SENSITIVITY OF STEEL PURLINS TO CHANGES IN APPLICATION OF WIND LOADS

Mary Douglas

Thesis submitted to the faculty of the Virginia Polytechnic Institute and State University in partial fulfillment of the requirements for the degree of

MASTER OF SCIENCE

In

CIVIL ENGINEERING

Matthew H Hebdon, Chair
Finley A Charney
Eric J Jacques

May 19, 2020

Blacksburg, Virginia

Keywords: wind tunnel, low-rise buildings, steel purlins, continuous beam analysis

SENSITIVITY OF STEEL PURLINS TO CHANGES IN APPLICATION OF WIND LOADS

Mary Douglas

Abstract

This project studied the effects of wind tunnel test loads applied to purlins in low rise steel buildings compared to those determined with currently recognized wind loading provisions. The National Institute of Standards and Technology (NIST) database of low-rise building wind tunnel test data, which was collected at the University of Western Ontario (UWO) boundary layer wind tunnel, was used to model a realistic wind load scenario. Pressure coefficient data recorded in the database was applied statically to individual purlins in a typical design for the size of buildings studied. These results were then compared to those obtained using the wind design provisions in ASCE 7-16 Chapter 30 for Components and Cladding. The primary data of interest was shear and moment values along the length of the purlins, which were modeled as continuous beams. Comparisons were made between the resultant shear and moment from both the wind tunnel load and ASCE 7-16 load values at 1-foot increments along the length of the purlin. The results showed that the overall peak values obtained from wind tunnel test loads were 3% to 49% higher than those calculated using ASCE 7-16 for purlins that were on the windward edge of the building. Purlins on the interior of the building varied in whether they exceeded the loads calculated with ASCE 7. Changing the height of the structure and the terrain roughness both increased the number of purlins that were lower than the values provided in ASCE 7-16 in the interior of the structure.

SENSITIVITY OF STEEL PURLINS TO CHANGES IN APPLICATION OF WIND LOADS

Mary Douglas

General Audience Abstract

Purlins are roof members used in low rise steel buildings to transmit wind loads applied to the roof of the structure to the frame of the building. This project studied the effects of applying loads to purlins using methods specified by the code compared to those found in a wind tunnel, to look at the similarity of the values and model the actual behavior of the purlins more accurately. For this study, wind tunnel test data obtained from the National Institute of Standards and Technology (NIST) database was applied to the purlins and the shear and moment was calculated. These results were compared to the current code requirements provided in the American Society of Civil Engineers (ASCE) 7 document: Minimum Design Loads and Associated Criteria for Buildings and Other Structures. The results showed that the loads developed in the purlins subjected to wind tunnel test loadings were 3% to 49% higher on the edge of the building than those that had the ASCE 7 design loads applied. More accurately modeling the behavior of the purlins using wind tunnel test data and beam models showed that in locations where the purlins received the maximum wind force, the ASCE 7 requirements for components and cladding tended to be lower than the wind tunnel test data. However, in locations where the purlins were not experiencing the maximum wind force, the ASCE 7 requirements tended to overpredict the loads, based on the use of symmetric high wind areas to design for all wind angles.

Dedication

To my family, whose endless support and encouragement made this possible.

Acknowledgments

I would like to thank my committee chair, Dr. Matthew Hebdon, for his support in pursuing this project, his excellent guidance throughout its development, and for surpassing his role as an advisor. I would also like to thank my committee members: Dr. Finley Charney, for sparking my interest in the topic through his courses and his contribution of continuous beam Matlab functions used in the analyses, and Dr. Eric Jacques for his knowledge and support.

I would like to thank the Insurance Institute for Business and Home Safety (IBHS), the Metal Building Manufacturers Association (MBMA), and the American Iron and Steel Institute (AISI) for funding this project. I would also like to thank Murray Morrison, for his patience in helping me learn and manipulate the NIST Wind Tunnel Database, and along with Mark Detwiler, and Lee Shoemaker for sharing their expertise and for taking the time to guide me through this project. I appreciate you trusting me with this opportunity.

Table of Contents

List of Figures

List of Tables

CHAPTER 1: Introduction

1.1 Background

In the current American Society of Civil Engineers (ASCE) specification, ASCE 7-16 chapter 30, which describes the wind provisions for Components and Cladding, the forces acting on a roof surface are determined based on an envelope of the peak pressures for each zone (ASCE, 2016). These zones are calculated based on "the latest boundary-layer wind tunnel and full-scale tests and from previously available literature" according to ASCE 7-16 Commentary on Wind Load Provisions. In the development of the most recent version of ASCE 7, the roof zones and pressure coefficients were updated to reflect new results based on the analysis of a database of low-rise building wind tunnel data available from the National Institute of Standards and Technology (NIST) (Ho, et al. 2003). This database was also utilized in this project.

In the NIST wind tunnel tests, conducted at the University of Western Ontario (UWO) Boundary Layer Wind Tunnel, pressure taps were placed across the walls and roof of the building (shown in Figure 1) (Ho, et al. 2003). Pressure coefficients (C_p) were then recorded at each of these locations to measure the variation in load at different points of the structure over time. Data was recorded for multiple test configurations with variation in wind direction, exposure, building height, and building size. For low rise buildings, such as the ones tested in these studies, ASCE 7 implements this data by separating zones of similar pressure coefficient values evaluated across all wind angles, that vary across the surface being considered and are dependent on building height(ASCE, 2016).

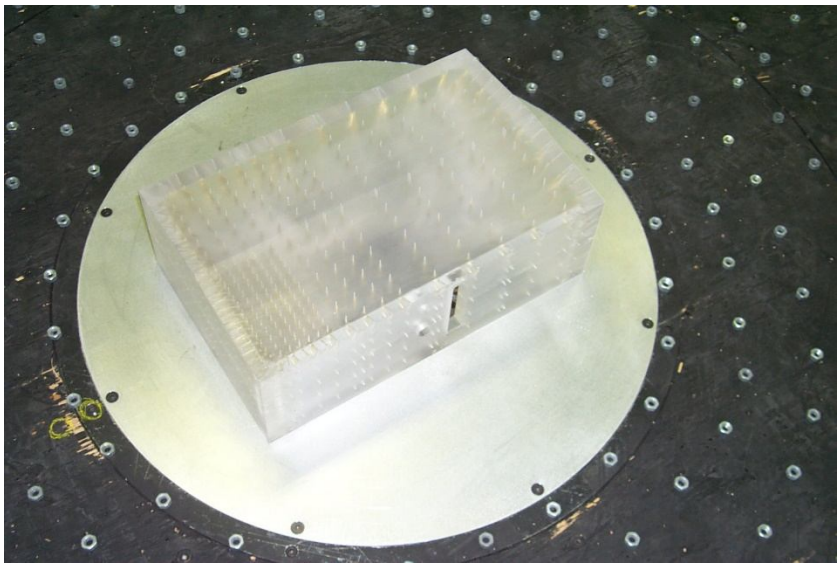

Figure 1: Image of test building with pressure taps (The Boundary Layer Wind Tunnel Laboratory, UWO)

In typical low-rise steel building design, purlins are used to span multiple girders and provide support for roofing attachment. Because of this design, purlins are long continuous members that often span multiple wind zones. Due to the simplified pressure coefficient zones used in ASCE 7, component and cladding loads on a roof purlin are determined using a combination of pressure coefficients along the length of the member. However, this does not always accurately model the true loads on a purlin at any one instance in time. Since these pressure coefficients are an envelope of the actual pressures measured at the taps within that particular zone, it is likely that at each snapshot in time, most of the actual pressures on the purlin would be much lower. When formulating the pressure coefficients for the standard, an envelope is drawn for multiple structures at multiple wind angles so that one pressure coefficient curve can be used for all structures to which the standard applies.

The structural response of a long continuous member will be very different under these two loading scenarios described above. In the actual loading on a purlin, there are a series of varying loads acting along the length of the purlin. In contrast, using the established wind zones in ASCE 7, there will be between two and four different line loads placed on the purlin depending on the building size and location of the purlin. An example of these differences is shown in Figure 2 and Figure 3. Figure 2 shows the measured forces on a purlin for fifteen-time steps, each block corresponds to the width of the pressure tap tributary area. Figure 3 shows a diagram of the design loads on a purlin using the ASCE 7 component and cladding loading zones.

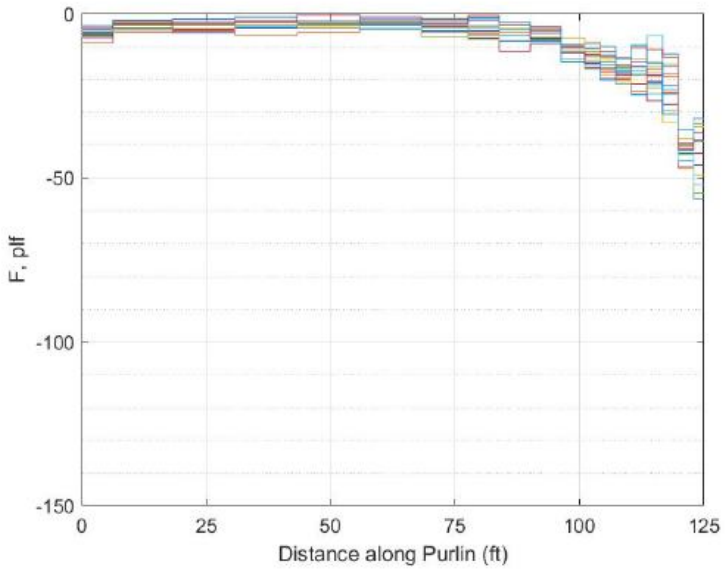

Figure 2:Loading pattern for a purlin subjected to wind tunnel loads at 360° wind angle

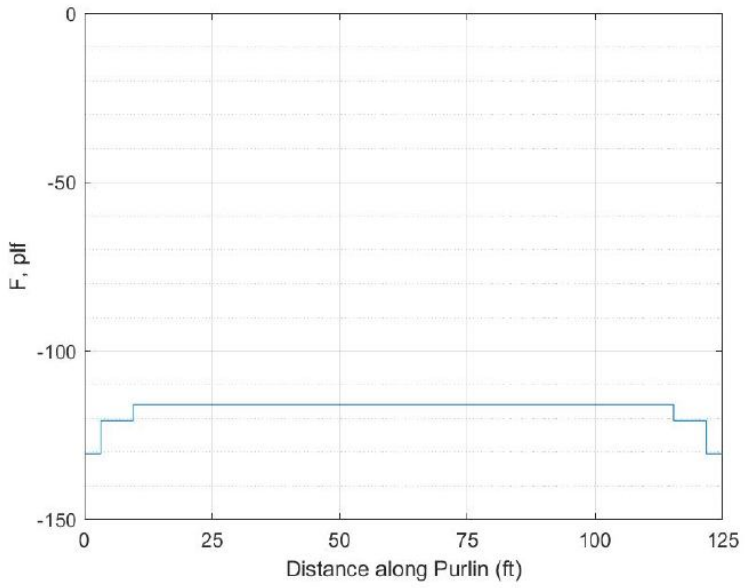

Figure 3: Loading pattern for a purlin subjected to ASCE 7 C&C Loads

Figure 2 and Figure 3 show the distinct differences between the two load scenarios applied to the structure. While the loads for ASCE 7 do represent an envelope of all the maximum values that the purlin could experience, Figure 2 shows that in individual time steps for the 360° wind direction, the maximum loads will not be experienced across the entire purlin, and the behavior with different wind directions will vary, while not being applied exactly as the loads in Figure 3 show.

1.2 Objective and Scope

The goal of this project was to explore methods of analyzing low rise buildings under wind loads to more accurately model the behavior of the structural system. In conducting this analysis, the behavior of a purlin under wind loads was modeled. The project used pressure coefficient data from wind tunnel testing and distributed the measured roof pressures to the purlins based on their tributary widths. By creating incremental wind loads along the length of the member, rather than a series of zone loadings as is dictated by ASCE-7, a more accurate load envelope was derived for each loading condition. The behavior of a continuous beam under the proposed loading was expected to be different from the current recommendations in the standard, due to the differences in the loading patterns using wind tunnel test results compared to the pressure envelope used in ASCE 7-16.

While time-varying data was used, the loads were applied to the structure statically at each time step and wind angle. According to the equations provided in Chapter 26 of ASCE 7-16 for calculating natural frequency, these buildings are designed as rigid, with a natural frequency larger than 1 Hz (ASCE, 2016). This structure also does not meet the properties provided in the ASCE 7-16 Commentary on Chapter 26 for buildings with the potential for large dynamic response characteristics. Finally, as this study compared wind tunnel test results with ASCE 7-16 design provisions, in which dynamic effects are taken into account using the gust-effect factor, the loads were applied statically corresponding to assumptions in ASCE 7-16 assumptions in design of rigid buildings.

Using this method, a reduction in the wind loads on some of the purlins was expected, as this removes some of the built-in conservatism present in the ASCE 7 component and cladding procedures. Currently, ASCE 7 uses an envelope of peak pressures in a zone across all angles and building sizes to determine the loads for components and cladding. Using this method, specific time steps that are expected to generate higher loads can be isolated for the building under consideration.

1.3 Thesis Organization

The first two chapters of this thesis provide an introduction to the topic and project, and a review of relevant literature on wind loading, low-rise steel buildings, and computer analysis methods. Chapter 3 contains a manuscript that will be submitted to the Journal of Structural Engineering that discusses the research conducted for this thesis. Chapter 4 is a conclusion discussing the findings and potential for expansion of the study. Appendix A contains an extended description of the methods used for research. A copy of the MATLAB routines used for the analysis of the wind tunnel data, conversion to force, and analysis of the purlins are attached in Appendix B.

CHAPTER 2: Literature Review

2.1 Wind Loading

ASCE 7-16

For determination of the wind loads on a structure, ASCE 7 utilizes a series of equations for the Main Wind Force Resisting System and Component and Cladding loads (ASCE, 2016). These equations are generally based on a target wind speed and adjusted for factors relating to site and structure conditions, such as elevation, topography, and building height. The primary equation used is equation 26.10-1 from ASCE 7-16 and calculates the velocity pressure at the height being considered (q_z) (ASCE, 2016):

$$q_z = 0.00256 K_z K_{zt} K_d K_e V^2 \quad \text{(Equation 1.1)}$$

The velocity pressure exposure coefficient (K_z) is determined based on the height along the structure (typically either floor elevation or roof height) and exposure categories (ASCE, 2016). In ASCE 7-16, there are three exposure categories (B, C, or D) that are determined based on upwind ground surface roughness. Examples of these exposures are urban and suburban, open, and flat, for Exposures B, C, and D respectively. The K_z factor accounts for variations in the wind speed profile with height and exposure. With increases in height, there tends to be a reduction in turbulence and an increase in wind speed, however; the values of K_z are limited at a height of 15 feet, where no further reduction is permitted below that value.

The topographic factor (K_{zt}) accounts for wind speed-up on hills, ridges, and escarpments (ASCE, 2016). This condition only applies where the topography significantly extends beyond the other upwind features. This is taken from observations of significant increases in the wind speed experienced by a structure located along or on an elevated feature compared to those on relatively flat terrain. Both the velocity pressure exposure coefficient and topographic factor increase the calculated wind pressure (with values larger than 1) to account for higher velocities based on site conditions.

The directionality factor (K_d) accounts for a low probability of having the maximum wind and maximum pressure coefficient occurring in any one direction (ASCE, 2016). In the standard, there is a table of directionality factors that vary depending on the type of structure. The elevation factor (K_e) accounts for changes in air density with elevation. This reduction is based on the ratio of air density at elevation, to the benchmark air density at zero feet above sea level that is assumed in the equation for calculating wind pressure. Both of these factors reduce the wind pressure, however; a value of 1.0 can be used conservatively.

Equation 26.10-1 uses the wind speed (V) obtained from a wind speed hazard map as the basis for determining wind pressure (ASCE, 2016). In the current standard, there are separate maps used for each risk category based on the target return period. Using wind speed maps broken down by mean return interval as opposed to an importance factor, as was previously done, allows there to be a consistent target reliability between zones and risk categories, separate regions of the country who only experience non-hurricane wind loads, and have a clear design wind for a certain building. In each map, there are contour lines showing wind speeds on a 3-second gust basis. These wind speed maps were developed from available non-hurricane data and hurricane model simulations. Depending on the region and return period, the controlling case between non-hurricane and hurricane cases varies. An example of a wind speed hazard map for Risk Category II is shown in Figure 4.

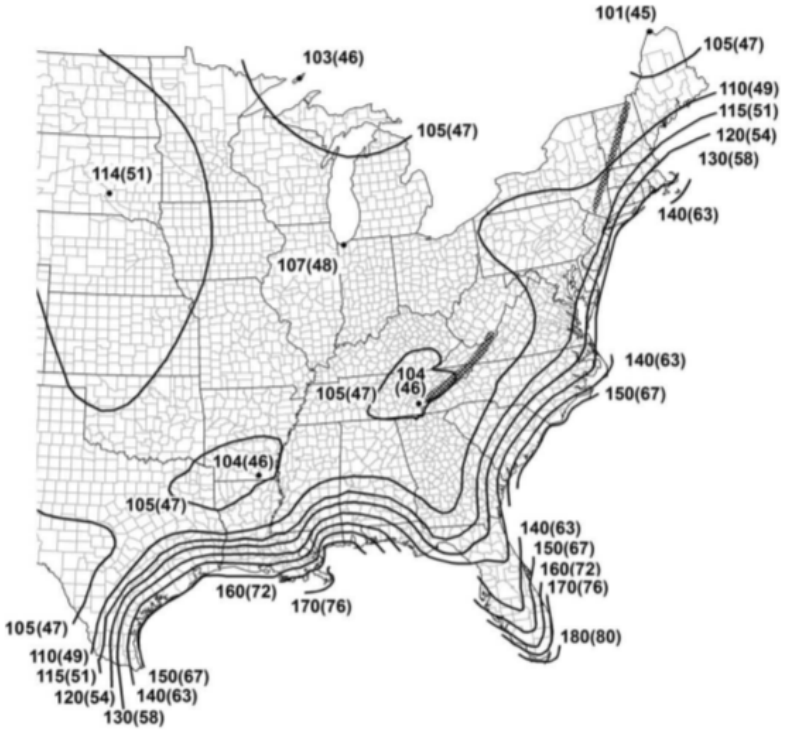

Figure 4: Example of wind speed maps for the East coast of the United States for Risk Category II (ASCE, 2016)

Main Wind Force Resisting System

An additional equation (Eq. 27.3-1) is used to convert from velocity pressure to the design wind pressure (ASCE, 2016). This equation uses the velocity pressures determined in equation 1.1 along the height of the structure along with a gust-effect factor and pressure coefficients to determine the design wind pressure.

$$p = qGC_p - q_i(GC_{pi})$$ (Equation 1.2)

This equation is based on the velocity pressure (q) determined from the equation above (ASCE, 2016). For windward walls, q is equal to the velocity pressure at heights above the ground up the height of the structure (typically delineated by floor). For the roof and leeward walls, q is calculated at the mean roof height of the structure. For calculating the loads on the MWFRS, the gust-effect factor (G) is 0.85 for rigid buildings, but can be reduced with additional equations. Several equations are used to calculate G_f for flexible buildings. Whether a building is considered rigid or flexible depends on the calculated approximate natural frequency (less than 1 Hertz is considered flexible). The gust factor (G) accounts for all the dynamic effects of wind on the structure. For flexible buildings, this includes the effects of dynamic amplification, which is not accounted for in the calculation for rigid buildings.

The calculation of the pressure coefficient (C_p) is then determined using tables contained in Chapter 27, based on building geometry (ASCE, 2016). The calculation of these coefficients is based on the "actual loading on each surface of the building as a function of wind direction" according to the Chapter 27 commentary (ASCE, 2016). This is based on observations made in wind tunnel tests. In these tests, it was noted that roof structures experience both slightly positive and large negative pressures, leading to the selection of the given C_p values that require designers to account for this.

The internal pressure (q_i) is determined based on the height of the highest opening in the structure using the equation for velocity pressure (ASCE, 2016). The internal pressure coefficient (GC_{pi}) is determined using the tables provided in Chapter 26 based on the amount of enclosure in the building. The coefficients for internal pressure are based on both wind tunnel tests and full-scale data. Enclosed buildings are assumed to have small amounts of leakage paths throughout the structure that uniformly allow air transfer, leading to low internal pressure coefficients. For partially enclosed buildings, significant increases in loads can occur due to internal pressure, leading to higher internal pressure coefficients. The results of the studies used in the development of the standard did not account for the effects of the interior of the structure being compartmentalized, and so this was not considered in the design code. There is also a recommendation that breaching of cladding be considered when in a wind-born debris region, as this can create openings that have a significant impact on the internal pressures in the structure.

Components and Cladding

The wind loads on components and cladding are often larger than those that are calculated for the main wind force resisting system. Because they are subjected to turbulent flows around a bluff body, components can experience large peak loads over a small area (Kopp & Morrison, 2018). There are seven sections of

ASCE Chapter 30 on Components and Cladding (ASCE, 2016). These sections are based on the type of structure being considered. Part 1 is for enclosed and partially enclosed low-rise buildings and those shorter than 60 feet. Part 2 is a simplified method for enclosed low-rise buildings and those with a height greater than 60 feet. The additional parts of the chapter are for taller buildings, open buildings, building appurtenances, and non-building structures. Part 1 will be the focus of this study for comparison to wind tunnel loads, as it contains the recommendations for low rise buildings, with flat, gable, multi-span gable, hip, monoslope, stepped, or sawtooth roofs. Chapter 30 is limited to structures that are regularly shaped, have no characteristics that make it susceptible to strong dynamic loading, or site conditions that cause variations in wake behavior. The provisions of this chapter use the calculated velocity pressure and a combined gust effect factor and pressure coefficient in equation 30.3-1 to find the pressure on the components and cladding of the structure.

$$p = q_h\left[\left(GC_p\right) - \left(GC_{pi}\right)\right] \quad \text{(Equation 2.3)}$$

In this equation, the velocity pressure at the mean roof height of the building is used as the q_h value (ASCE, 2016). A separate set of external pressure coefficients is used in this chapter than those used for the MWFRS. The external pressure coefficients for components and cladding are provided as a combined GC_p that cannot be separated. Each component and cladding member must be designed for both the maximum positive and negative pressures. The internal pressure coefficients are the same as those obtained from Chapter 26.

The external pressure coefficients in Chapter 30 are provided in charts for both walls and roofs (ASCE, 2016). These are broken down by roof slope and roof type. The surface being considered is divided into zones based on regions of the surface that experienced similar loading measured in wind tunnel tests. The zones are created using an enveloping method of determining the peak pressure. Using the NIST wind tunnel database (Ho, 2003), updates were made to the existing roof zones and pressure coefficients in 2016 to be consistent with new data (ASCE, 2016). These new updates were based on a study that utilized the ability to find “spatially-averaged pressure” by using multiple pressure taps that were collecting data concurrently (Kopp & Morrison, 2018). The results of this study showed that pressures on the roof for low slope roofs are primarily dependent on the building height rather than building plan, as was previously assumed. New roof zones were drawn to implement the size as a function of building height, while also minimizing the high-pressure areas of the roof. In this method, buildings with lower plan to height ratios can have as few as two roof zones, while buildings with larger plan to height ratios will have up to four. These changes to roof zones and pressure coefficients predominantly increased loading at the corners of the roof and the pressure coefficient curves in the other zones were adjusted to more accurately fit the data.

These zones then correspond to a provided curve of values where external pressure coefficients are plotted on the vertical axis, and effective wind areas on the horizontal axis (ASCE, 2016). The effective wind area is defined as either the area that contributes to the load on the component (tributary area) or the span length of the component being considered multiplied by an effective width no less than a third of the span length. This definition of effective wind area varies for specific cladding systems such as membrane roof systems, windows and doors, et cetera. An example of the roof zones and plots for flat roof structures is shown in Figure 5.

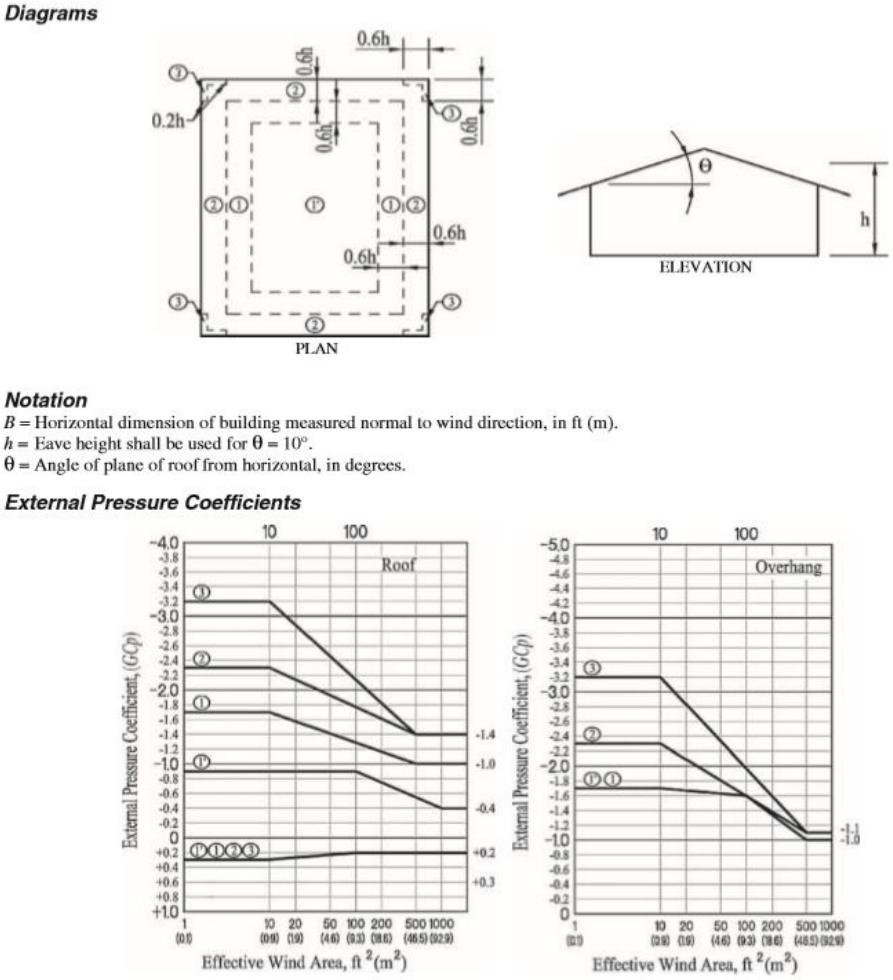

Figure 5: Example of Roof Zones and Pressure Coefficient Curves (ASCE, 2016)

Wind Tunnel Tests

In this study, wind tunnel test pressure coefficients were used to determine an alternate loading pattern on the purlins. Generally, for low-rise buildings there is significant variation in the results from different wind

tunnels and can be up to 50 percent different from the wind loads specified in ASCE 7 for the main wind force resisting system (MWFRS) (Duthinh, 2011). To quantify the differences between wind tunnel test results and full-scale results, tests were conducted in China where a full-scale building was instrumented and placed in the field to collect pressure histories during tropical storm events (Li, 2019). A scaled version of the building was then tested in the boundary layer wind tunnel at the Southwest Jiaotong University. While the results between the boundary layer wind tunnel tests and full-scale field tests were similar across most of the roof, there were significant differences along the ridge and on the leeward side of the roof. The lower values in the model scale are most likely due to inaccurate separation at the model ridge. This study gives a good picture of the variations in results between the two test methods, since there is a direct modeling of the buildings that are being tested at full size in actual site conditions.

This study will use wind tunnel data from the NIST database. The NIST data was collected at the University of Western Ontario (UWO) wind lab in a boundary layer wind tunnel (Ho, et al. 2003). To verify the data collected, the test results were compared with previous research that had been done at UWO and was the basis for the development of code provisions for low rise buildings under wind loading (Pierre, et al. 2005). The previous tests that were conducted and used for comparison were done on a variety of scales, were collected at 45-degree increments of approach angle, and had a lower sampling frequency and tap density than what was in the NIST database. This was due to less ability to store data with the technology that was used at the time. The turbulence profiles produced in the two studies were also different, which was attributed to a change in the "design" open country profile. The turbulence profiles used in the current tests were able to be matched to the Engineering Sciences Data Unit (ESDU) turbulence profile. Horizontal thrust and vertical uplift were calculated on the end bays of three building layouts for comparison of the results. The mean values for the tests were a close match, while the peak values in the current test database were much higher. After adjusting for differences in the tests, the data from the two databases matched well, and places where the results did not closely match could be attributed to the various parameters discussed previously. The results from the tests were also compared with full-scale building tests and field results from Texas Tech (T. C. E. Ho et al., 2005). The mean pressure coefficients from the tests matched well, but there was a significant difference in the root mean square pressure coefficients. This generally agrees with the results of other studies, where peaks aren't always captured by the wind tunnel tests, however; the trends are consistent.

NIST Database

The wind tunnel data being considered for this study is the NIST Aerodynamic Database containing results from tests conducted at the UWO Boundary Layer Wind Tunnel Laboratory (T. C. E. Ho et al., 2005). In

this database several building floor plans were tested with variations in building plan size, building height, roof slope, and exposure. All were tested at a length scale of 1:100. All buildings had approximately the same distribution of pressure taps, with some variation in the number of taps with the size of the floor plan. The windward corner of each building had a higher density of pressure taps than the rest of the structure to accurately measure the variation at the most turbulent corner of the building. For the buildings considered in this study, the tap spacing is the equivalent at the prototype scale to is 3.12 feet at the windward corner versus 12.5 feet at the furthest corner. The layout of pressure taps across the roof for one building is shown in Figure 6.

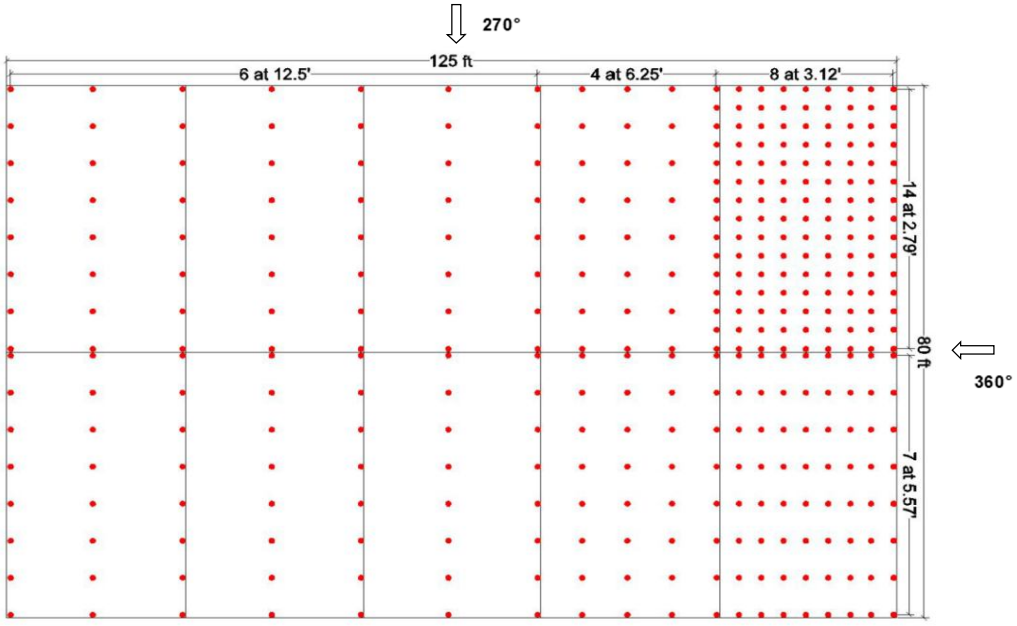

Figure 6: Layout of pressure taps on roof of 125 ft by 80 ft building

For each building, tests were run over 90 degrees at five-degree increments. The turbulence intensity profile was created using a combination of spires and roughness elements along the floor (shown in Figure 7) to recreate a benchmark turbulence from ESDU.

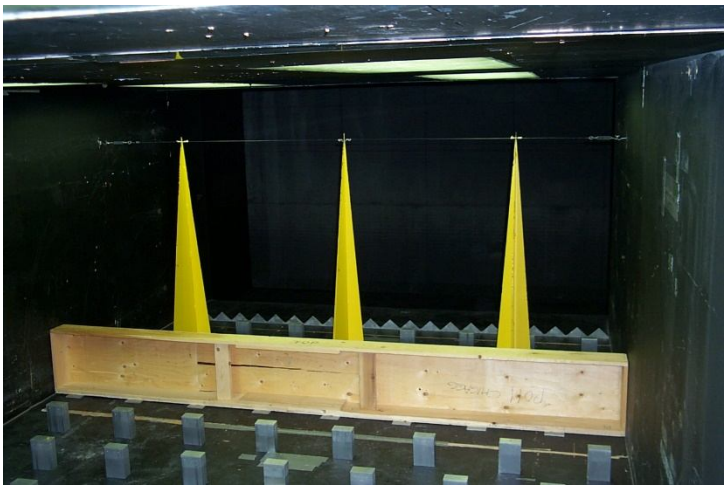

Figure 7: Setup of the elements used to create an accurate turbulence profile (The Boundary Layer Wind Tunnel Laboratory, UWO)

During the UWO tests, pressures were recorded at each tap simultaneously and any lag in data collection with time was accounted for (T. C. E. Ho et al., 2005). Data was collected at a frequency of 500 Hertz over 60 seconds for each test set up. The pressures were then converted into an equivalent pressure coefficient by referencing to the dynamic pressures measured in the upper level of the wind tunnel. They could then be compared to the standard design values by referencing to roof height using a conversion factor of the ratio of roof height to reference height. The wind speed profile was also measured to check the mean wind speed. Collected data was stored in Hierarchical Data Files (HDF) due to its ability to handle large arrays of data and be retrieved using a variety of accessible processing software.

To implement this pressure coefficient data as a parameter on the same scale as what is calculated in ASCE 7, it was converted into an equivalent $(GC_{pf})_{eq}$. After the completion of these wind tunnel studies, an equation was developed to perform this conversion (Pierre, et al. 2005):

$$(GC_P)_{eq} = \frac{\frac{1}{2}\rho V^2{}_{h,z_0,meanhrly} C_p}{\frac{1}{2}\rho V^2{}_{10m,o.c.,3secgust} K_{zt} K_h K_d I} \qquad \text{(Equation 2.4)}$$

This equation removes the impacts caused by the differences in averaging time and wind speed measurement height between what is used in the tests and what is used in the standard (Pierre et al., 2005). It also removes the impacts of the various factors that are typically applied, as this is already accounted for in the determination of pressure for the calculations in ASCE 7. The directionality factor, however, was left as 1.0 for this calculation since the wind tunnel data contained multiple wind angles, and therefore was not adjusted for variations in probability due to directionality.

2.2 Steel Building Systems

Typical Design

Industrial or other low rise steel building structures, such as the ones being considered for of this study, are designed very efficiently to minimize the amount of steel being used with the requirements for the structure (MBMA, 2018). Typically, these buildings consist of moment frames made of structural steel (hot rolled sections) spaced at 15 to 25 feet on center (J Ginger, 2015). These members use tapered sections of multiple sizes welded together to ensure that most of the steel is placed in locations with maximum loads (MBMA, 2018). They also serve as the MWFRS in one direction of the building. Cross bracing is used between frames to serve as the MWFRS in the other direction and to provide stability of the moment frames (J Ginger, 2015). Additionally, girts, purlins (cold-formed sections and joists), and cladding are attached to the frames and serve as secondary members and wall and roof diaphragms. The Metal Building Systems Manual, provided by Metal Building Manufacturers Association, details procedures for designing low-rise steel structures to meet load requirements. A typical design for a low-rise steel building with roof purlins is shown in Figure 8.

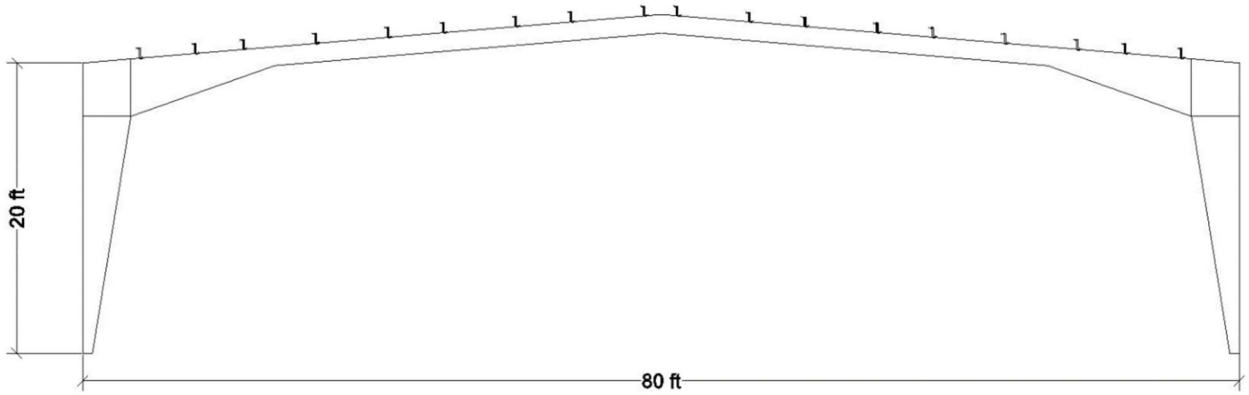

Figure 8: Profile view of typical low-rise building frame

The design of these structures for wind loads relies on ASCE 7, chapters 26 through 30, with a special focus on chapter 30 for purlin design for components and cladding loads (MBMA, 2018). For components and cladding, a minimum value of 16 pounds per square foot (psf) is specified. When selecting the *GCp* value discussed in previous sections, zones along the surface are used showing locations of higher and lower pressure values on the surface of the structure. It is common for a building member to lie within multiple zones, such as for a roof purlin like the ones being studied in this report. In this case, the approach to address this is up to the discretion of the designer based on the structure being considered, but the recommended

method is to employ a step function along the length of the structural member or a weighted average of the zone overlap with tributary area. For purlin design, where the values of pressure coefficient will be varying along the length, the best approach is to use a step function for each zone. A diagram showing a typical layout of purlin spacing with an overlay of roof zones is shown in Figure 9.

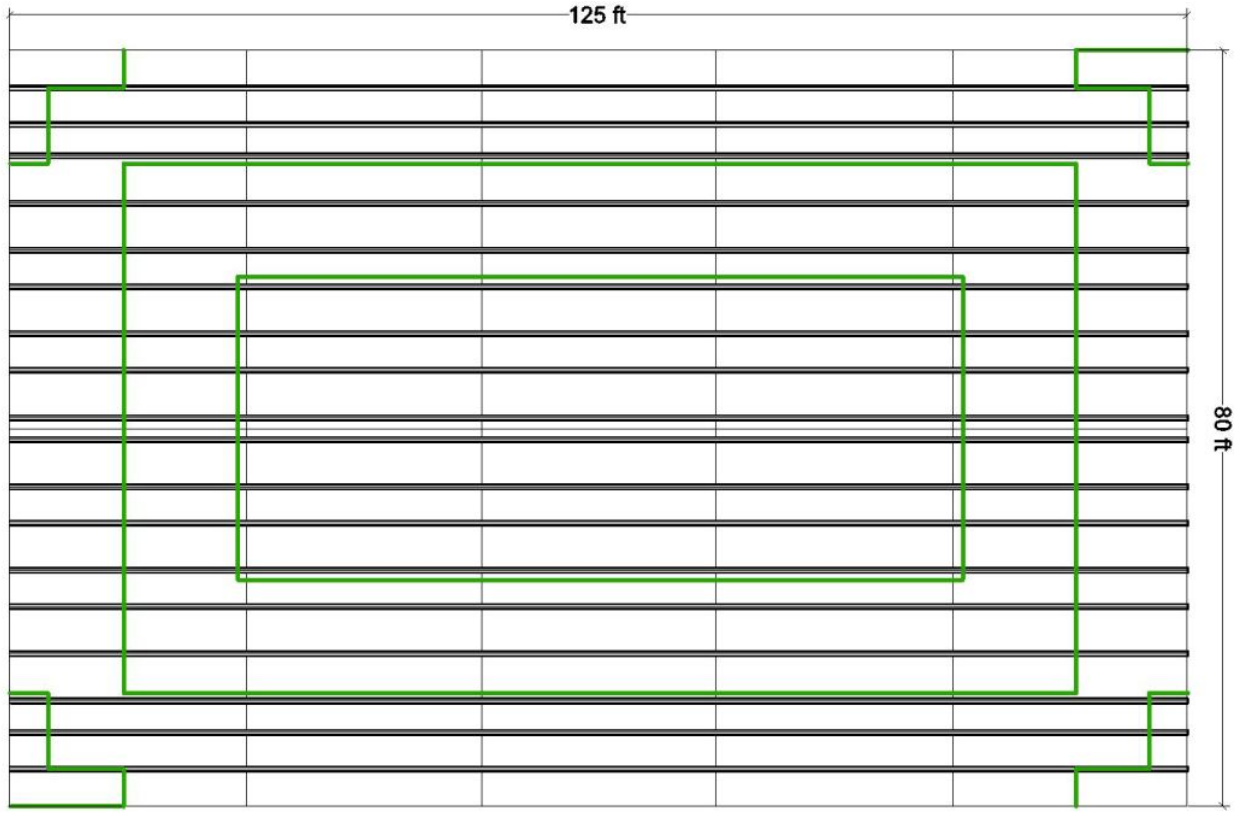

Figure 9: Purlin spacing with roof zones

In selecting the effective wind load area for determining the pressure coefficient, the maximum value between the average of the two adjacent tributary widths, or the span length over 3 times the tributary width should be used (MBMA, 2018). The resulting effective wind area has an impact on the pressure coefficient value obtained, as increases in effective wind area will decrease the calculated pressure coefficient value, and therefore, the loads on the member. This is due to the effect of determining pressure coefficients using area-averaged pressures. For the MWFRS, the pressure coefficient values are lower because they are an average of all of the pressure values contributing to the load on these members and are typically across multiple faces. For components and cladding members, the area averages are more localized, and each peak has more of an influence. As the effective wind areas decrease, the component and cladding loads increase.

Performance Under Wind Loads

The primary damage incurred in steel structures is related to the building envelope and cladding (Ji, 2017). Breach of roofing causes damage to the structure itself along with the contents which results in large economic losses. The results of disaster investigations from 1972 through 1988 found that the primary damage to these structures occurred in nine categories, two of which involved purlins (Perry, 1990). The categories were failures of purlin and roof assemblies that led to progressive collapse, and strut purlin failures led to collapse of the end bay. The requirements for these members have been updated to account for these failure mechanisms, but these examples provide insight into the importance of adequate purlin design for the entire structure. In high wind, the cladding of the structure serves as restraints for lateral-torsional buckling of the purlins, since they are often spanning long distances. The combination of sheeting and purlins also contributes to lateral resistance through diaphragm action. Because each member in the structure contributes to stability in some way, the failure of any member of the structure impacts the entire structure.

2.3 Computer Analysis Methods

To conduct structural analysis of the continuous purlins studied in this project, the direct stiffness method with a transformational approach was used. This analysis method is based on previous work conducted at Virginia Tech by Finley Charney and Jeena Jayamon (Jayamon, 2012). Computer codes were developed to implement this method and were confirmed using SAP2000 as part of a previous student's Master's Thesis (Jayamon, 2012). These computer codes have been adapted to analyze purlins for this project and independently verified. In this method of analysis, multiple levels of scope (Figure 10) are used to formulate the stiffness matrix and then solve for the element forces (shear and moment) and reactions.

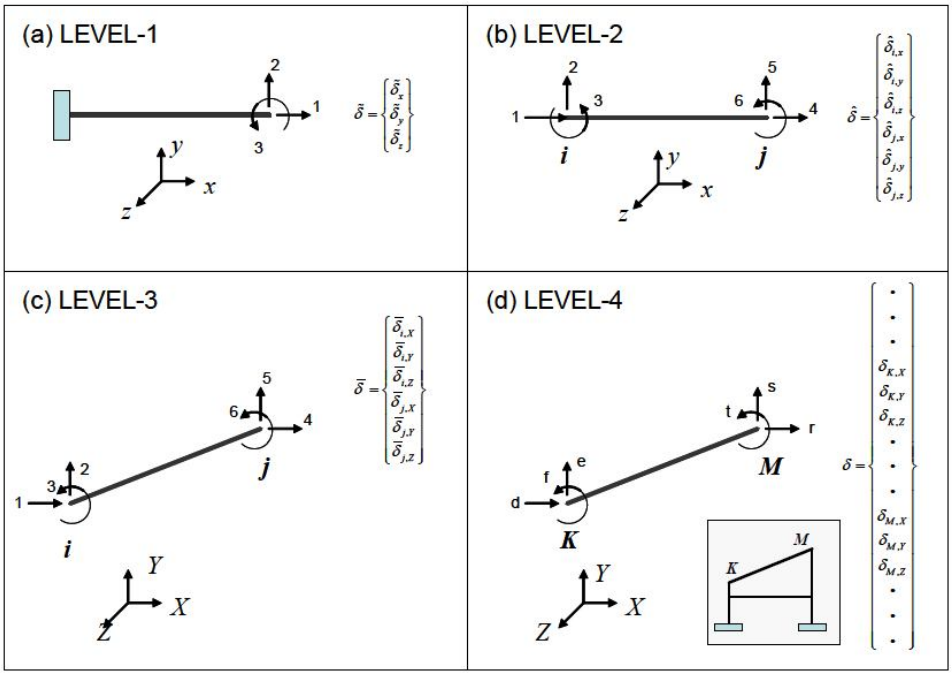

Figure 10: Diagram of Levels of Scope (Charney, 2008)

The element stiffness matrix is formulated in level 1 using a reduced element degree of freedom set in coordinates local to the element (Jayamon, 2012). This is done by calculating the element flexibility matrix using the principles of virtual work and then inverted to obtain the level one stiffness matrix. The equation of equilibrium at level 1 is shown in equation 2.5.

$$\tilde{k}\tilde{d} = \tilde{f} \qquad \text{(Equation 2.5)}$$

From there, transformations are used to move from level one to level two, where the full element degree of freedom set is considered in local element coordinates (Jayamon, 2012). This is done using transformation matrices (a and b) that are determined based on equations of compatibility (a) and equilibrium (b). The equations for converting from level one to level two and determining the transformation matrices are shown below (Charney, 2008).

$$\tilde{\delta} = a\hat{\delta} \qquad \text{(Equation 2.6)}$$

$$\hat{f} = b\tilde{f} \qquad \text{(Equation 2.7)}$$

$$b = a^T \qquad \text{(Equation 2.8)}$$

$$\hat{k} = b\tilde{k}a \qquad \text{(Equation 2.9)}$$

Using the same concept, transformations are used to move from level two to level three, where the full element degree of freedom set is used, but the coordinates are converted from the local element coordinates to the global system coordinates (Jayamon, 2012). This is done using similar transformation matrices (T and U) based on equations of compatibility (T) and equilibrium (U). These equations are shown below (Charney, 2008).

$$\hat{\delta} = T\bar{\delta} \quad \text{(Equation 2.10)}$$

$$\bar{f} = U\hat{f} \quad \text{(Equation 2.11)}$$

$$U = T^T \quad \text{(Equation 2.12)}$$

$$\bar{k} = U\hat{k}T \quad \text{(Equation 2.13)}$$

Equations of transformation can be used to then convert from level three to level four where the global coordinates are used and the total degree of freedom set is considered (Jayamon, 2012). The global stiffness matrix can then be assembled using transformation matrices (A and B) or it can be assembled directly to reduce computational demands (Charney, 2008). An equation representing the total transformation is shown below.

$$K = \sum_{i=1}^{n_{elements}} B_i U_i b_i \tilde{k}_i a_i T_i A_i \quad \text{(Equation 2.14)}$$

The basic equation of equilibrium shown above in equation 2.5 can be expanded to account for nodal loads and member loads (Charney, 2008). This expanded version that accounts for the two types of loading considered and using the stiffness matrix developed as described above is then used to solve for the displacements and element forces. In order to account for member loads using the standard equilibrium equations, they are converted into equivalent fixed end forces. In solving the system, the fixed end forces will be accounted for in the total values of force calculated. Because of this, the fixed end forces have to be added back into the element forces at level two to find the true element force. The expanded version of the equation is shown below where P is the nodal loads and Q is the fixed end forces (using the full system degree of freedom set and global coordinates).

$$K\Delta = P - Q \quad \text{(Equation 2.15)}$$

Where:

$$Q = -\sum_{i=1}^{n_{elements}} B_i U_i \hat{q}_i \quad \text{(Equation 2.16)}$$

For continuous beam structures, such as the purlins that will be analyzed in this project, a reduced set of these equations can be used (Jayamon, 2012). The level one stiffness matrix can be formed and then moved to level two using the equations provided above. Alternatively, the level two stiffness matrix can be formed directly using the full element degree of freedom set. From there, a conversion between level two and level three is unnecessary as the local and global coordinate systems are equal for beam structures. The stiffness matrix will then be built using the full system degree of freedom set and can be used to solve the system. In formulating the equations for a continuous beam, four degrees of freedom are considered for each element. There is a transverse deformation and rotation at each end of the element, and axial deformations are not considered.

CHAPTER 3: Manuscript

3.1 Foreword

This manuscript has been written with the intent of submission to the Journal of Structural Engineering. This manuscript is co-authored by Dr. Matthew Hebdon, who served as the primary advisor on this project, Murray Morrison, who provided programs to access the wind tunnel data and expertise on how to use these files to get the data of interest, and Mark Detwiler, who assisted with selecting the typical building design and other aspects of the project related to the steel sections and structural analysis.

3.2 Manuscript

A COMPARISON OF STEEL PURLIN BEHAVIOR UNDER WIND TUNNEL TEST LOADS AND ASCE 7-16

Mary K. Douglas, Murray Morrison, Matthew Hebdon

Abstract

This paper compares the behavior of steel roof purlins under wind loads based on wind tunnel tests to wind loading specifications in ASCE 7-16. Data from the National Institute of Standards and Technology (NIST) database of low-rise building wind tunnel tests were applied to a typical steel building. The load at each time step from the data was applied to the individual purlin statically and subsequent incremental shear and moment values along the length were determined. The results from the in-depth wind analysis were compared to the resulting shear and moment values at the same locations obtained from ASCE 7-16 specified loading based on specific roof zones. The purlins were analyzed as a continuous beam using the direct stiffness method. The maximum shear and moment on the purlins due to the wind tunnel test data were higher than those calculated using ASCE 7-16, ranging from 0.75-12% for shear, and 0.54-19% for moment on buildings with a mean roof height of 16 feet and 1.9-38% for shear and 0.82-49% for moment on buildings with a mean roof height of 40 feet. The largest deviation from the current specification was found to be for purlins experiencing the greatest loads on the windward edge. Purlin spans in the interior of the building had less correlation and varied in which procedure produced the most conservative loading results.

Introduction

Background

In typical low-rise steel building design, purlins are used to span the length of the roof and provide support for roofing attachment. Because of this design, purlins are long continuous members that often span multiple wind zones. The current American Society of Civil Engineers (ASCE) specification, ASCE 7-16 chapter 30, determines forces acting on a roof surface based on an envelope of the peak pressures for specified zones set by the height of the building and location on the roof (ASCE, 2016). These zones are calculated based on boundary layer wind tunnel test results that record pressure coefficients on sample buildings of a variety of sizes across multiple wind angles. Because purlins often will span multiple roof zones, under this enveloping procedure described, this does not represent the actual loads on the purlin at any instance in time. Since the pressure coefficients used in ASCE 7-16 envelope pressures measured at the taps within each zone, it is likely that at each snapshot in time, most of the actual pressures on the purlin would be much lower.

The structural response of a long continuous member, like a purlin, was expected to be very different under ASCE 7-16 loads compared to those that the structure would experience. In the actual loading on a purlin, there are multiple wind loads fluctuating in both magnitude and direction. The method used in ASCE 7 for forces acting away from the surface would result in between two and four different line loads placed on each purlin depending on the building height and the location of the purlin (ASCE, 2016). There is one consistent value used for each roof zone in ASCE 7-16 for forces acting towards the roof surface. The values found for forces acting towards and away from the surface independently represent the full range of loads the members could experience according to ASCE 7-16, whereas in actual loading scenarios, the purlins could be simultaneously experiencing pressures both towards and away from the surface at different locations along the length.

This project focused on the analysis of purlins in low rise steel buildings. These structures are typically designed very efficiently to minimize the amount of steel being used while meeting the load requirements (MBMA, 2018). Typically these types of buildings consist of frames made of structural steel spaced 15 to 25 feet apart (J Ginger, 2015). These frames are typically made of welded built-up tapered sections to ensure steel isn’t unnecessarily placed in locations with lower loads (MBMA, 2018). They also serve as the MWFRS in one direction. Cross bracing is used between frames for stability and as the MWFRS in the opposite direction. Girts, purlins, and cladding are attached to the frames and serve as secondary members. Purlins and girts are typically cold-formed sections or joists. The Metal Building Systems manual provides procedures for designing low-rise steel structures to meet load requirements (MBMA, 2018).

This project utilized the National Institute of Standards and Technology (NIST) database of low rise wind tunnel test results conducted in the boundary layer wind tunnel at University of Western Ontario (UWO) (T.C.E. Ho, et al. 2003). This database contains results of wind tests performed on buildings with a variety of floor plans, with varying size (40'x30' to 250'x60'), height (12ft to 60ft), roof slope (1/4:12 to 6:12), and exposure (open or suburban) (T.C.E. Ho, et al. 2005). Figure 11 shows the test set up for one building configuration in both open (left) and suburban (right) terrain.

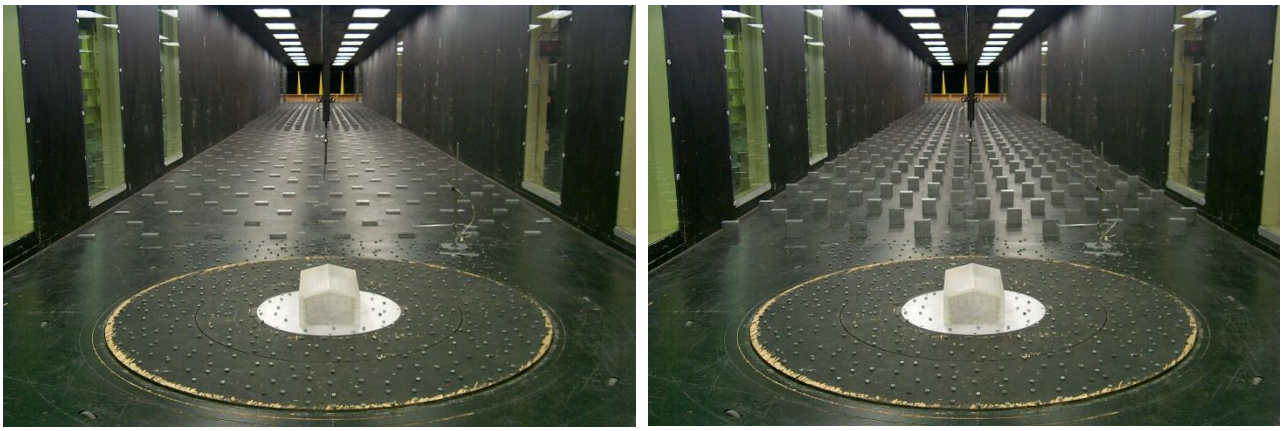

Figure 11: Images showing open terrain test (left) and suburban terrain test (right) (The Boundary Layer Wind Tunnel Laboratory, UWO)

All buildings were tested at a scale of 1:100. Pressure taps were placed at varying spacings along the walls and roof with different spacings used in each test configuration. In each of the tests, the highest density of taps was used at the windward corner of the roof, with lower tap densities on the leeward side longitudinally and transversely. The tests were performed across 90 degrees of approach angle at 5-degree increments.

In each test, the pressure was recorded at each tap essentially simultaneously and any lag in data collection with time was adjusted (T. C. E. Ho et al., 2005). Measured pressure was converted into an equivalent pressure coefficient by referencing to the dynamic pressures measured in the upper level of the wind tunnel. To compare the obtained pressure coefficient values from the wind tunnel test data with the pressure coefficient (C_p) used in ASCE 7, the measured values were converted into an equivalent combined gust-effect factor and external pressure coefficient $(GC_{pf})_{eq}$ using the following equation (Pierre, et al. 2005).

$$(GC_P)_{eq} = \frac{\frac{1}{2}\rho V^2{}_{h,z_0,meanhrly} C_p}{\frac{1}{2}\rho V^2{}_{10m,o.c.,3secgust} K_{zt} K_h K_d I} \qquad \text{(Equation 1)}$$

Equation 1 accounts for differences in averaging time and wind speed measurement height and removes any impacts from factors that are applied in calculations for ASCE 7, where ρ is air density, $V_{h,z_0,meanhrly}$

is the mean hourly wind speed measured at roof height, $V_{10m,o.c.,3secgust}$ is the 3-second gust wind speed at 10 meters in open country, and each of the factors in the denominator are those corresponding with ASCE7-10 (Pierre, et al. 2005). A directionality factor (K_d) of 1.0 was used in this equation rather than 0.85, which is specified, since this study was performed across multiple wind angles and the results were not adjusted to consider peak load with directionality.

ASCE 7 provides a series of equations for the calculation of wind loads on a structure. The equations are based on a target wind speed and adjustment factors that account for conditions that impact the wind pressure on a structure. The primary equation used to calculate the pressures on the roof under wind tunnel test loads was equation 26.10-1 from ASCE 7-16 for the calculation of velocity pressure at a certain height (q_z) (ASCE, 2016):

$$q_z = 0.00256 K_z K_{zt} K_d K_e V^2 \quad \text{(Equation 2)}$$

Where K_z is a velocity pressure exposure coefficient based on the height along the structure and the exposure category, B, C, or D. K_{zt} is a topographic factor that accounts for increases in wind speed on hills, ridges, and escarpments. K_d is a directionality factor that accounts for the fact that it is unlikely that the maximum pressure coefficient will occur simultaneously with high wind coming from the direction producing the highest wind speeds (ASCE, 2016). K_e is an elevation factor which accounts for changes in air density with elevation. These factors reduce the calculated wind pressure but can be substituted with 1.0 conservatively.

This equation uses wind speed (V) obtained from the wind speed hazard maps provided in ASCE 7 (ASCE, 2016). In ASCE 7-16, separate maps are used for each risk category based on the target return period. These maps are based on both non-hurricane data and hurricane model simulations. The goal of moving to separate maps for each risk category is to maintain a consistent target reliability.

In order to obtain the design wind pressure from the previously calculated velocity pressure, Equation 3 incorporates a gust-effect factor (G) and pressure coefficient (C_p) and takes into account internal pressure (ASCE, 2016). This equation is used for both the Main Wind Force Resisting System (MWFRS) and components and cladding; however, for components and cladding the terms are used as a combined factor that cannot be separated. It is provided as equation 27.3-1 for the MWFRS and in an alternate form as equation 30.3-1 for components and cladding.

$$p = q_h\left[\left(GC_p\right) - \left(GC_{pi}\right)\right] \quad \text{(Equation 3)}$$

This equation uses the previously determined velocity pressure (q) along with a combined GC_p value (ASCE, 2016). The internal pressure coefficients are equivalent to those calculated for the MWFRS in chapter 26. All components and cladding members must be designed for the maximum positive and negative pressures. Pressure coefficients for components and cladding are provided in charts where roof and wall surfaces are divided into zones based on areas of the surface that experience higher and lower pressures during the wind tunnel tests considered for the development of the standard. The wind pressure zones are a function of building height, with an envelope of the peak pressures being used to determine the pressure coefficient values (Kopp & Morrison, 2018).

The zones are numbered and curves are provided for each of these zones (ASCE, 2016). These curves are a plot of the external pressure coefficient on the vertical axis and effective wind area on the horizontal axis. The effective wind area is defined as either the tributary area or the span length of the component by one third of the span length.

The design of purlins uses the provision of ASCE 7-Chapter 30 for components and cladding (MBMA, 2018). When selecting the GC_p it is recommended that a step function along the length of the structural member be used; however, alternative methods are allowed, such as using a weighted average. In high wind, the cladding of the structure contributes to restraint against lateral torsional buckling for purlins by bracing the member (Perry, 1990). The combination of sheeting and purlins also contributes to lateral resistance through diaphragm action. Since metal buildings are designed with maximum efficiency, each member is critical to the buliding stability, and the failure of any member could result in a system-wide failure.

Objectives

The project used measured pressure coefficients from the NIST wind tunnel database to determine the loads on a roof purlin in a typical low-rise steel building under more realistic wind scenarios. The behavior of a continuous beam under the proposed loading was expected to be different from the zones that are currently considered in ASCE 7, based on the differences in loading patterns between ASCE 7-16 and the application of wind tunnel test loads. While time-varying data was used, the loads were applied to the structure statically for each time step, allowing an envelope of loads for each of the purlins to be constructed using the direct stiffness method and modelling the purlins as continuous beams. In conducting this analysis, a more refined analysis of the behavior of a purlin under wind loads was able to be modeled more accurately.

The goal of this study was to use the proposed method, to asses the possibility of a reduction in the wind loads on purlins in low rise buildings and to determine how accurate the ASCE 7-16 method is in

determining the loads on the components. A reduction in the loads on the purlins was expected as this removes some of the built-in conservatism present in the ASCE 7 component and cladding pressures. Currently, ASCE 7 uses an envelope of peak pressures in a zone across all angles and building sizes to determine the loads for components and cladding. Using a combination of the wind tunnel test database and continuous beam analysis, specific time steps that were expected to generate higher loads were isolated for the building under consideration.

Materials and Methods

Building Plans and Models

The data contained in the NIST database is accessible through Hierarchical Data Format (HDF) files that can be downloaded (Ho, 2003). For this study, the data used was primarily time histories of pressure coefficient (C_p) values. A variety of building plans, heights, and roof slopes were tested during these wind tunnel studies for use in the database. For the purposes of this project, a 125 foot by 80-foot building with a 1:12 roof slope was selected to represent a typical low rise steel building, shown in Figure 12.

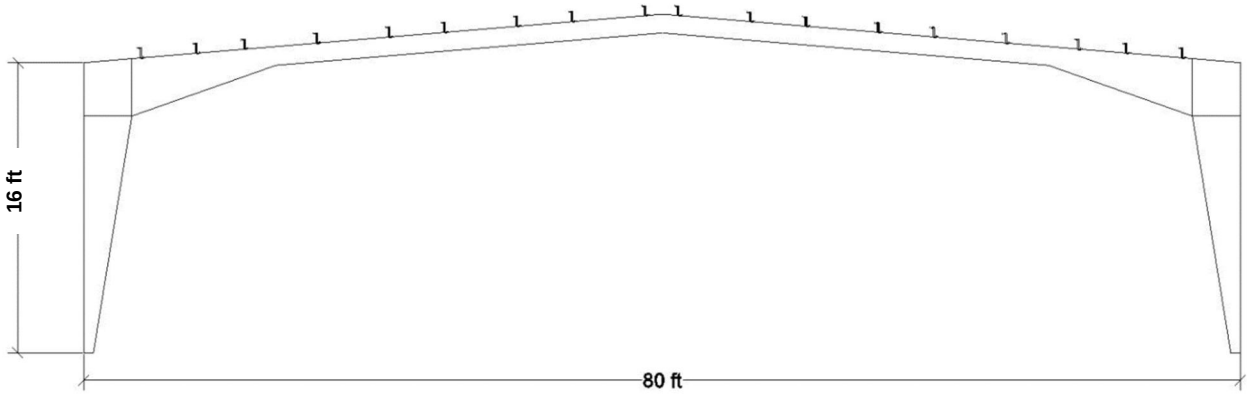

Figure 12: Profile view of selected building plan and roof slope

This building was used in open and suburban terrain in order to look at the effects of turbulence of the variation in pressure coefficient. Building heights of 16 and 40 feet were used. These heights were chosen out of the heights tested in the wind tunnel studies to consider roof zone layouts containing and not containing the 1’ roof zone in ASCE 7-16 Chapter 30, which are based on wall length to height ratio (ASCE, 2016). Diagrams of the roof zones for the 16 foot height and 40 foot heigh are shown in Figure 13.

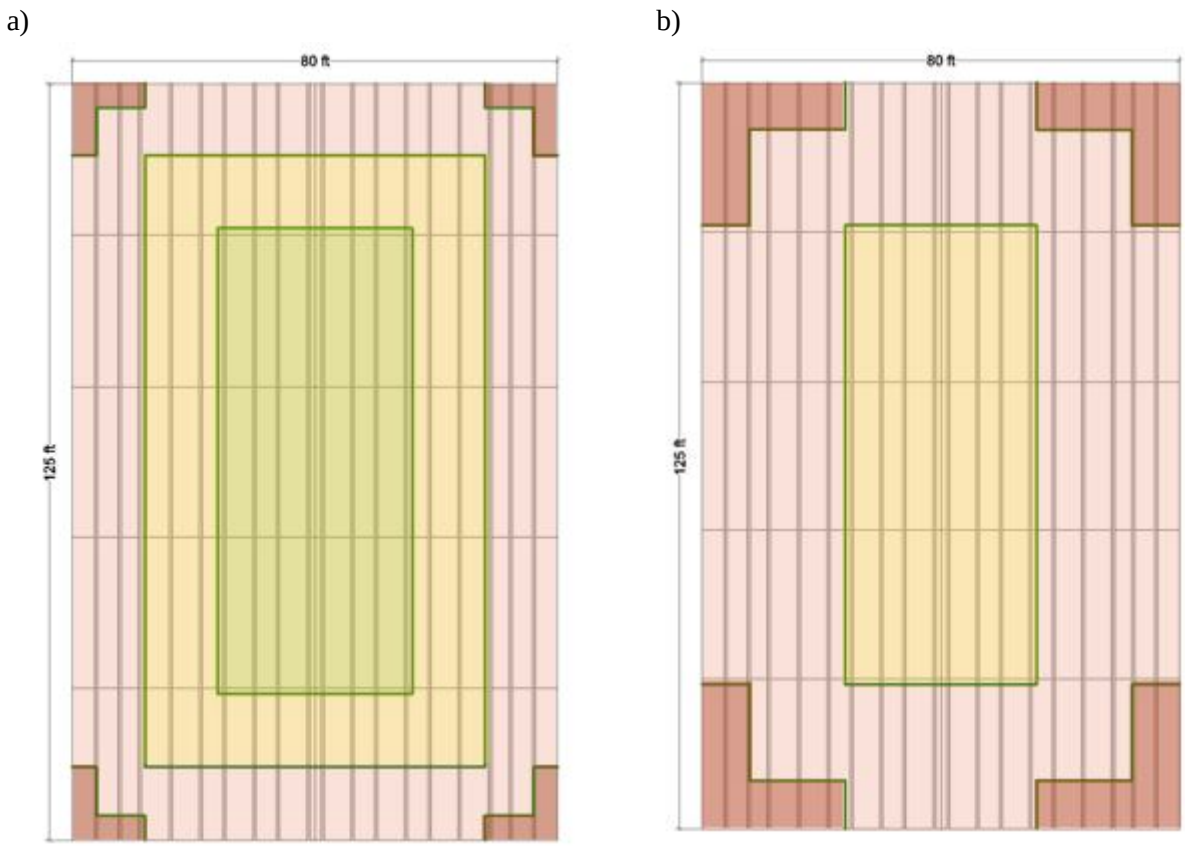

Figure 13: ASCE 7-16 roof zones for buildings with a height of 16' (a) and 40’ (b)

The tests were conducted in the UWO boundary layer wind tunnel. Each test setup contained approximately 600 taps, but only the 350 taps located on the roof were considered for this analysis. The actual number of active pressure taps varied based on the test setup, and so it was necessary to filter out the inactive taps containing artificial values. The files used to read the HDF data in Matlab were obtained from the Insurance Institute for Business and Home Safety (IBHS). To obtain a pressure coefficient value for a specific location on the building, an area of interest was set, based on coordinates along the roof, and the extents of the area being considered. The program then finds the taps whose tributary area overlaps with this area of interest. The percent of overlap from each of the contributing taps was used to weight the pressure coefficient value from each tap to obtain an area-averaged pressure coefficient for the set area of interest. The area of interest used in this study was the tributary width of the purlin in the transverse direction by the longitudinal dimension of one tap’s tributary area.

This was repeated for all the taps along the entire length of the purlin, and again for each purlin, in each test angle. Using this area of interest separated the purlin into segments that experienced different loads based on the measurements recorded in the tests. Using this method, data files were generated containing

pressure coefficient values with columns for each change in pressure tap and with rows corresponding to time histories for the duration of the test. The C_p values generated were then converted into an equivalent force using Equations 2 and 3.

For Equation 2, the exposure coefficient (K_z) used in was calculated based on the roof height and exposure of the given test setup, read from the HDF file (in this case: Exposure B at a height of 16ft). The topographic factor (K_{zt}), directionality factor (K_d), and elevation factor (K_e) were each taken as 1.0. The internal pressures were not considered in these models, as the project compared the pressures on the purlins between what is required in ASCE 7-16 and what can be calculated using wind tunnel pressures, and the internal pressure values would be equivalent for each and would not contribute to any differences observed. A reference wind speed (V) of 100 mph was used for these tests.

The pressure coefficient values from the wind tunnel HDF files were converted into an equivalent GC_P at each point using Equation 1. The factors contributing to Equation 1 were provided in the initial program obtained from IBHS and were multiplied by C_p to obtain the equivalent GC_p used in equation 27.3-1 when calculating the force on the purlin. Using the pressure that was obtained, the load on each purlin was calculated by multiplying by the tributary width of the purlin, resulting in a series of line loads for each purlin in force per length. In this project, the spacing of the purlins along the roof varied, from 3 feet-4 inches at the smallest to 5 feet at the largest, to simulate a typical design for a structure of this size. Purlin spacings are typically varied across the roof to account for higher loads at the edges. Once the force was obtained, the distributed force data was plotted along the length of the purlin and used to calculate the resulting shear and moment. Each of these steps is repeated across a 90-degree series of wind angles from 270 to 360 degrees at five-degree increments (Figure 14) to capture the behavior of the structure under all angles, since each building was symmetric.

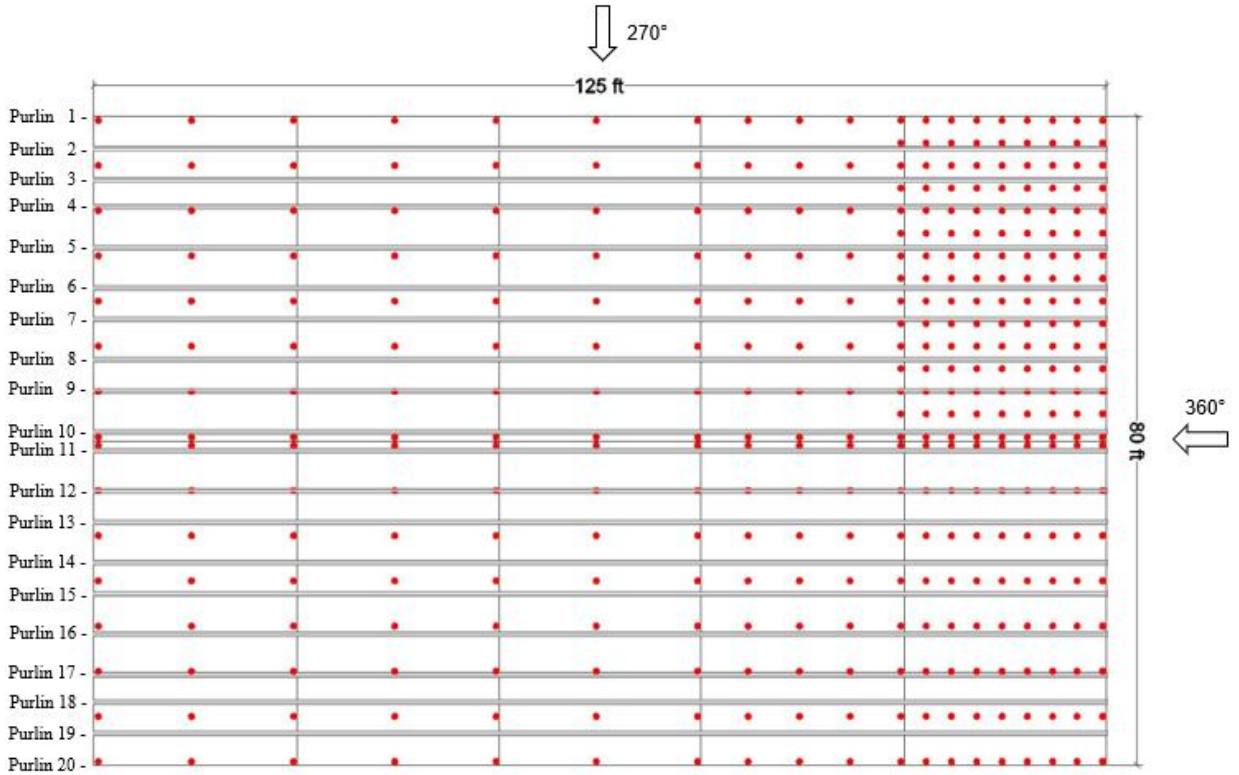

Figure 14: Tap layout with purlin locations

Analysis methods

For this study, the purlins were analyzed as continuous beams through the whole length of the structure. In design, bolted laps are used at the ends of the purlins to form as the connection for continuous design (AISI, 2009). A common analysis assumption used in design is to ignore the additional moment of inertia at the lap. With this method, full continuity is not achieved, but will be used for the analysis of these sections as a baseline comparison with ASCE 7-16. The supports for this structure were taken to be rigid, rather than accounting for any flexibility in the girders with applied load. While girders are large stiff members, some deflection under wind loads would be expected. The main basis for this assumption was to keep a consistent baseline, as the main goal was to look at the effects of using the wind tunnel test loads compared to the ASCE 7 loads.

To analyze the purlins as continuous beams, previously developed functions were obtained that use the direct stiffness method with a transformational approach (Jayamon, 2012). The function and input file were adjusted to meet the needs of this project. The material properties of the sections being used were set in a series of matrices. A modulus of elasticity of 29000 kips per square inch (ksi) and Poisson's ratio of 0.27 were used. A restraint matrix was developed to set the locations of the supports. In the typical design of

purlins, the Z-Sections in the end bays of the structure would be designed with larger moments of inertia. In this study, a consistent Z-Section size, corresponding with a typical design for a building of this size in the end bay, was used. A Z-Section of 8X2.5Z14 was used as the purlin section, and the cross-sectional dimensions are given in Figure 15.

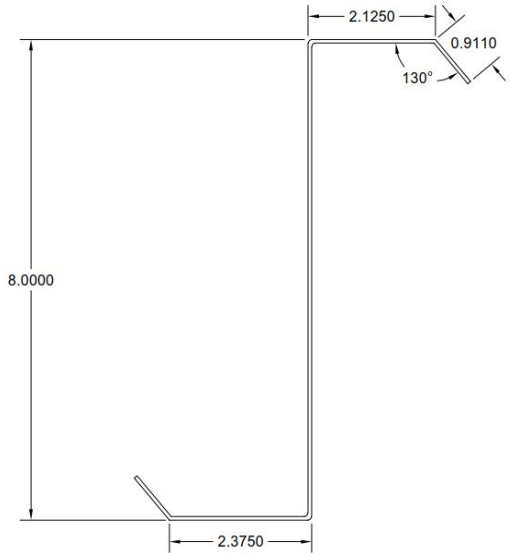

Figure 15: 8X2.5Z14 section with dimensions

A matrix was built containing the location of node and element and the load case that was applied to it. The nodes were defined at each location where a change of load was recorded (corresponding to tap tributary area) and each support. The text files containing force values were then read and input into a member load matrix. The beam analysis function was called to calculate the reactions at each support and the element forces (shear and moment) and deflections at each node using the method discussed above. The values that were output were stored in text files with rows corresponding to each time step and columns corresponding to different nodes. The accuracy of the generated reactions, element forces, and deflections were verified by checking four cases by hand in MASTAN (R.D. Ziemian). The cases considered were uniform positive load, uniform negative load, a negative actual load case, and an actual load case with positive and negative pressures. The percent error values between the beam functions used and the MASTAN analysis had a range of 0.0005% and 1.988%, indicating good agreement.

Once the shear and moment values at the nodes were determined, intermediate shear and moment values were calculated by breaking each purlin element into 100 segments and calculating the internal forces at each increment. The overall maximum and minimum shear and moment values across the entire purlin were

calculated for each time step. Using the one-foot increment combined with the values obtained previously at the nodes captures the calculated “true maximum” obtained with the smaller segment increment and allows a shear and moment envelope to be built at a one-foot step across the length.

The shear and moment values obtained were compared with the values determined from the loads prescribed in ASCE 7 Chapter 30. This was done by finding the longitudinal location corresponding to changes in the roof zone, corresponding to the locations of the nodes, and the associated pressure coefficients for calculation of the member loads. Once these values were obtained for each purlin, they were read into the input file and the beam analysis function was called to calculate the reactions, element forces, and deflections caused by the loads from ASCE 7. This also generated a maximum and minimum value of shear and moment across the whole purlin for each purlin, and captured shear and moment values at one-foot increments. These values were used to compare with those generated using wind tunnel pressure coefficients. A comparison of these loading diagrams is shown in Figure 16, for a case of a wind approach angle of 360° for the wind tunnel test loads (a) and the ASCE 7-16 loads (b).

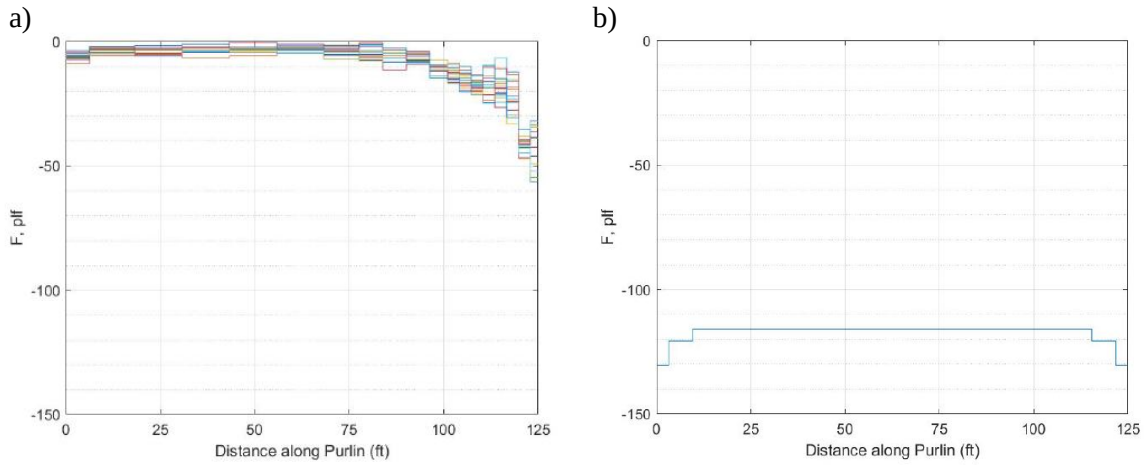

Figure 16: Loading diagrams for wind tunnel test loads (a) and ASCE 7-16 loads (b)

Only the first 10 purlins on the structure (those from the eave to the ridge line) were evaluated using the ASCE 7-16 method, as the building and purlin spacing are symmetric. A directionality factor of 0.85 was used in accordance with the ASCE 7-16 recommendation for building design, since in this case, these values represent all wind angles.

Results

The primary data obtained from the continuous beam models were the shear and moment along the length of each purlin. First, the maximum shear and moment values across the entire purlin for all time steps and wind angles were found and compared to the maximum shear and moment observed in the beam subjected to wind pressures according to the ASCE 7-16 Chapter 30 provisions.

Configuration 1

The first configuration was the building with a mean roof height of 16 feet in open terrain exposure conditions. The maximum magnitude of shear and moment values were determined, and the percent difference between the maximum magnitude value calculated from ASCE 7 and from the wind tunnel test loads were also found. Negative values of percent difference corresponded with a wind tunnel test load higher than what is specified in ASCE 7-16. The maximum shear and moment values generated for each purlin across all angles and times steps for the wind tunnel tests and both the required positive and negative pressures specified by ASCE 7-16 are shown in Table 1 and Table 2.

Table 1: Maximum shear in each purlin for all time steps and wind angles compared with ASCE 7-16 provisions (125'x80'x16' building, open terrain)

		Max Shear (kip)									
	Purlin #	1	2	3	4	5	6	7	8	9	10
ASCE -	Max	0.8362	1.6524	1.5299	1.3763	1.6271	1.2782	1.2513	1.2513	1.2513	1.0686
	Min	-0.8933	-1.7667	-1.6363	-1.4670	-1.7339	-1.3435	-1.3117	-1.3117	-1.3117	-1.1201
ASCE +	Max	0.0920	0.1841	0.1714	0.1985	0.2382	0.2104	0.2104	0.2104	0.2104	0.1796
	Min	-0.0860	-0.1721	-0.1602	-0.1855	-0.2226	-0.1967	-0.1967	-0.1967	-0.1967	-0.1679
Wind Tunnel	Max	0.9086	1.8895	1.5132	1.3935	1.3962	1.1879	1.2772	1.3939	1.3558	1.1226
	Min	-0.9565	-1.8374	-1.6001	-1.6076	-1.5392	-1.3722	-1.3215	-1.2333	-1.1539	-1.0136
% Diff		-6.83	-6.72	2.24	-9.15	11.90	-2.11	-0.75	-6.08	-3.30	-0.22

		Max Shear (kip)									
	Purlin #	11	12	13	14	15	16	17	18	19	20
ASCE -	Max	1.0686	1.2513	1.2513	1.2513	1.2782	1.6271	1.3763	1.5299	1.6524	0.8362
	Min	-1.1201	-1.3117	-1.3117	-1.3117	-1.3435	-1.7339	-1.4670	-1.6363	-1.7667	-0.8933
ASCE +	Max	0.1796	0.2104	0.2104	0.2104	0.2104	0.2382	0.1985	0.1714	0.1841	0.0920
	Min	-0.1679	-0.1967	-0.1967	-0.1967	-0.1967	-0.2226	-0.1855	-0.1602	-0.1721	-0.0860
Wind Tunnel	Max	1.0781	1.2682	1.2194	1.2249	1.2023	1.6664	1.1989	0.9336	1.0420	0.6068
	Min	-1.0043	-1.2394	-1.1355	-1.1678	-1.2908	-1.3752	-1.3299	-1.1756	-1.1941	-0.6441
% Diff		3.82	3.37	7.29	6.84	4.00	3.97	9.80	32.76	38.68	32.41

Table 2: Maximum moment in each purlin for all time steps and wind angles compared with ASCE 7-16 provisions (125'x80'x16' building, open terrain)

		Max Moment (kip-in)									
	Purlin #	1	2	3	4	5	6	7	8	9	10
ASCE -	Max	46.70	92.23	85.37	77.00	91.05	69.27	67.39	67.39	67.39	57.55
	Min	-35.89	-69.35	-63.48	-63.35	-75.43	-68.50	-68.82	-68.82	-68.82	-58.77
ASCE +	Max	3.55	7.11	6.62	7.67	9.20	8.13	8.13	8.13	8.13	6.94
	Min	-4.80	-9.60	-8.94	-10.35	-12.42	-10.97	-10.97	-10.97	-10.97	-9.37
Wind Tunnel	Max	51.05	96.98	81.13	79.80	73.62	56.79	58.49	61.14	61.24	52.44
	Min	-47.41	-81.49	-63.73	-66.50	-87.71	-83.88	-81.18	-78.85	-76.80	-63.37
% Diff		-8.92	-5.02	5.09	-3.57	3.74	-19.07	-16.48	-13.58	-10.96	-7.54

		Max Moment (kip-in)									
	Purlin #	11	12	13	14	15	16	17	18	19	20
ASCE -	Max	57.55	67.39	67.39	67.39	69.27	91.05	77.00	85.37	92.23	46.70
	Min	-58.77	-68.82	-68.82	-68.82	-68.50	-75.43	-63.35	-63.48	-69.35	-35.89
ASCE +	Max	6.94	8.13	8.13	8.13	8.13	9.20	7.67	6.62	7.11	3.55
	Min	-9.37	-10.97	-10.97	-10.97	-10.97	-12.42	-10.35	-8.94	-9.60	-4.80
Wind Tunnel	Max	49.65	58.76	54.61	55.91	56.01	69.67	56.89	49.66	53.11	30.65
	Min	-60.97	-71.62	-72.63	-71.23	-70.41	-94.49	-88.71	-65.68	-61.80	-34.99
% Diff		-3.67	-3.98	-5.39	-3.44	-1.63	-3.70	-14.12	26.07	39.51	28.67

Purlins 1 through 10 are on the windward side of the ridgeline, while purlins 11 through 20 are on the leeward side of the ridgeline, as shown in Figure 14. While the calculated overall maximums obtained from the wind test data for each purlin typically exceeded the values calculated using the current ASCE 7 wind load provisions, the behavior of the purlins between the two cases were similar. For this configuration, the maximum magnitude shear and moment values were larger than ASCE 7 for all purlins on the windward side except purlins 3 and 5. Purlins 11 through 20 are on the leeward side of the structure, and although they have some locations with values significantly less than ASCE 7-16 (26%-40%). These purlins would need to be subjected to the same wind tunnel loads as purlins 1-10 to account for the maximum case for wind blowing around all 360° of the structure. To show differences in the behavior of the purlins between the three types of loading considered, the time step and angle corresponding to the maximum value of shear for the first purlin after the eave (purlin 2), was determined and the full shear diagram was plotted. This occurred at a wind angle of 285° and is shown in Figure 17.

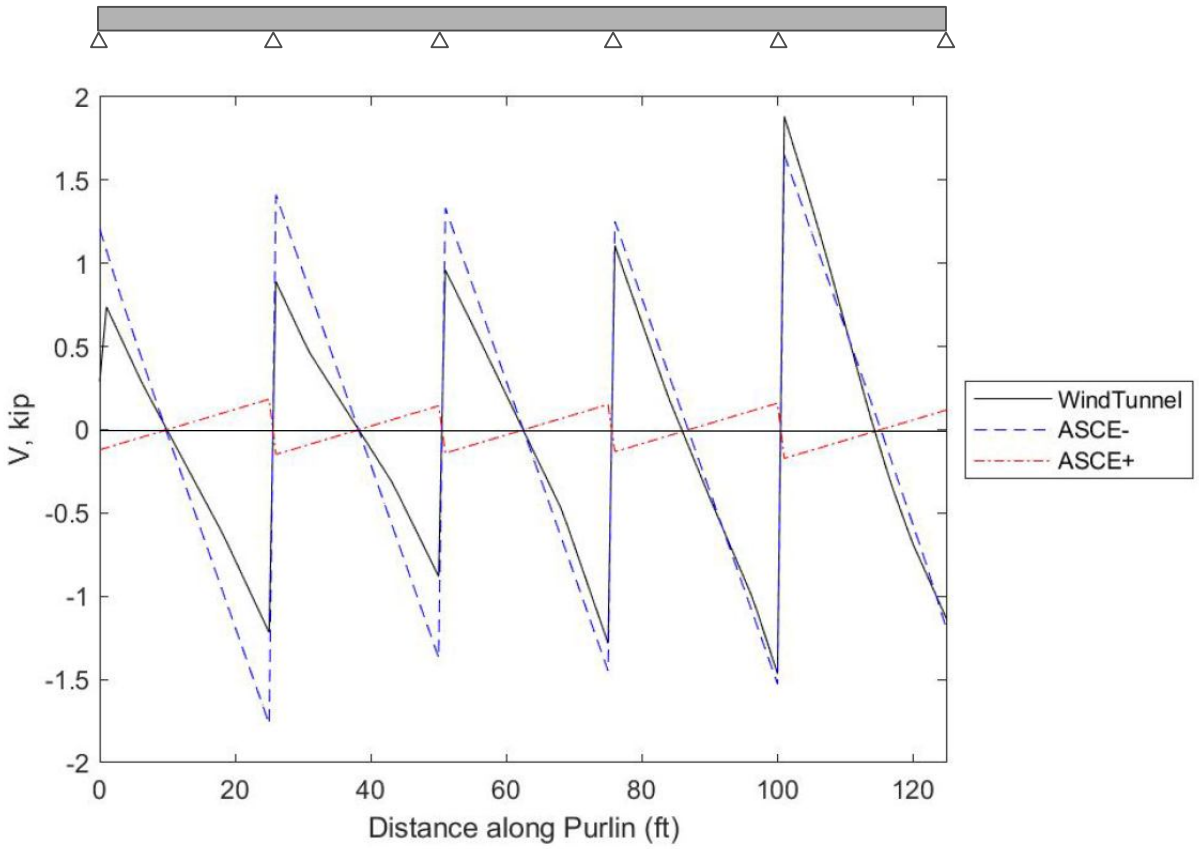

Figure 17: Shear diagram for case causing maximum shear at 285° (125'x80'x16' building, open terrain)

Similar behavior was observed in the moment diagrams for the maximum case. The time step and wind angle corresponding to the maximum value of moment on purlin 2 were determined, and the corresponding moment diagram was drawn. This occurred at a wind angle of 275° and is shown in Figure 18.

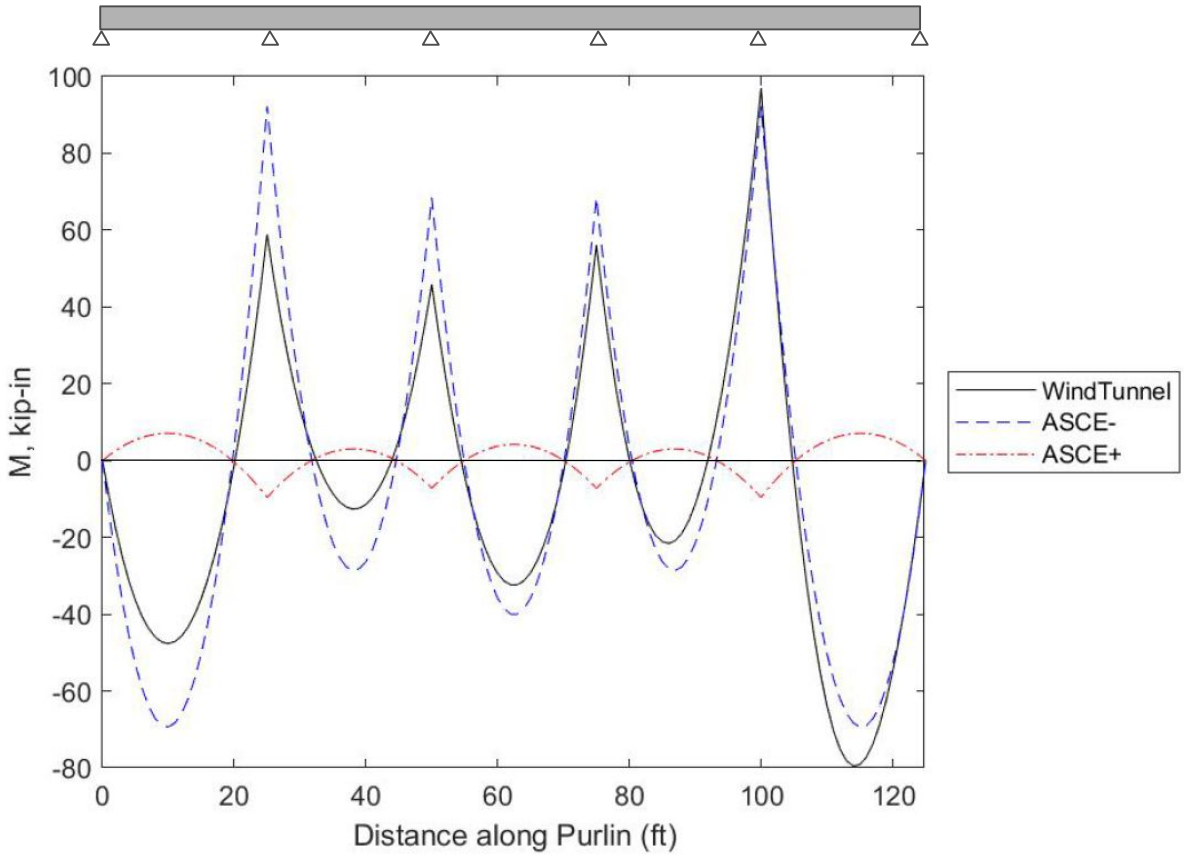

Figure 18: Moment diagram for case causing maximum moment at 275° (125'x80'x16' building, open terrain)

Figure 17 and Figure 18 show similar behavior for the purlin under the negative ASCE 7-16 and wind tunnel test loads, with the shear values fitting those obtained using component and cladding provisions better than the moment values. In each of the cases corresponding to Figure 17 and Figure 18, the values obtained using wind tunnel tests follow a similar behavior and the ASCE 7 value is exceeded in the last bay of the structure, corresponding to the windward corner.

Configuration 2

The second configuration` used was the building with a mean roof height of 16 feet in suburban terrain exposure conditions. This corresponds with Exposure Category B as specified by ASCE 7-16. In this case, the maximum values of shear developed in the purlin were higher than those determined using ASCE 7 on all of the purlins on the windward edge with the exception of purlin 3, with a percent difference range of -12% to -2%. However, in the interior of the building, they tended to be lower than what was specified in ASCE 7, with a percent difference range of 6.66% to 17.58%. The maximum values of moment had more variation across the windward side in whether they exceeded the values obtained using ASCE 7 when

compared to shear and had lower values of percent difference than those obtained for shear. The maximum values of moment developed in the purlin were higher than those determined using ASCE 7 for purlins 1 and 4 on the windward edge, with a percent differences of -10.7% and -0.54%, respectively. While all of the internal purlins had shear values lower than those calculated with ASCE 7-16, the moment values were higher for all purlins except 5 and 8. Purlin 5 had a percent difference for moment of 11.56%, and purlin 8 had a percent difference for moment of 1.32%. The values obtained for shear and moment and the percent difference between the two methods are shown in Table 3 and Table 4.

Table 3: Maximum shear in each purlin across all time steps and wind angles compared with ASCE 7 provisions (125'x80'x16' building, suburban terrain)

		Max Shear (kip)									
	Purlin #	1	2	3	4	5	6	7	8	9	10
ASCE -	Max	0.5689	1.1242	1.0408	0.9363	1.1070	0.8696	0.8513	0.8513	0.8513	0.7270
	Min	-0.6077	-1.2019	-1.1132	-0.9980	-1.1796	-0.9140	-0.8924	-0.8924	-0.8924	-0.7621
ASCE +	Max	0.0626	0.1252	0.1166	0.1350	0.1620	0.1431	0.1431	0.1431	0.1431	0.1222
	Min	-0.0585	-0.1171	-0.1090	-0.1262	-0.1515	-0.1338	-0.1338	-0.1338	-0.1338	-0.1143
Wind Tunnel	Max	0.6468	1.2437	1.0436	1.0191	0.8238	0.7379	0.7671	0.7628	0.7389	0.7129
	Min	-0.6907	-1.1860	-1.0515	-1.0182	-0.9890	-0.7620	-0.7547	-0.7845	-0.8163	-0.6830
% Diff		-12.78	-3.42	5.70	-2.08	17.58	18.14	15.11	12.86	8.91	6.66
		Max Shear (kip)									
	Purlin #	11	12	13	14	15	16	17	18	19	20
ASCE -	Max	0.7270	0.8513	0.8513	0.8513	0.8696	1.1070	0.9363	1.0408	1.1242	0.5689
	Min	-0.7621	-0.8924	-0.8924	-0.8924	-0.9140	-1.1796	-0.9980	-1.1132	-1.2019	-0.6077
ASCE +	Max	0.1222	0.1431	0.1431	0.1431	0.1431	0.1620	0.1350	0.1166	0.1252	0.0626
	Min	-0.1143	-0.1338	-0.1338	-0.1338	-0.1338	-0.1515	-0.1262	-0.1090	-0.1171	-0.0585
Wind Tunnel	Max	0.6676	0.8093	0.7697	0.7429	0.7515	0.8244	0.7352	0.5726	0.6084	0.3704
	Min	-0.7901	-0.7783	-0.7160	-0.6798	-0.6997	-0.8460	-0.7250	-0.5789	-0.6682	-0.4826
% Diff		-3.62	9.77	14.76	18.29	19.51	32.94	30.33	63.15	57.07	22.95

Table 4: Maximum moment in each purlin for all time steps and wind angles compared with ASCE 7-16 provisions (125'x80'x16' building, suburban terrain)

		Max Moment (kip-in)									
	Purlin #	1	2	3	4	5	6	7	8	9	10
ASCE -	Max	31.77	62.75	58.08	52.39	61.95	47.13	45.85	45.84	45.85	39.15
	Min	-24.41	-47.18	-43.19	-43.10	-51.32	-46.61	-46.82	-46.82	-46.82	-39.98
ASCE +	Max	2.42	4.84	4.50	5.21	6.26	5.53	5.53	5.53	5.53	4.72
	Min	-3.27	-6.53	-6.08	-7.04	-8.45	-7.46	-7.46	-7.46	-7.46	-6.37
Wind Tunnel	Max	35.35	62.33	53.36	52.67	47.80	35.80	33.31	34.71	34.00	32.90
	Min	-33.56	-62.55	-48.28	-43.50	-55.18	-47.36	-47.53	-46.20	-48.73	-42.91
% Diff		-10.66	0.31	8.46	-0.54	11.56	-0.48	-1.50	1.32	-4.00	-7.07
		Max Moment (kip-in)									
	Purlin #	11	12	13	14	15	16	17	18	19	20
ASCE -	Max	39.15	45.85	45.84	45.85	47.13	61.95	52.39	58.08	62.75	31.77
	Min	-39.98	-46.82	-46.82	-46.82	-46.61	-51.32	-43.10	-43.19	-47.18	-24.41
ASCE +	Max	4.72	5.53	5.53	5.53	5.53	6.26	5.21	4.50	4.84	2.42
	Min	-6.37	-7.46	-7.46	-7.46	-7.46	-8.45	-7.04	-6.08	-6.53	-3.27
Wind Tunnel	Max	33.40	36.85	38.07	36.14	34.54	40.11	39.40	26.74	29.28	19.36
	Min	-42.02	-44.62	-45.85	-43.54	-41.81	-49.73	-43.81	-35.14	-36.29	-22.46
% Diff		-4.98	4.81	2.09	7.25	11.97	21.87	17.83	49.22	53.44	34.34

The shear and moment diagrams for the loading case causing the maximum moment of the first purlin from the eave (purlin 2) were plotted. The maximum shear and moment occurred at a wind approach angle of 270 degrees, which corresponds to wind perpendicular to the ridge. The shear and moment diagram comparing the wind tunnel tests and loads obtained using ASCE 7-16 at the time step the maximum load on purlin 2 at this wind angle are shown in Figure 19 and Figure 20.

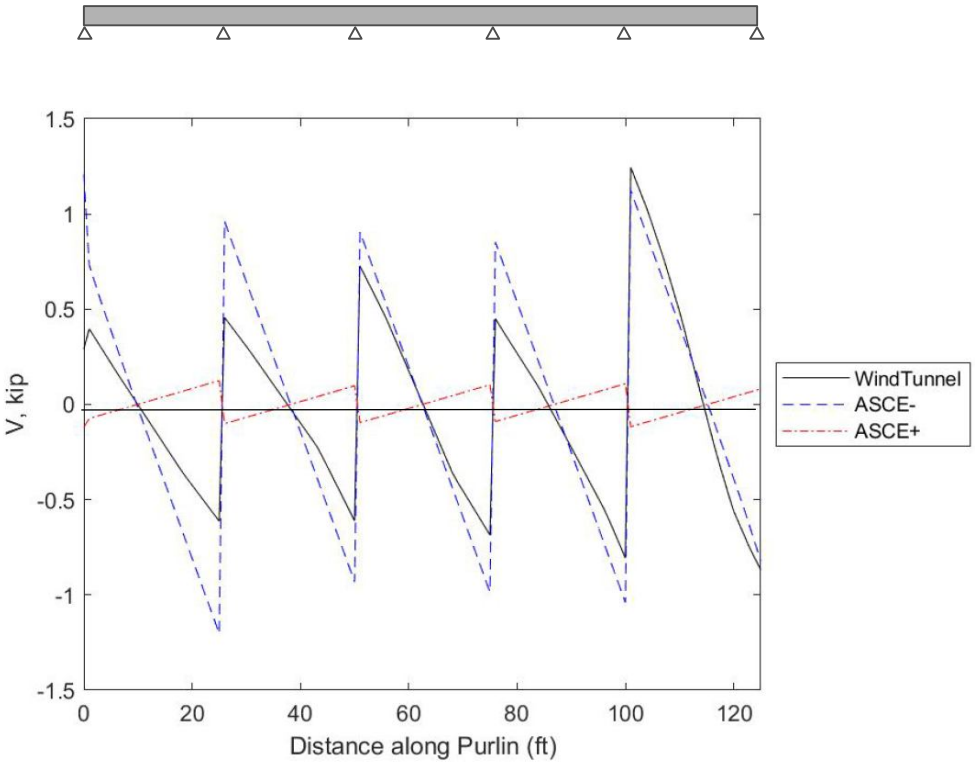

Figure 19: Shear diagram for case causing maximum shear at 270° (125'x80'x16' building, suburban terrain)

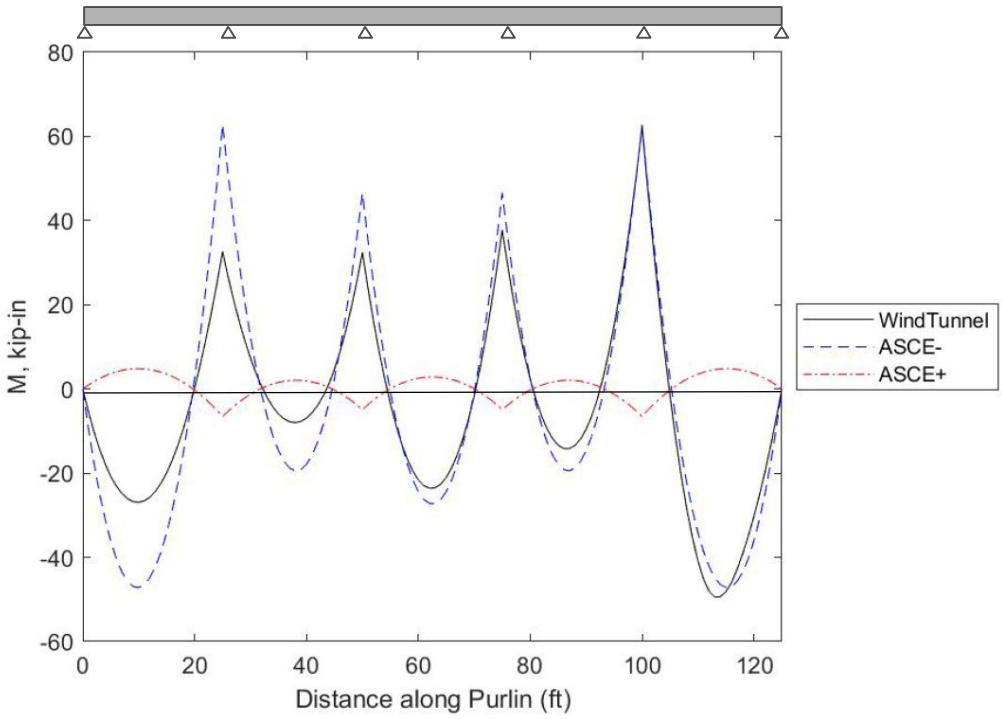

Figure 20: Moment diagram for case causing maximum moment at 270° (125'x80'x16' building, suburban terrain)

Configuration 3

The next configuration considered was the tests conducted with a mean roof height of 40 feet in open terrain exposure conditions. This corresponds with Exposure Category C as specified by ASCE 7-16. The maximum shear and moment values for each purlin were obtained, similar to the previous two cases. In this case, the maximum values of shear and moment developed in the purlin were consistently higher than those determined using ASCE 7 on the windward edge, with percent differences ranging from -38.44% to -13.46% for shear and -49.7% to -10.9% for moment. In the interior of the building, the shear values were consistently lower than what was specified in ASCE 7, with percent differences ranging from 6.45% to 21.22%. All of the internal purlins on the windward face had moment values higher than those determined using the loads in ASCE 7-16, with the exception of purlins 5 and 6. Purlin 6 had both shear and moment lower than ASCE 7-16, while purlin 5 had a higher shear value than ASCE 7-16 with a lower moment. The values obtained for shear and moment and the percent difference between them are shown in Table 6 and Table 5.

Table 6: Maximum shear in each purlin across all time steps and wind angles compared with ASCE 7 provisions (125'x80'x40' building, open terrain)

		Max Shear (kip)									
	Purlin #	1	2	3	4	5	6	7	8	9	10
ASCE -	Max	1.1090	2.2180	1.9920	2.1715	2.6059	2.3019	2.2435	2.2259	2.2260	1.9009
	Min	-1.1793	-2.3586	-2.1229	-2.3230	-2.7877	-2.4625	-2.3699	-2.3419	-2.3420	-1.9999
ASCE +	Max	0.1116	0.2232	0.2079	0.2407	0.2888	0.2551	0.2551	0.2551	0.2551	0.2179
	Min	-0.1043	-0.2087	-0.1943	-0.2250	-0.2700	-0.2385	-0.2385	-0.2385	-0.2385	-0.2037
Wind Tunnel	Max	1.7405	2.9640	2.3283	2.3793	2.8354	2.1705	2.1379	1.9551	1.8926	1.7835
	Min	-1.6758	-2.7279	-2.5041	-2.6583	-2.8415	-2.3086	-1.9330	-1.9641	-1.7845	-1.4671
% Diff		-38.44	-22.75	-16.48	-13.46	-1.91	6.45	10.29	17.55	21.22	11.44

		Max Shear (kip)									
	Purlin #	11	12	13	14	15	16	17	18	19	20
ASCE -	Max	1.9009	2.2260	2.2259	2.2435	2.3019	2.6059	2.1715	1.9920	2.2180	1.1090
	Min	-1.9999	-2.3420	-2.3419	-2.3699	-2.4625	-2.7877	-2.3230	-2.1229	-2.3586	-1.1793
ASCE +	Max	0.2179	0.2551	0.2551	0.2551	0.2551	0.2888	0.2407	0.2079	0.2232	0.1116
	Min	-0.2037	-0.2385	-0.2385	-0.2385	-0.2385	-0.2700	-0.2250	-0.1943	-0.2087	-0.1043
Wind Tunnel	Max	1.6990	1.8415	1.7430	1.6847	1.7724	2.1562	1.8556	1.5852	1.6261	0.9552
	Min	-1.6169	-1.6453	-1.5298	-1.5346	-1.5186	-1.7515	-1.6115	-1.5557	-1.6943	-0.9533
% Diff		16.27	23.93	29.33	33.80	32.59	25.55	22.37	29.00	32.78	20.99

Table 5: Maximum Moment in each purlin across all time steps and wind angles compared with ASCE 7 provisions (125'x80'x40' building, open terrain)

	Purlin #	1	2	3	4	5	6	7	8	9	10
ASCE -	Max	59.77	119.54	108.81	121.38	145.66	128.67	116.92	113.39	113.39	96.83
	Min	-47.26	-94.52	-84.78	-92.21	-110.65	-97.74	-98.78	-99.09	-99.09	-84.62
ASCE +	Max	4.31	8.62	8.03	9.30	11.16	9.85	9.85	9.85	9.85	8.42
	Min	-5.82	-11.64	-10.84	-12.55	-15.06	-13.31	-13.31	-13.30	-13.31	-11.36
Wind Tunnel	Max	91.52	154.93	121.34	143.56	141.59	108.63	100.77	98.55	96.98	79.76
	Min	-99.30	-139.74	-104.48	-113.59	-134.17	-115.56	-119.35	-118.88	-121.18	-97.62
% Diff		-49.70	-25.79	-10.89	-16.74	2.84	10.73	-2.05	-4.73	-6.64	-0.82

		Max Moment (kip-in)									
	Purlin #	11	12	13	14	15	16	17	18	19	20
ASCE -	Max	96.83	113.39	113.39	116.92	128.67	145.66	121.38	108.81	119.54	59.77
	Min	-84.62	-99.09	-99.09	-98.78	-97.74	-110.65	-92.21	-84.78	-94.52	-47.26
ASCE +	Max	8.42	9.85	9.85	9.85	9.85	11.16	9.30	8.03	8.62	4.31
	Min	-11.36	-13.31	-13.30	-13.31	-13.31	-15.06	-12.55	-10.84	-11.64	-5.82
Wind Tunnel	Max	78.51	88.60	89.75	88.69	88.25	109.70	86.10	69.16	75.25	47.44
	Min	-95.07	-98.96	-93.89	-88.41	-89.12	-106.61	-100.21	-84.82	-90.69	-50.43
% Diff		1.83	13.59	18.81	27.46	36.32	28.16	19.11	24.78	27.44	16.96

The shear and moment diagrams for the loading case causing the maximum moment of the first purlin from the eave (purlin 2) were plotted. The maximum loading case occurred at a wind angle of 325 degrees for both shear and moment in this configuration. The shear and moment diagrams for the ASCE 7-16 loads and the wind tunnel test loads at the time step producing the maximum values on purlin 2 at this wind angle are shown in Figure 21 and Figure 22, respectively.

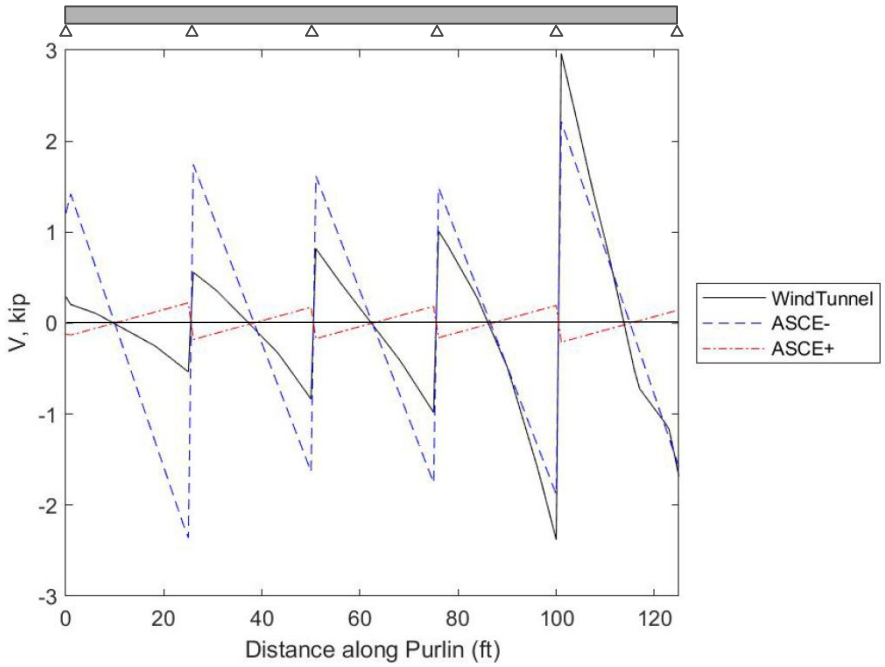

Figure 21: Shear diagram for case causing maximum shear at 325° (125'x80'x40' building, open terrain)

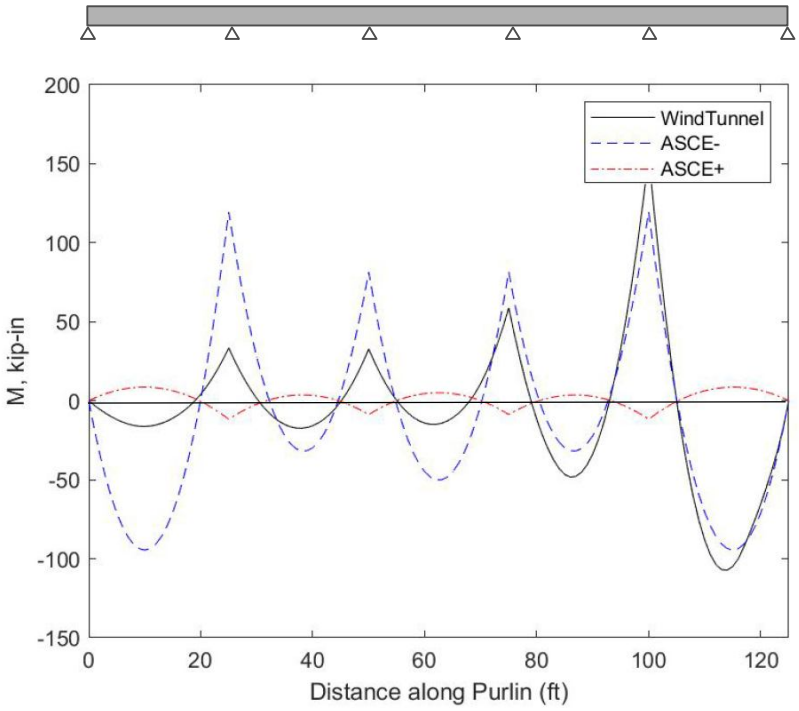

Figure 22: Moment diagram for case causing maximum moment at 325° (125'x80'x40' building, open terrain)

Configuration 4

The final configuration used was the building with a mean roof height of 40 feet in suburban terrain exposure conditions. In this configuration, the purlins on the windward edge of the building had consistently higher maximum shear and moment values than what was calculated using ASCE 7, with percent differences ranging from -16.35% to -9.8% for shear and -22.97% to -12.4% for moment. The purlins on the interior of the building had shear and moment values with lower magnitude than what was specified in ASCE 7, with percent differences ranging from 5.01% to 30.9% for shear and 8.17% to 21.26% for moment. The maximum shear and moment values for each purlin across all wind angles and time steps are shown in Table 7 and Table 8.

Table 7: Maximum shear in each purlin across all time steps and wind angles compared with ASCE 7 provisions (125'x80'x40' building, suburban terrain)

		Max Shear (kip)									
	Purlin #	1	2	3	4	5	6	7	8	9	10
ASCE -	Max	0.8083	1.6166	1.4519	1.5827	1.8993	1.6777	1.6352	1.6224	1.6224	1.3854
	Min	-0.8595	-1.7190	-1.5472	-1.6931	-2.0318	-1.7948	-1.7273	-1.7069	-1.7070	-1.4576
ASCE +	Max	0.0813	0.1627	0.1515	0.1754	0.2105	0.1859	0.1859	0.1859	0.1859	0.1588
	Min	-0.0760	-0.1521	-0.1416	-0.1640	-0.1968	-0.1738	-0.1738	-0.1738	-0.1738	-0.1484
Wind Tunnel	Max	0.9530	1.8963	1.7174	1.8076	1.8009	1.4041	1.2443	1.3148	1.2518	1.0675
	Min	-0.9891	-1.7398	-1.6372	-1.9946	-1.9326	-1.5144	-1.3311	-1.1799	-1.0825	-0.9722
% Diff		-14.02	-9.80	-10.43	-16.35	5.01	16.94	25.91	25.95	30.77	30.90

		Max Shear (kip)									
	Purlin #	11	12	13	14	15	16	17	18	19	20
ASCE -	Max	1.3854	1.6224	1.6224	1.6352	1.6777	1.8993	1.5827	1.4519	1.6166	0.8083
	Min	-1.4576	-1.7070	-1.7069	-1.7273	-1.7948	-2.0318	-1.6931	-1.5472	-1.7190	-0.8595
ASCE +	Max	0.1588	0.1859	0.1859	0.1859	0.1859	0.2105	0.1754	0.1515	0.1627	0.0813
	Min	-0.1484	-0.1738	-0.1738	-0.1738	-0.1738	-0.1968	-0.1640	-0.1416	-0.1521	-0.0760
Wind Tunnel	Max	1.1111	1.1992	1.1851	1.2209	1.2414	1.5144	1.0599	0.8945	1.0231	0.6339
	Min	-1.0015	-1.0454	-0.9923	-0.9605	-1.0306	-1.3138	-1.1631	-0.9605	-0.9374	-0.5903
% Diff		26.98	34.95	36.09	34.35	36.45	29.18	37.11	46.79	50.76	30.22

Table 8: Maximum moment in each purlin across all time steps and wind angles compared with ASCE 7 provisions (125'x80'x40' building, suburban terrain)

		Max Moment (kip-in)									
	Purlin #	1	2	3	4	5	6	7	8	9	10
ASCE -	Max	43.56	87.12	79.31	88.47	106.17	93.78	85.22	82.64	82.64	70.57
	Min	-34.44	-68.89	-61.79	-67.20	-80.65	-71.24	-72.00	-72.22	-72.22	-61.68
ASCE +	Max	3.14	6.28	5.85	6.78	8.13	7.18	7.18	7.18	7.18	6.13
	Min	-4.24	-8.48	-7.90	-9.15	-10.98	-9.70	-9.70	-9.70	-9.70	-8.28
Wind Tunnel	Max	51.61	99.60	90.14	100.17	97.83	75.76	69.12	63.06	63.72	56.26
	Min	-54.87	-98.08	-81.97	-79.48	-80.90	-72.48	-71.84	-74.03	-71.96	-57.59
% Diff		-22.97	-13.37	-12.79	-12.40	8.17	21.26	17.04	10.99	13.82	20.27

		Max Moment (kip-in)									
	Purlin #	11	12	13	14	15	16	17	18	19	20
ASCE -	Max	70.57	82.64	82.64	85.22	93.78	106.17	88.47	79.31	87.12	43.56
	Min	-61.68	-72.22	-72.22	-72.00	-71.24	-80.65	-67.20	-61.79	-68.89	-34.44
ASCE +	Max	6.13	7.18	7.18	7.18	7.18	8.13	6.78	5.85	6.28	3.14
	Min	-8.28	-9.70	-9.70	-9.70	-9.70	-10.98	-9.15	-7.90	-8.48	-4.24
Wind Tunnel	Max	50.80	55.92	58.94	59.68	59.79	66.65	55.96	45.85	50.38	30.79
	Min	-59.12	-64.84	-61.68	-61.30	-65.44	-82.47	-70.50	-51.10	-57.25	-36.71
% Diff		17.65	24.14	29.05	32.66	35.60	25.12	22.61	43.25	41.38	17.08

In this test configuration, the maximum shear value for purlin 2 occurred at an approach angle of 325 degrees, while the maximum moment value for purlin 2 occurred at an approach angle of 270 degrees. The shear and moment diagrams for purlin 2 at the time step where the maximum value occurred for each of these angles is shown in Figure 23 and Figure 24.

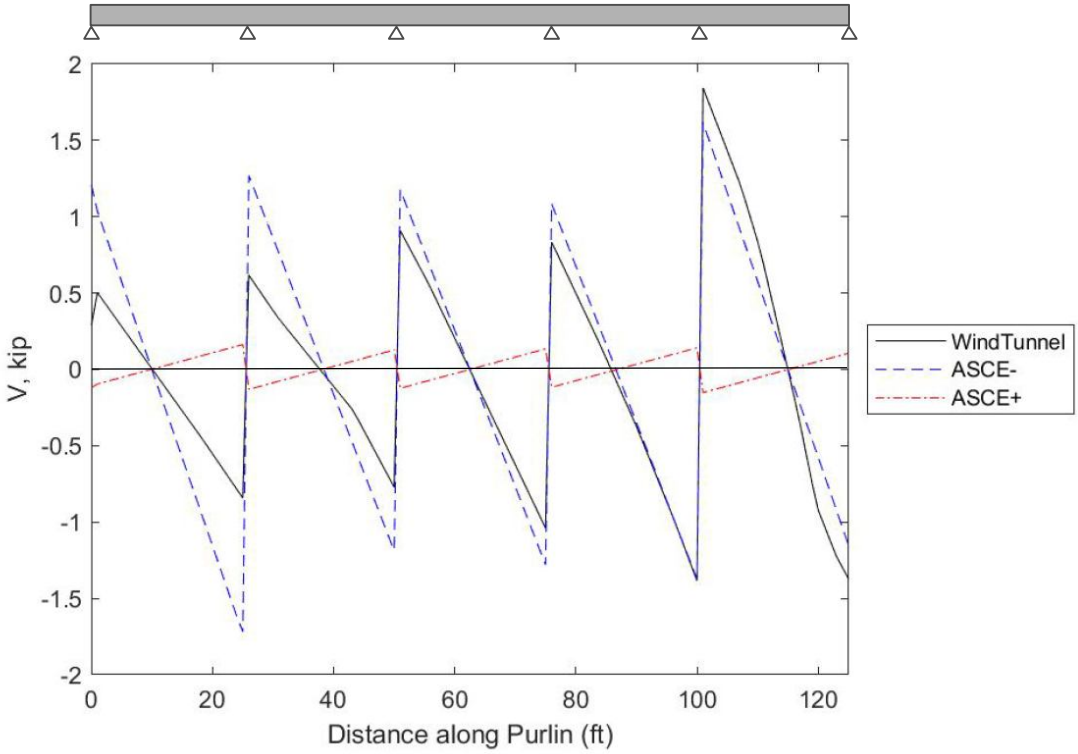

Figure 23: Shear diagram for case causing maximum shear at 325° (125'x80'x40' building, suburban terrain)

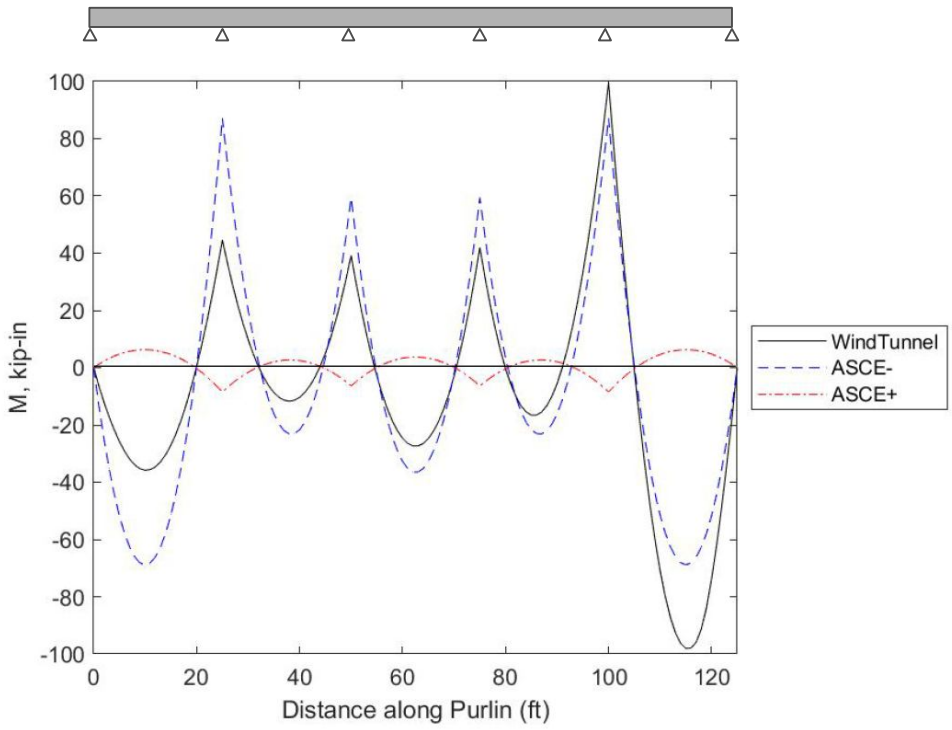

Figure 24: Moment diagram for case causing maximum moment at 270° (125'x80'x40' building, suburban terrain)

Discussion

This project set out to model the behavior of steel purlins under wind loads more accurately than the current design wind loads used in ASCE 7 for components and cladding. The results showed that the overall maximum values for shear and moment on the purlins that were obtained with ASCE 7 were lower than what the structure experienced in a wind tunnel test, particularly near the edge of the windward corner of the structure. However, this was not the case for the purlins and segments of purlins that were not on the windward corner of the structure. For interior purlins and portions of purlins, the loads obtained in the wind tunnel varied in whether they were higher or lower what was calculated based on the methods provided in ASCE 7. The provisions in Chapter 30 on components and cladding use roof zones symmetrically placed around the building to account for winds at all approach angles, shown in Figure 13. Therefore, it is reasonable that purlins and portions of purlins not located on the windward corner would experience loads lower than what ASCE 7 specifies. It is necessary for all purlins to be designed for the maximum load they could experience, and since the purlins for this model were placed symmetrically, these purlins on the leeward side would have similar behavior to their counterparts on the opposite side of the ridge line (1 and 20, 2 and 19, etc) if the tests were run for a full 360 degrees.

These results show that while the shear and moment diagrams follow the same general patterns between the wind tunnel and code provision loads, the actual internal loads the section will experience do have differences in location and maximum magnitude. As the wind angle shifts from perpendicular to the ridge at 270 degrees (shown in Figure 19, Figure 20, & Figure 24) to parallel to the ridge at 360 degrees, the similarity of the shear and moment diagrams decreases, with much higher shear and moment values towards the windward corner. Figure 19, Figure 20, and Figure 24, while based on loads from the angle perpendicular to the ridge, seem to experience higher loads at the windward corner of the building for angles 275 to 360 degrees. Typically for wind perpendicular to the ridge, it is expected that the load on the purlin would be symmetric. In these tests, a higher density of pressure taps is placed on the windward side of the building, and the tap density decreases as you move away from the windward edge at the 360-degree approach angle. A higher tap density in the windward corner allows this area of the building to more precisely read more variation in values. This allowed this corner of the building to read more peak values throughout the test which seemed to be causing the higher values of shear and moment on this corner while under the 270-degree approach angle. This effect is demonstrated in the decrease in pressure coefficient with an increase in effective wind area that is specified in Chapter 30 of ASCE 7-16.

Figures 17 through 24 show that the windward corner of the buildings tend to be the location where the wind tunnel test data exceeds the values calculated using ASCE 7. This is not the case for all of the buildings, but does suggest that if the direction were to be reversed and a consistent tap density was placed across the building, what was previously the leeward corner where the ASCE 7 loads were higher, would now experience the maximum load value. While the equations for calculating the loads in ASCE 7 are applied symmetrically, those generated in the wind tunnel test vary significantly between the windward and leeward corner. In order to implement wind tunnel test data in the design of purlins, they would need to be designed for loads placed at all angles, as is considered in ASCE 7, therefore; the purlins would have to be designed symmetrically about their midpoint and purlins that are symmetric about the ridge line would need to be designed equally (e.g. purlins 2 and 19).

For the buildings with a mean roof height of 16 feet, purlins 3 and 5 had maximum values with magnitudes lower than those that were calculated using the ASCE 7 provisions, with larger percent differences than those around it. Purlins 3 and 5 were both located on the windward side of the ridge line. Purlin 3 was located in Zone 3 for the first and last 3.2 feet, and the rest of the purlin was in Zone 2, according to the zone diagram shown in 30.3-2A of ASCE 7-16 (ASCE, 2016). Purlin 5 was located in Zone 2 for the first and last 9.6 feet and the internal part of the purlin was in Zone 1 according to the same diagram. This shift from loads lower than ASCE 7, to higher, and back to lower that was observed with purlins 3, 4, and 5 at lower heights may be explained by the phenomenon of the wind reattaching at a certain distance along the

length as shown in the contour plots for this data set that are shown in figure 3 of the paper "Components and Cladding Wind Loads for Low-Slope Roofs on Low-Rise Buildings" (Kopp & Morrison, 2018). This reattachment length is dependent on the ratio between wall length to building height and occurs along the edge, due to the principles of flow around a bluff body.

For the configurations with a mean roof height of 40 feet when compared to the 16 foot mean roof height cases, more of the internal purlins had shear and moment values with magnitudes lower than ASCE 7-16 when wind tunnel test loads were used. For open terrain, only purlin 5 had both shear and moment with lower magnitudes than ASCE 7-16 for the 16 foot case, while purlin 6 had both shear and moment with lower magnitudes than ASCE 7-16 for the 40 foot case. For suburban terrain, purlins 5 and 8 had both shear and moment values with lower magnitudes than ASCE 7-16 for the 16 foot case, but purlins 5-10 all had shear and moment values with lower magnitudes than ASCE 7-16 for the 40 foot case. There also were larger percent differences between shear and moment values with the maximum magnitude obtained from ASCE 7-16 loads and wind tunnel data loads with the increase in mean roof height. For the 16 foot case, the range of percent differences was -20% to +18%, whereas for the 40 foot case, the range of percent differences was -50% to +30%. The most extreme case considered overall was the 40 foot mean roof height configuration with suburban exposure. This case had the highest number of purlins that had values with lower magnitudes than ASCE 7-16, with percent differences ranging from 5% to 31%. This case also had windward purlins with values of higher magnitude than ASCE 7-16 with large percent differences, ranging from -23% to -9%.

The terrain roughness has a significant influence on the turbulence around the building. When changing from open to suburban terrain, more internal purlins had lower magnitude shear and moment maximum values based on wind tunnel data than on ASCE 7-16 loads. For the 16 foot mean roof height case, only purlin 5 had both shear and moment with lower magnitudes than ASCE 7-16 in open terrain, whereas purlins 5 and 8 both had shear and moment with lower magnitudes than ASCE 7-16 in suburban terrain. For the 40 foot mean roof height case, only purlin 6 had both shear and moment with lower magnitudes than ASCE 7-16 in open terrain, whereas purlins 5-10 had shear and moment values with lower magnitudes than ASCE 7-16 in suburban terrain. The change in terrain from open to suburban also corresponded with an increase in percent difference for purlins with shear and moment values lower than ASCE 7-16. For the 16 foot mean roof height case, changing from open to suburban shifted the maximum percent difference from 12% to 16%. For the 40 foot mean roof height case, changing from open to suburban shifted the maximum percent difference from 21% to 31%. Shifting from open terrain to suburban terrain increases the turbulence, while decreasing the velocity profile. In the code provisions for surface roughness, changing from Exposure B (suburban) to Exposure C (open) increases the velocity pressure exposure coefficient

(K_Z), leading to an increase in the velocity pressure (q_Z). The larger percent differences with suburban terrain may be caused by the adjustment for velocity profile, while not adjusting for the larger turbulence.

For the purposes of purlin design, these methods indicate that while some of the interior purlins are suitable for a reduction in loads, the purlins in the edge zones will have significant increases in shear and moment compared to designing using ASCE 7-16. For buildings of a lower mean height and in open terrain, many of the purlin loads would have to be increased. The most probable situation where reduction in purlin size would be possible is in the interior purlins for the taller mean roof height case in suburban terrain. This configuration had 6 of the 10 purlins on the windward side of the structure with shear and moment lower than those calculated with ASCE 7-16. For this case, if the loads were then applied symmetrically to the leeward side of the structure, 12 of 20 purlins would be able to be reduced, while 8 of 20 would need to be increased. In order to implement this method for design, an iterative approach would have to be used, where purlin sizes spacings would be adjusted to account for changes in the loading, and shear and moment values regenerated each time, until a suitable design is determined. This system would determine if there are potential cost savings associated with applying wind tunnel test loads to the structure, but would require a large amount of computational effort to analyze the purlin at each time step multiple times.

The results indicate that the largest differences in the shear and moment in the purlins found using ASCE 7-16 and the wind tunnel loads was in the case of changing terrain roughness. This indicates that the change in turbulence with surface roughness is not being sufficiently accounted for in the development of the component and cladding pressures. Shifting the roof zones or applying a factor to Equation 3 to account for changes in turbulence could yield a more accurate representation of the behavior.

Conclusion

In this study, comparisons were made between the shear forces and moments that continuous purlins experienced for load cases determined using both ASCE 7-16 and from wind tunnel test data. Using the NIST database of low-rise building wind tunnel test data, buildings that are similar to a typical low rise steel building were considered. The results indicated that purlins 1, 2, and 4, which were close to the windward edge of the structures studied, consistently experienced higher maximum shear and moment values under the wind tunnel test loads than those using ASCE 7-16 components and cladding loads, with percent differences ranging from -38% to -2% for shear and -50% to -0.54% for moment. Those closer to the interior of the structure experienced both higher and lower overall maximum shear and moment values under the wind tunnel test loads than those using ASCE 7-16 depending on which test configuration was considered.

For buildings with lower height, fewer purlins on the interior had shear and moment values lower than those found using ASCE 7-16. For buildings with higher height, more purlins on the interior had shear and moment values lower than those found using ASCE 7-16. Changes in terrain roughness had a similar effect, where test configurations with open terrain had fewer purlins on the interior with shear and moment values lower than ASCE 7-16 and test configurations with suburban terrain had more purlins on the interior with shear and moment values lower than those found using ASCE 7-16. The case with the overall largest differences for internal purlins was the test configuration with a mean roof height of 40 feet with suburban terrain. In this case, purlins 1 through 4 all had shear and moment values higher than ASCE 7-16, and purlins 5 through 10 all had shear and moment values lower than ASCE 7-16.

In addition, for cases where the maximum values were produced by wind angles perpendicular to the ridge, the behavior of the purlins was similar between the two load applications with the values of shear and moment on the diagrams following a similar pattern. However, for these cases, the maximum magnitude of shear and moment were located in the bay with closest tap spacing, while the ASCE 7-16 loads had shear and moment values that were symmetric on the purlin. In cases where the maximum values were produced by wind angles parallel to the ridge, the shear and moment diagrams had significant differences between the loads determined using ASCE 7-16 and the wind tunnel test. The ASCE 7-16 loads were symmetric on the purlin, while the wind tunnel test loads concentrated most of the load in the windward bay.

References

AISI (2009). D111-09: Design Guide For Cold-Formed Steel Purlin Roof Framing Systems. Washington, DC, American Iron and Steel Institute.

ASCE. (2016). ASCE/SEI 7-16: Minimum Design Loads and Associated Criteria for Buildings and Other Structures. In. Reston, VA: American Society of Civil Engineers.

Association, M. B. M. (2018). Metal Building Systems Manual. In. Cleveland, OH: Metal Building Manufacturers Association.

Charney, F. (2008). *A Transformational Approach to Teaching Matrix Structural Analysis, and Visual Implementation using Mathcad*. Paper presented at the 18th Analysis and Computation Specialty Conference.

Ho, E. S., D.; Morrish, D.; Nywening, M.; Kopp, G. (2003). *NIST Aerodynamic Database*.

Ho, T. C. E., Surry, D., Morrish, D., & Kopp, G. A. (2005). The UWO contribution to the NIST aerodynamic database for wind loads on low buildings: Part 1. Archiving format and basic aerodynamic data. *Journal of Wind Engineering and Industrial Aerodynamics, 93*(1), 1-30. doi:10.1016/j.jweia.2004.07.006

J Ginger, D. H., and M Humphreys. (2015). Wind loads on the frames of industrial buildings. *Australian Journal of Structural Engineering, 16*, 8.

Jayamon, J. (2012). Static and Dynamic Analysis of Various Structural Systems Using Matlab and Mathcad Simulations.

Kopp, G. A., & Morrison, M. J. (2018). Component and Cladding Wind Loads for Low-Slope Roofs on Low-Rise Buildings. *Journal of Structural Engineering, 144*(4). doi:10.1061/(asce)st.1943-541x.0001989

Perry, D. C. M., James R.; Saffir, Herbert S. (1990). Performance of Metal Buildings in High Winds. *Journal of Wind Engineering and Industrial Aerodynamics, 36*, 14.

Pierre, L. M. S., Kopp, G. A., Surry, D., & Ho, T. C. E. (2005). The UWO contribution to the NIST aerodynamic database for wind loads on low buildings: Part 2. Comparison of data with wind load provisions. *Journal of Wind Engineering and Industrial Aerodynamics, 93*(1), 31-59. doi:10.1016/j.jweia.2004.07.007

R.D. Ziemian, W. McGuire. MASTAN2.

CHAPTER 4: Conclusions

4.1 Summary

The objective of this study was to use the NIST wind tunnel database of low-rise building tests to more accurately model continuous purlin behavior. This was done by applying varying line loads along the length of each purlin and calculating the shear and moment values using a continuous beam model. The loads were applied statically, and the shear and moment calculated at 1-foot increments along the length. Each building plan was evaluated using wind tunnel test data across 90 degrees of varying wind angle at 5-degree increments. At each of these time histories, pressure coefficients were collected across the roof using pressure taps with varying spacing. The internal forces in the purlins were calculated individually for each of the wind angle and time step cases, to simulate the loads for each instant in time.

Additional continuous beam analyses were run using the loads specified in ASCE 7-16 Chapter 30 for components and cladding loads. These loads are based on symmetric roof zones across the building, that specify higher loads on all edges of the structure and decrease towards the interior area of the roof. This method accounts for winds at any approach angle. Both positive and negative pressures were calculated using the code provisions for components and cladding for comparison with the wind tunnel test results.

Each of these analyses were run for several different cases provided in the wind tunnel database. The building selected for consideration was the 125 foot by 80-foot building with a roof slope of 1:12, as this represents a typical low rise steel building plan. Cases were run for both open and suburban terrain exposures to analyze the effects of varying terrain, and for mean roof heights of 16 feet and 40 feet to analyze the effects of varying height.

4.2 Conclusions

When compared to the loads calculated using ASCE 7-16 Chapter 30, the overall maximum values of shear and moment that were calculated for the purlins 1, 2, and 4, on the windward corner, were consistently higher using the wind tunnel test pressures with percent differences from -38% to -2% for shear and -50% to -0.54% for moment. The interior purlins under the wind tunnel test loads depended on the building configuration considered in whether the shear and moment values exceeded the loads determined with ASCE 7-16. The most significant difference in interior purlins was the building with a mean roof height of 40 feet and suburban terrain. For this case, purlins 1 through 4 all had shear and moment values higher than ASCE 7-16, and purlins 5 through 10 all had shear and moment values lower than ASCE 7-16. The purlins closest to the leeward edge of the building were consistently lower than those calculated using ASCE 7-16

Chapter 30, which is a product of the direction that the wind angles were applied at (90 degrees versus 270 degrees). These building configurations that were tested were symmetric, therefore; the purlins closest to the leeward edge would be subjected to the same loads as was calculated for the windward edge, to take into account wind from a 360-degree range.

Increasing the mean roof height of the building also increased the number of purlins on the interior of the windward side of the roof that had shear and moment values with magnitudes lower than those found using ASCE 7-16. Changing the terrain roughness from open terrain to suburban terrain also increased the number of purlins on the interior with shear and moment values with magnitudes lower than ASCE 7-16.

For cases with wind angles perpendicular to the ridge, the shear and moment diagrams for the purlins under ASCE 7-16 loads and wind tunnel test loads followed a similar pattern. For these cases, the maximum magnitude of shear and moment were still located in the bay with closest tap spacing, while the ASCE 7-16 loads had shear and moment values that were symmetric on the purlin. This effect was attributed to higher tap density capturing more peak values in wind pressure during the testing. For cases with wind angles parallel to the ridge, the shear and moment diagrams had significant differences between the loads determined using ASCE 7-16 and the wind tunnel test. The ASCE 7-16 loads were symmetric on the purlin, while the wind tunnel test loads concentrated most of the load in the windward bay, with a significant drop in both shear and moment at the leeward edge of the purlin.

4.3 Future Work

In future studies, the effects of considering the purlins as fully continuous should be studied, with increased moment of inertia at the laps being taken into account. In addition, the effects of the girders not being fully rigid should also be considered. Two methods for this would be to use existing data on girder stiffnesses and model them as a spring using the existing program, or to use the tap data on each wall to calculate the wind loads the girders are experiencing at each time step and apply these displacements to the purlin supports. The second method is much more computationally expensive.

This study used the assumption of the roof system distributing forces to the purlins based on tributary areas. Whether the tributary area method is accurate for these roof systems is debated, with previous studies finding that with increases in roof membrane stiffness compared to the purlin stiffness, the roof system distributes the forces as a continuous beam (Henderson, 2013). With future studies, the forces due to wind could be applied to the structure from the pressure taps using a double continuous beam model, where both the roof and purlins are behaving as continuous beams. This would have a significant impact on the distribution of forces and the purlins experiencing peak loads.

For the purposes of purlin design, these methods indicate that while some of the interior purlins are suitable for a reduction in loads, the purlins in the edge zones will have significant increases in shear and moment compared to designing using ASCE 7-16. For buildings of a lower mean height and in open terrain, many of the purlin loads would have to be increased. The most probable situation where reduction in purlin size would be possible is in the interior purlins for the taller mean roof height case in suburban terrain. This configuration had 6 of the 10 purlins on the windward side of the structure with shear and moment lower than those calculated with ASCE 7-16. For this case, if the loads were then applied symmetrically to the leeward side of the structure, 12 of 20 purlins would be able to be reduced, while 8 of 20 would need to be increased. In order to implement this method for design, an iterative approach would have to be used, where purlin sizes spacings would be adjusted to account for changes in the loading, and shear and moment values regenerated each time, until a suitable design is determined. This system would determine if there are potential cost savings associated with applying wind tunnel test loads to the structure, but would require a large amount of computational effort to analyze the purlin at each time step multiple times. An alternative method would be to use the pressure data in combination with an existing building analysis software. This method was pursued, and programs were put together that could be implemented by Metal Building Systems (MBS) to conduct this analysis.

The results indicate that the largest differences in the shear and moment in the purlins found using ASCE 7-16 and the wind tunnel loads was in the case of changing terrain roughness. This indicates that the change in turbulence with surface roughness is not being sufficiently accounted for in the development of the component and cladding pressures. Shifting the roof zones or applying a factor to Equation 3 to account for changes in turbulence could yield a more accurate representation of the behavior. Future research into the effects of terrain roughness on a larger variety of building floor plans and mean roof heights would help isolate this effect.

References

AISI (2009). D111-09: Design Guide For Cold-Formed Steel Purlin Roof Framing Systems. Washington, DC, American Iron and Steel Institute.

ASCE. (2016). ASCE/SEI 7-16: Minimum Design Loads and Associated Criteria for Buildings and Other Structures. In. Reston, VA: American Society of Civil Engineers.

Association, M. B. M. (2018). Metal Building Systems Manual. In. Cleveland, OH: Metal Building Manufacturers Association.

Charney, F. (2008). *A Transformational Approach to Teaching Matrix Structural Analysis, and Visual Implementation using Mathcad*. Paper presented at the 18th Analysis and Computation Specialty Conference.

Duthinh, D. S., E. (2011). The Use of Wind Tunnel Measurements in Building Design. In *Wind Tunnels and Experimental Fluid Dynamics Research* (pp. 23): InTech.

Henderson, D., et al. (2013). "Failure mechanisms of roof sheathing under fluctuating wind loads." Journal of Wind Engineering and Industrial Aerodynamics 114: 27-37.

Ho, E. S., D.; Morrish, D.; Nywening, M.; Kopp, G. (2003). *NIST Aerodynamic Database*.

Ho, T. C. E., Surry, D., Morrish, D., & Kopp, G. A. (2005). The UWO contribution to the NIST aerodynamic database for wind loads on low buildings: Part 1. Archiving format and basic aerodynamic data. *Journal of Wind Engineering and Industrial Aerodynamics, 93*(1), 1-30. doi:10.1016/j.jweia.2004.07.006

J Ginger, D. H., and M Humphreys. (2015). Wind loads on the frames of industrial buildings. *Australian Journal of Structural Engineering, 16*, 8.

Jayamon, J. (2012). Static and Dynamic Analysis of Various Structural Systems Using Matlab and Mathcad Simulations.

Ji, X. H., G.; Zhang, X.; Kopp, G.A. (2017). Vulnerability analysis of steel roofing cladding-influence of wind directionality. *Engineering Structures, 156*, 11. doi:10.1016/j.engstruct.2017.11.068

Kopp, G. A., & Morrison, M. J. (2018). Component and Cladding Wind Loads for Low-Slope Roofs on Low-Rise Buildings. *Journal of Structural Engineering, 144*(4). doi:10.1061/(asce)st.1943-541x.0001989

Li, J. L., Q.; Hu, S. (2019). Monitoring of wind pressures on gable roof of a low rise building during tropical cyclones and compariisons with wind tunnel test results. *Wiley & Sons: Structural Control Health Monitoring, 26*, 20. doi:10.1002/stc.2380

Perry, D. C. M., James R.; Saffir, Herbert S. (1990). Performance of Metal Buildings in High Winds. *Journal of Wind Engineering and Industrial Aerodynamics, 36*, 14.

Pierre, L. M. S., Kopp, G. A., Surry, D., & Ho, T. C. E. (2005). The UWO contribution to the NIST aerodynamic database for wind loads on low buildings: Part 2. Comparison of data with wind load provisions. *Journal of Wind Engineering and Industrial Aerodynamics, 93*(1), 31-59. doi:10.1016/j.jweia.2004.07.007

R.D. Ziemian, W. McGuire. MASTAN2.

APPENDIX A: Extended Materials and Methods

A.1 Wind Database

The NIST Database of wind tunnel tests conducted at UWO was used as the basis for the wind loading considered (Ho, et al. 2003). The data is accessible from NIST through downloadable Hierarchical Data Format (HDF) files. For the purpose of this study, the data being accessed was primarily pressure coefficient (C_p) values along with test setup information and relevant measurements. The pressure coefficients in these tests were the pressure values measured in the wind tunnel adjusted for the wind velocity to provide a unitless number that can be compared between the model scale and full-scale. These tests were conducted in the UWO boundary layer wind tunnel. In each test configuration approximately 600 pressure taps were used. For the purposes of this project, only the pressure taps on the roof were considered, of which there were approximately 350. The actual number of pressure taps that were active in each test configuration varies.

Contained in the NIST Database are 81 different test configurations of realistic low-rise buildings that were run at UWO. For this project, a test configuration typical of the steel low rise buildings of interest was selected. After discussion with the industry partners on this project, the 125 foot by 80-foot building was selected. From there, the scope was narrowed to those with 1:12 roof slopes. Both open and suburban terrain were considered and compared. Mean roof heights of 16 and 40 feet were selected to compare results. Considering these heights allows two roof zone layouts (one including zone 1' and one without) per the provisions in ASCE 7-16 Chapter 30 to analyze this effect.

For the initial set up of the analysis system, baseline files to read the data files in Matlab were obtained from the Insurance Institute for Business and Home Safety (IBHS). These files were updated and tested against previous work using the database and the values in ASCE 7 to confirm that the analysis was being done correctly. These programs extracted the pressure taps that were active in the test being considered (inactive taps stored artificial values). The roof data was then separated by identifying the face number based on which surface was considered (walls and roof were numbered 1 through 6). From there, the program uses the variable ZROOF to establish an area of interest on the roof. This is done by writing a vector of the starting x and y coordinates followed by the extents in the x- and y-direction. The program then finds each pressure tap's tributary area that overlaps with the area specified in ZROOF. Using the percent of overlapping area for each tap, corresponding weights are multiplied by the C_p values that correspond with each tap. Using this weighted C_p value for each tap, an area-averaged pressure coefficient for the entire area of interest was calculated. After matching the output of the program to some baseline

checkpoints from previous studies using the database and the provisions in the ASCE 7 Chapter 30 on components and cladding, the files were altered to be able to isolate loads for each purlin and consider multiple wind angles.

The variable ZROOF was used in this project by setting the area of interest equal to the width of the purlin tributary area by the width of one tap's tributary area. This served to separate the variation in loading along the length of the purlin by creating a series of line loads. Loops were implemented here to repeat the process of setting ZROOF for each tap tributary width along the purlin. The result of this process is a plot of pressure coefficient values along the length of the purlin. An example of a plot for the first 15-time steps for one wind angle and one purlin is shown in Figure 25.

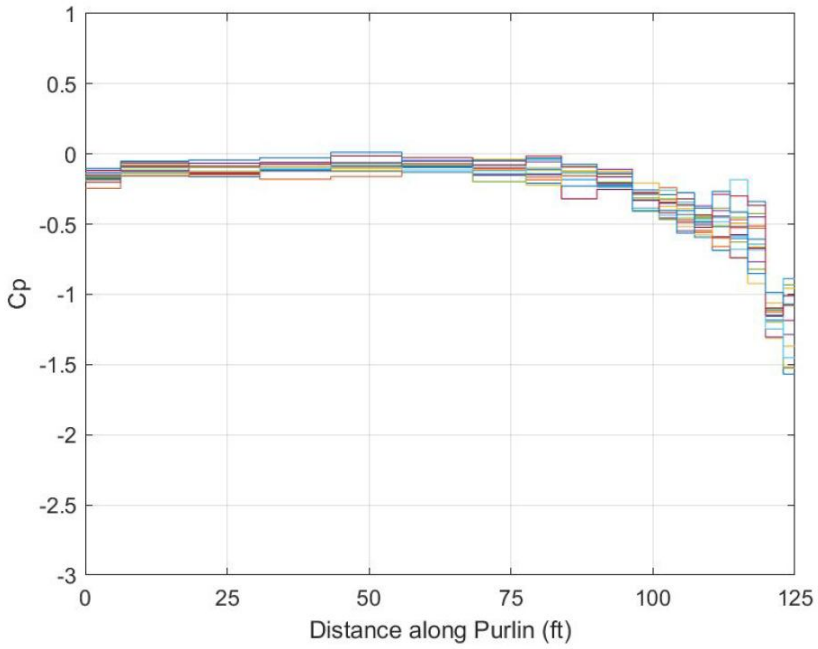

Figure 25: Pressure coefficient varying along purlin length for 15 time steps

This process also generates text files containing C_p values with rows of time histories across columns of pressure taps. One table of approximately 19 columns and 50,000 rows was generated per purlin (varying based on location on the building and test setup), each column corresponding to one of the pressure coefficients shown in Figure 25, and each row corresponding to a time step.

In order to convert to an equivalent force, equations 26.10-1 and 30.3-1 from ASCE 7-16 were used (ASCE, 2016):

$$q = 0.00256 K_z K_{zt} K_d K_e V^2 \quad \text{(Equation A.1)}$$

$$p = q_h\left[\left(GC_p\right) - \left(GC_{pi}\right)\right] \quad \text{(Equation A.2)}$$

The exposure coefficient (K_z) was calculated based on the roof height and exposure of the given test setup, read from the HDF file (in this case: Exposure B at a mean roof height of 16ft). The topographic factor (K_{zt}) was taken as 1.0 for the test setup. The directionality factor (K_d) was taken as 1.0, as the wind tunnel tests were run over a range of angles, removing the effects that lead to the use of this factor defined in the literature review. The internal pressures are not being considered in these models. Because the primary interest of the project is to compare the pressures on the purlins between what is required in ASCE 7-16 and what can be calculated using wind tunnel pressures, the internal pressure values would be equivalent for each and will not contribute to any differences observed. A reference wind speed (V) of 100 mph was used for the initial tests but may be varied, as the effects of changing wind speed are nonlinear.

The pressure coefficient values from the wind tunnel HDF files are converted into an equivalent GC_P at each point using the following equation (Pierre et al., 2005):

$$\left(GC_P\right)_{eq} = \frac{\frac{1}{2}\rho V^2{}_{h,z_0,meanhrly} C_p}{\frac{1}{2}\rho V^2{}_{10m,o.c.,3secgust} K_{zt} K_h K_d I} \quad \text{(Equation A.3)}$$

The factors determined using the above equation were part of the initial program obtained from IBHS and can be multiplied by C_p to obtain the equivalent GC_p to use in equation 27.3-1 when calculating the force on the purlin.

After the pressure coefficient was converted into a corresponding pressure over the specified area, it was multiplied by the tributary width of the purlin being considered to obtain a tributary load in pounds per linear foot. For this project, the spacing of the purlins was varied across the roof to simulate a typical design for a structure of this size. Additional text files were created containing rows of force values at each time step across columns of each tap, with the same formatting as described above for pressure coefficient files. The Matlab files used for these steps are located in Appendix B. The Matlab files used to generate the plots shown in Figure 25 and Figure 26 are located in Appendix C. The calculated line loads are plotted to show the distribution of tributary loads along each purlin as shown in Figure 26.

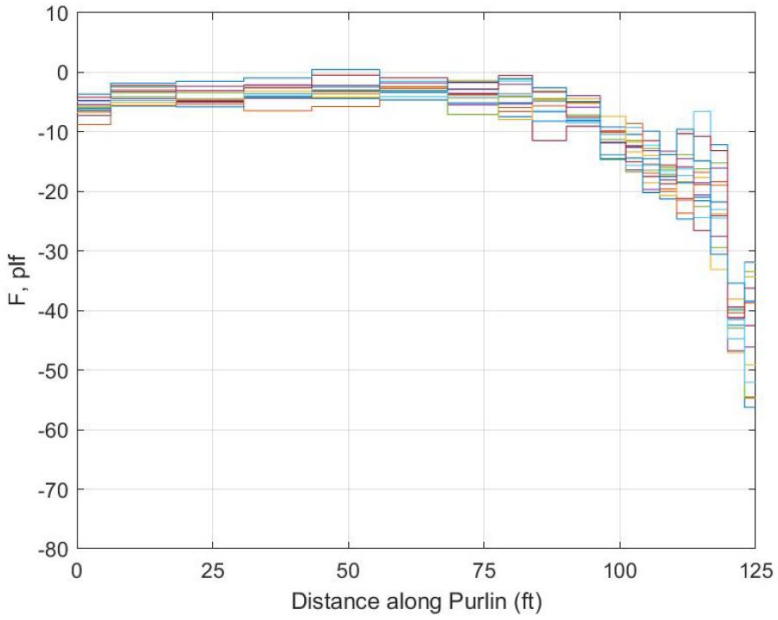

Figure 26: Varying line loads along the length of the purlin for 15 time steps

Finally, the sequence of block loads that were generated at each time step for each purlin were used to determine the resulting shear and moment. These steps were repeated across wind angles 270 to 360 degrees. This 90-degree series captures the behavior of the wind around the structure for all directions, as the buildings being tested are symmetric.

A.2 Beam Analysis and Comparison Methods

Continuous Beam Analysis

As discussed in the literature review, previously developed functions to analyze continuous beam structures using the direct stiffness method were adapted to work with the previously saved text files and conduct a basic analysis of each purlin. This analysis was done by first setting the material properties of the structural material being used, including section moment of inertia and shear area, along with Modulus of Elasticity, coefficient of thermal expansion, and Poisson's ratio. For this project, an 8x2.5Z14 Z-section was used to represent a typical purlin member. The moment of inertia and shear area values were obtained from the industry partners for this section. The Modulus of Elasticity was taken as 29,000 kips per square inch (ksi), and the Poisson's ratio used was 0.27. No thermal load was applied to the structure and so the coefficient of thermal expansion did not have an impact. A constant section size was used throughout the structure but could be varied in future studies, with further adjustment to the beam analysis files. A restraint matrix was

developed to set the locations of the supports and a matrix of zeros is built to represent that there are no point loads at the supports to be considered.

Next a matrix describing the connectivity of the system was built (called CON) that was used to determine the member loads applied to each element, the nodes corresponding to the ends of each element, and which of the specified material properties corresponds with each element. The nodes for this project were set at each change of load and each reaction. Each change of load corresponds with the edges of the pressure tap tributary areas. Finally, the text files containing force values were read and the values input into a member load matrix containing each of the different distributed load values. The Matlab files used to generate these input files are shown in Appendix D. After setting these initial values, the function was called and used the series of equations and methods discussed above to output the reactions, element forces (shear and moment), and deflections. The function used for the continuous beam analysis is contained in Appendix E.

Shear, moment, and deflection values were output at each node, while the reactions were output at each support. Additional outputs that can be accessed are a diagram of the deflection of the structure, and shear and moment diagrams. The values that were output were then stored in text files with rows corresponding to each time step and columns corresponding to the nodes. Separate sets of text files were created for each purlin and each wind angle. These files were then accessed to create shear and moment envelopes, as well as, to verify the program, and for use with comparison to ASCE 7. The accuracy of the generated reactions, element forces, and deflections were verified by checking four cases by hand in MASTAN. The cases considered were uniform positive load, uniform negative load, an actual load case with negative pressures, and an actual load case with both positive and negative pressures. For each of these, the values that were obtained from MASTAN matched the results from the Matlab programs to approximately the 3rd or 4th decimal place (depending on the number of leading zeros).

Development of Shear and Moment Envelopes

Intermediate shear and moment values were primarily obtained by breaking each element of the purlin into smaller segments (approximately 100 segments per element, or 2300 segments for the whole purlin). Using these intermediate length values and the already calculated shear and moment values at each end of the element, the internal forces at each segment were calculated. The overall maximum and minimum values of the 2300 shear and moment values were taken for each time step along the length of purlin. In addition, one-foot increments along the length were calculated and recorded for each time step. In using a one-foot increment, the goal was to capture the closest value to the maximum possible, to get the most accurate envelope. To create the envelope, the maximum and minimum shear and moment values at each increment

along the purlin across all time steps and wind angles were calculated. The Matlab files used to create the shear and moment envelopes are located in Appendix G.

Comparison with ASCE 7

One of the main goals of this project was to compare the results obtained using the wind tunnel data from the NIST database to what is currently used in ASCE 7-16. To do this comparison, the forces along each of the purlins needed to be calculated using the design loads determined using ASCE7-16 Chapter 30 for components and cladding. This is done by using the same equations in A.1 and A.2 discussed previously, while using the GC_p values specified for roofs in ASCE 7 Chapter 30. Since the purlins span multiple zones, the method of determining a stepped load used in the examples contained in the Metal Building Systems Manual was implemented (MBMA, 2018).

Calculations of the pressure coefficient values along different lengths of each purlin were calculated in Excel and then input into the member load matrices in the continuous beam analysis Matlab files. Matlab generated reactions, element forces, and displacements at the nodes as well as an overall minimum and maximum shear and moment based on the segmented elements and the shear and moment values at one-foot increments. These files used the same method as used for the analysis of wind tunnel data and were compared to the files described previously when generating the shear and moment envelopes. The Matlab files used to generate the function input are located in Appendix F. The function being called is located in Appendix E. Since these buildings and the purlin spacings are symmetric about the ridge line, for these configurations, only the purlins from one the windward eave to the ridge are calculated and can be used to create the full set. In this case, the nodes will be set at each change in load (0.2*height, 0.6*height, or 1.2*height) based on the changes in roof zones as well as a node at each support. A directionality factor of 0.85 was used per ASCE 7 recommendation for design, since this will be the same values calculated for comparison with all the angles of wind tunnel test data.

A.3 Metal Building Systems Analysis

Program Interface

Programs were developed that would allow the user to apply the wind loads determined in the wind tunnel tests to the building models commonly used by metal building designers. This project worked with Metal Building Systems by providing data that could be integrated with their design system. This was done by taking the text files containing time steps of load data and breaking this down into a series of distributed loads over a certain area for one purlin at one time step. The text files generated with this system can then

be input into this software to determine the structural response at time steps of interest. The output for this system is formatted as one file per case, where one case is one time step of one purlin at one wind angle. Each row of this file contains one of the line loads to be applied to the structure and the columns contain data on the amount of load (in pounds per linear foot) and the coordinates of the purlin that the load is acting on.

APPENDIX B: Code for accessing database files

```
clear all
clc
testname='ADW100o100D016a';
Vdesign=100; %design wind speed, mph
tribwidth=[0;1.9321;5.7963;9.3951;13.5617;18.5617;22.9784;27.3951;31.8117;
            36.2284;40;43.6515;48.0682;52.4848;56.9015;61.3182;
            66.3182;70.4649;74.0836;77.9478;80]; %tributary width of a
purlin, ft
numangles=19;
k=9;
GREGFACTORS=[0.392112615000000,0.282864238355351,0.382977213000000,0.27357646
8929597,0.422145941000000,0.281568891530027,0.437681598000000,0.2778499960547
97,0.421503034000000,0.282864238355351,0.422145941000000,0.281568891530027,0.
434699238000000,0.296072983042682,0.437681598000000,0.277849996054797,0.38297
7213000000,0.273576468929597,0.401957158000000,0.282864238355351,0.3921126150
00000,0.282864238355351,0.422145941000000,0.281568891530027,0.437681598000000
,0.277849996054797,0.382977213000000,0.289262222211370,0.382977213000000,0.30
6021605233478,0.424794520000000,0.307806910967542,0.430574079000000,0.3273044
63140754,0.397322345000000,0.309287705569391,0.434699238000000,0.313489140440
821];
GCpfactor=GREGFACTORS(k);

expname=char(testname);
exp=expname(7);
%finds zg and alpha based on exposure category (from name of file)
if isequal(exp,'s')
    zg=1200;
    alpha=7.0;
else
    zg=900;
    alpha=9.5;
end

for ANGLE_COUNTER=1:numangles
    ang=2700+(ANGLE_COUNTER-1)*50;
    name=strcat(testname,string(ang));
    %direct=unzip(strcat('D:\NIST\NIST3\ee1\',name,'.zip'),'D:\Mary\Beam
analysis\All Angles\EE1\');
    filepath=strcat('D:\Mary\Beam analysis\All Angles.v2\EE1\',name,'.HDF');
    [ALL_DATA Tap_Coordinates_3D Roof_Height_Velocity_Ratio
Tap_Max_Min_Mean_RMS Building_Height_Ft
Wind_Speed_Profile]=Read_Nistdata(filepath);

    [~,J]=(min(abs(ALL_DATA.RoofHeightFt*12*2.54/100-
Wind_Speed_Profile(1,:))));
    [~,JJ]=(min(abs(10-Wind_Speed_Profile(1,:))));
    SUB_CONV_FACTOR=1/((Wind_Speed_Profile(3,J(1))*3/100+1)^2);
    V_V10RATIO=Wind_Speed_Profile(2,J(1))./Wind_Speed_Profile(2,JJ(1));
%ratio of speed at roof height vs reference height
    a=max([min([0.4*ALL_DATA(1).RoofHeightFt
0.1*min([ALL_DATA(1).BuildingLengthFt ALL_DATA(1).BuildingWidthFt])]) 3
0.04*min([ALL_DATA(1).BuildingLengthFt ALL_DATA(1).BuildingWidthFt])]);
    %dimension a in ASCE 7
```

```
roof=surface_data(ALL_DATA,Tap_Coordinates_3D,Tap_Max_Min_Mean_RMS,Roof_Heigh
t_Velocity_Ratio,[5 6]);
    for h=1:length(roof)
        ROOF.Cp_data(:,h)=roof(h).Time_Series;
    end
    [ROOF.trib,
ROOF.taprect]=trib_area(roof,roof(1).BuildingLengthFt,roof(1).BuildingWidthFt
,2,1);
    ROOF.width=roof(1).BuildingWidthFt;
    ROOF.length=roof(1).BuildingLengthFt;
    ROOF.height=roof(1).RoofHeightFt;
    ROOF.slope=roof(1).RoofSlopein12;
    ROOF.Tap_Coordinates_3D=Tap_Coordinates_3D;

    OUTPUT{k,ANGLE_COUNTER}.V_V10RATIO=V_V10RATIO;
    OUTPUT{k,ANGLE_COUNTER}.SUB_CONV_FACTOR=SUB_CONV_FACTOR;
    OUTPUT{k,ANGLE_COUNTER}.width=ROOF.width;
    OUTPUT{k,ANGLE_COUNTER}.length=ROOF.length;
    OUTPUT{k,ANGLE_COUNTER}.height=ROOF.height;
    OUTPUT{k,ANGLE_COUNTER}.a=a;

    rootdir='D:\Mary\Beam analysis\All Angles.v2\EE1_Results';
    Folder1=string(ang);
    mkdir('EE1_Results',Folder1);

    for ii=1:(size(tribwidth,1)-1)

        Folder2=strcat('Purlin',string(ii));
        mkdir(strcat(rootdir,'\',Folder1),Folder2);

        Zroof=[tribwidth(ii) 0 tribwidth(ii+1)-tribwidth(ii)
OUTPUT{k,ANGLE_COUNTER}.length];
        INTERCECTGRID=single(rectint(ROOF.taprect,Zroof));
        temp2=ROOF.trib(INTERCECTGRID~=0,2:3);
        temp3=sort(unique(temp2(:,2)),'descend');
        temp4=[temp3(1:end-1)+diff(temp3)/2; 0];
        temp5=-diff([125; temp4]);
        SIZE=size(temp4,1);
        Zroof2=zeros(SIZE,4);
        Zroof2(:,2)=temp4;
        Zroof2(:,4)=temp5;
        Zroof2(:,1)=tribwidth(ii);
        Zroof2(:,3)=tribwidth(ii+1)-tribwidth(ii);
        INTERCECTGRID=single(rectint(ROOF.taprect,Zroof2));

INTERCECTGRID=INTERCECTGRID./repmat(sum(INTERCECTGRID),size(INTERCECTGRID,1),
1);
        temp_data=ROOF.Cp_data*INTERCECTGRID;

        header=string(transpose(Zroof2(:,2)));

        %calculates Kz based on roof height and zg and alpha
        if ROOF.height<15
            Kz=2.01*(15/zg)^(2/alpha);
        else
            Kz=2.01*(ROOF.height/zg)^(2/alpha);
```

```
        end
        Kd=1;    %Use Kd=0.85 if needed
        qz=0.00256*Kz*Kd*Vdesign^2;
        GCp=temp_data*GCpfactor;
        p=qz*GCp;                   %in psf

        Force=p*(tribwidth(ii+1)-tribwidth(ii));              %in plf

        filen1='Cp.txt';
        filen2='Force.txt';
        fileID1=fopen(fullfile(rootdir,Folder1,Folder2,filen1),'w+');

        formatting='%g\t';
        for jj=1:size(temp_data,2)-1
            formatting=strcat(formatting,' %g\t');
        end
        fprintf(fileID1,strcat(formatting,'\n'),header);
        for ll=1:size(temp_data,1)
            fprintf(fileID1,strcat(formatting,'\n'),temp_data(ll,:));
        end

        fileID2=fopen(fullfile(rootdir,Folder1,Folder2,filen2),'w+');
        fprintf(fileID2,strcat(formatting,'\n'),header);
        for mm=1:size(Force,1)
            fprintf(fileID2,strcat(formatting,'\n'),Force(mm,:));
        end
        fclose(fileID1);
        fclose(fileID2);
    end
end
```

APPENDIX C: Code for creating pressure coefficient and force plots

```
clear all
clc

tribwidth=[0;1.9321;5.7963;9.3951;13.5617;18.5617;22.9784;27.3951;31.8117;
            36.2284;40;43.6515;48.0682;52.4848;56.9015;61.3182;
            66.3182;70.4649;74.0836;77.9478;80]; %tributary width of a
purlin, ft
numangles=19;
rooflength=125;
numtimes=15;

for ANGLE_COUNTER=1:numangles

    ang=2700+(ANGLE_COUNTER-1)*50;

    for ii=1:(size(tribwidth,1)-1)

        rootdir='D:\Mary\Beam analysis\All Angles.v2\EE1_Results';
        Folder1=string(ang);
        Folder2=strcat('Purlin',string(ii));
        filen1='Cp.txt';
        filen2='Force.txt';

        filename1 = strcat(rootdir,'\',Folder1,'\',Folder2,'\',filen1);
        filename2 = strcat(rootdir,'\',Folder1,'\',Folder2,'\',filen2);
        delimiterIn = '\t';
        headerlinesIn = 0;
        Cp = importdata(filename1,delimiterIn,headerlinesIn);
        F = importdata(filename2,delimiterIn,headerlinesIn);
        [l,m]=size(Cp);
        taparea=[rooflength Cp(1,:)];
        Cp_data=Cp(2:l,:);
        F_data=F(2:l,:);

        plot_data=Cp_data(1:numtimes,:);
        plot_data=transpose(plot_data);
        [n,p]=size(plot_data);
        t=zeros(n,1);
        plotdat=zeros(n,p);
        Fplot=zeros(n,p);
        for i=1:n
            a=2*(i-1)+1;
            b=2*(i-1)+2;
            t(a,1)=taparea(i);
            t(b,1)=taparea(i+1);
            plotdat(a,:)=plot_data(i,:);
            plotdat(b,:)=plot_data(i,:);
        end
        plot(t,plotdat)
        xlabel('Distance along Purlin (ft)')
        ylabel('Cp')
        xlim([0 125])
        savefig(strcat(rootdir,'\',Folder1,'\',Folder2,'\CpPlot'));
```

```
        F_plot=F_data(1:numtimes,:);
        F_plot=transpose(F_plot);

        for i=1:n
            a=2*(i-1)+1;
            b=2*(i-1)+2;
            Fplot(a,:)=F_plot(i,:);
            Fplot(b,:)=F_plot(i,:);
        end
        plot(t,Fplot)
        xlabel('Distance along Purlin (ft)')
        ylabel('F, plf')
        xlim([0 125])
        savefig(strcat(rootdir,'\',Folder1,'\',Folder2,'\FPlot'));
    end
end
```

APPENDIX D: Code for creating continuous beam input files for wind tunnel tests

```
clear all
clc

interiorsupports=[25;50;75;100]; %in feet
tribwidth=[0;1.9321;5.7963;9.3951;13.5617;18.5617;22.9784;27.3951;31.8117;
            36.2284;40;43.6515;48.0682;52.4848;56.9015;61.3182;
            66.3182;70.4649;74.0836;77.9478;80]; %tributary width of a
purlin, ft
numangles=19;
rooflength=125;
numtimes=15;

ANGLE_COUNTER=1;

for ANGLE_COUNTER=1:numangles

    ang=2700+(ANGLE_COUNTER-1)*50;
    PURLIN_COUNTER=1;
    for PURLIN_COUNTER=1:(size(tribwidth,1)-1)

        rootdir='D:\Mary\Beam analysis\All Angles.v2\EE1_Results';
        Folder1=string(ang);
        Folder2=strcat('Purlin',string(PURLIN_COUNTER));
        filen2='Force.txt';
        filename2 = strcat(rootdir,'\',Folder1,'\',Folder2,'\',filen2);
        delimiterIn = '\t';
        headerlinesIn = 0;

        F = importdata(filename2,delimiterIn,headerlinesIn);
        [l,m]=size(F);
        taparea=[rooflength F(1,:)];
        F_data=F(2:l,:); %in pounds per linear foot
        F_dataflip=flip(F_data,2);

        X=transpose(taparea);
        X=[X;interiorsupports];
        X=sort(X,'ascend'); %in feet

        % PROP=[Moment of inertia, Shear area]
        PROP=[9.177, 0.976]; %In inches
        % MAT= [Modulus of Elasticity,coefficent of thermal expansion,
Poisson's ratio]
        MAT=[29000,0.00000108,.27];

        nnodes=size(X,1);
        nels=nnodes-1;

        % Restraint Matrix is given by
        % R=[X displacement , Y displacement restraint]

        R=[1,0;
            zeros(nnodes-2,2);
```

```
            1,0];
        P=zeros(nnodes,2);
        % Connectivity Matrix is given by
        % CON=[iend,jend,material property no:,section property no:,member
load type]
        CON=zeros(nels,5);

        ii=1;
        for i=1:nels
            CON(i,:)=[i, i+1,  1,  1,  0];
            if ismember(X(i),interiorsupports)
                CON(i,5)=ii-1;
                R(i,:)=[1,0];
            else
                CON(i,5)=ii;
                ii=ii+1;
            end
        end

        ntimes=size(F_data,1);

        X=X*12; %convert to inches
        TIME_COUNTER=1;
        for TIME_COUNTER=1:ntimes
            %[uniform load (kip/in), upto 3 point load, fraction of distance
from iend ]
            for j=1:size(F_data,2)
                % For member load type zero indicate there is no member load
where as any
                % number greater than zero indicate the corresponding row in
the member
                % load matrix.
                MLOAD(j,:)=[F_dataflip(TIME_COUNTER,j)/12/1000,   0,  0,  0,
0,  0,  0];
            end
            % The number of segments to which the structure needs to be
divided
            % plot the deflected and undeflected shape
            nsegD=[100];
            % The magnification of displacement for plotting the shape of the
structure.
            % The magnification factor of 0 is used to plot the undeflected
shape and
            % the magnification factor greater than 1 is used to plot the
undflected shape.

            mg=[1,2];

            % For the given example the undeflected shape is plotted with the
            % magnification factor  of 10

            % The number segments to which the elements has to be divided to
plot the
            % bending moment diagram is given by
            nsegBM=[100];
```

```
            % The side on which the bending moment digarm needs to be plotted
is given
            % by
            SIDE='T';
            % The character T represents tension side and the character C
represenst
            % the compression side


[L,ID,FVEC,khat,KG,FEF,Q,D,UOUT,F,S,React,EQ,FullMoment,FullShear,FullPlotX]=
Beam_Functions(CON,X,R,P,MAT,PROP,MLOAD,nsegD,mg,nsegBM,SIDE);

%[L,ID,FVEC,khat,KG,FEF,Q,D,UOUT,F,S,React,EQ,ESHAPE,SHEAR,BMD]=Beam_Function
s(CON,X,R,P,MAT,PROP,MLOAD,nsegD,mg,nsegBM,SIDE,rootdir,Folder1,Folder2,jj);
            kk=1;
            jj=1;
            for k=1:nnodes
                if abs(React(k,1))>0.00001
                    R_Force(TIME_COUNTER,kk)=React(k,1);
                    kk=kk+1;
                end
                if abs(React(k,2))>0.00001
                    R_Moment(TIME_COUNTER,jj)=React(k,2);
                    jj=jj+1;
                end
                D_VERT(TIME_COUNTER,k)=UOUT(k,1);
                D_ROT(TIME_COUNTER,k)=UOUT(k,2);
            end
            for l=1:nels
                V_ELEM_i(TIME_COUNTER,l)=F(1,1,l);
                V_ELEM_j(TIME_COUNTER,l)=F(3,1,l);
                M_ELEM_i(TIME_COUNTER,l)=F(2,1,l);
                M_ELEM_j(TIME_COUNTER,l)=F(4,1,l);
            end

            %MaxMin file will be 4 columns, 1 row per time step. [MaxV,
            %MaxM, MinV, MinM]
            MaxMin(TIME_COUNTER,2)=max(FullMoment);
            MaxMin(TIME_COUNTER,1)=max(FullShear);
            MaxMin(TIME_COUNTER,4)=min(FullMoment);
            MaxMin(TIME_COUNTER,3)=min(FullShear);

            FullX=FullPlotX/12;

            for mm=1:125
                [val,idx]=min(abs(FullX-mm));
                FullX2(mm)=FullX(idx);
                FullV2(mm)=FullShear(idx);
                FullM2(mm)=FullMoment(idx);
            end

            FullX3(TIME_COUNTER,:)=FullX2;
            FullV3(TIME_COUNTER,:)=FullV2;
            FullM3(TIME_COUNTER,:)=FullM2;

        end
```

```
filen='Reactions.txt';
fileID=fopen(fullfile(rootdir,Folder1,Folder2,filen),'w+');
formatting='%g\t';
for m=1:size(R_Force,2)-1
    formatting=strcat(formatting,' %g\t');
end
for mm=1:size(R_Force,1)
    fprintf(fileID,strcat(formatting,'\n'),R_Force(mm,:));
end

filen='VerticalDisp.txt';
fileID=fopen(fullfile(rootdir,Folder1,Folder2,filen),'w+');
formatting='%g\t';
for n=1:size(D_VERT,2)-1
    formatting=strcat(formatting,' %g\t');
end
for nn=1:size(D_VERT,1)
    fprintf(fileID,strcat(formatting,'\n'),D_VERT(nn,:));
end

filen='RotationalDisp.txt';
fileID=fopen(fullfile(rootdir,Folder1,Folder2,filen),'w+');
formatting='%g\t';
for o=1:size(D_ROT,2)-1
    formatting=strcat(formatting,' %g\t');
end
for oo=1:size(D_ROT,1)
    fprintf(fileID,strcat(formatting,'\n'),D_ROT(oo,:));
end

filen='ShearIEnd.txt';
fileID=fopen(fullfile(rootdir,Folder1,Folder2,filen),'w+');
formatting='%g\t';
for p=1:size(V_ELEM_i,2)-1
    formatting=strcat(formatting,' %g\t');
end
for pp=1:size(V_ELEM_i,1)
    fprintf(fileID,strcat(formatting,'\n'),V_ELEM_i(pp,:));
end

filen='ShearJEnd.txt';
fileID=fopen(fullfile(rootdir,Folder1,Folder2,filen),'w+');
formatting='%g\t';
for q=1:size(V_ELEM_j,2)-1
    formatting=strcat(formatting,' %g\t');
end
for qq=1:size(V_ELEM_j,1)
    fprintf(fileID,strcat(formatting,'\n'),V_ELEM_j(qq,:));
end

filen='MomentIEnd.txt';
fileID=fopen(fullfile(rootdir,Folder1,Folder2,filen),'w+');
formatting='%g\t';
for r=1:size(M_ELEM_i,2)-1
    formatting=strcat(formatting,' %g\t');
end
for rr=1:size(M_ELEM_i,1)
```

```
            fprintf(fileID,strcat(formatting,'\n'),M_ELEM_i(rr,:));
        end

        filen='MomentJEnd.txt';
        fileID=fopen(fullfile(rootdir,Folder1,Folder2,filen),'w+');
        formatting='%g\t';
        for q=1:size(M_ELEM_j,2)-1
            formatting=strcat(formatting,' %g\t');
        end
        for qq=1:size(M_ELEM_j,1)
            fprintf(fileID,strcat(formatting,'\n'),M_ELEM_j(qq,:));
        end

        filen='FullMoment.txt';
        fileID=fopen(fullfile(rootdir,Folder1,Folder2,filen),'w+');
        formatting='%g\t';
        for r=1:size(FullM3,2)-1
            formatting=strcat(formatting,' %g\t');
        end
        for rr=1:size(FullM3,1)
            fprintf(fileID,strcat(formatting,'\n'),FullM3(rr,:));
        end
        filen='FullX.txt';
        fileID=fopen(fullfile(rootdir,Folder1,Folder2,filen),'w+');
        formatting='%g\t';
        for s=1:size(FullX3,2)-1
            formatting=strcat(formatting,' %g\t');
        end
        for ss=1:size(FullX3,1)
            fprintf(fileID,strcat(formatting,'\n'),FullX3(ss,:));
        end
        filen='FullShear.txt';
        fileID=fopen(fullfile(rootdir,Folder1,Folder2,filen),'w+');
        formatting='%g\t';
        for t=1:size(FullV3,2)-1
            formatting=strcat(formatting,' %g\t');
        end
        for tt=1:size(FullV3,1)
            fprintf(fileID,strcat(formatting,'\n'),FullV3(tt,:));
        end
        filen='MaxMin.txt';
        fileID=fopen(fullfile(rootdir,Folder1,Folder2,filen),'w+');
        formatting='%g\t';
        for t=1:size(MaxMin,2)-1
            formatting=strcat(formatting,' %g\t');
        end
        for tt=1:size(MaxMin,1)
            fprintf(fileID,strcat(formatting,'\n'),MaxMin(tt,:));
        end
        fclose('all');
    end
end
```

APPENDIX E: Function for continuous beam analysis

```
function
[L,ID,FVEC,khat,KG,FEF,Q,D,UOUT,F,S,React,EQ,FullMoment,FullShear,FullPlotX]
= Beam_Functions(CON,X,R,P,MAT,PROP,MLOAD,nsegD,mg,nsegBM,SIDE)
%function [L,ID,FVEC,khat,KG,FEF,Q,D,UOUT,F,S,React,EQ,ESHAPE,SHEAR,BMD] =
Beam_Functions(CON,X,R,P,MAT,PROP,MLOAD,nsegD,mg,nsegBM,SIDE,rootdir,Folder1,
Folder2,jj)

% The above expression is the function name with the input and the output
% arguments. The name of the function is Beam_functions. The input arguments
% are given in a separate Matlab script with the name as
'Beam_Input_WithSheardeformations'.

% The arguments in the left side represents the output and those on the
% right side represents the input arguments.

% The output quantities of interest are

% L  - Length of individual elements
% ID - ID matrix to automatically number the degree of freedom
% FVEC -Nodal force vector
% khat - element stiffness matrix in local cordinates
% KG - global stiffness matrix
% FEF - Fixed end in element local cordinates
% Q   - Fixed end force vector
% D  - Displacement Vector
% UOUT - Displacement formatted to table form
% F  -  Local element forces
% S- Spring forces
% React-Support reactions in global cordinates
% EQ - Checking the global equilibrium
% ESHAPE - Plot the deflected and undeflected shape



% The Matlab routines are given below.

% the rows and columns of the CON matrix are stored in nels and cols

[nels,cols]=size(CON);

% calculate the element length

for n=1:nels
    i=CON(n,1);
    j=CON(n,2);
    dx=X(j,1)-X(i,1);
    L(n)=sqrt(dx.*dx);

end

% Create the equation number array ID

[nr,nc]=size(R);
```

```
% The size of the restraint matrix is stored in nr and nc

eqn=0;

for i=1:nr
    for j=1:nc
        ID(i,j)=0;
        if R(i,j)<=0
            eqn=eqn+1;
            ID(i,j)=eqn;

        end

    end
end

% The routine assigns a zero for restraint degree of freedom . The
% unrestraint degree of freedom are numbered starting from node 1. .


% Create the nodal force vector

% The nodal force vector will have the size of the maximum degreee of
% freedom which is obtained from the iD matrix. The given routine will
% convert the nodal force matrix into a force vector.

[nr,nc]=size(ID);
for i=1:nr
    for j=1:nc
        if ID(i,j)~=0
            k=ID(i,j);
            FVEC(k,1)=P(i,j);
        end
    end
end


% Create the 4 x 4 element local stiffness matrix khat

for n=1:nels
    matno=CON(n,3);
    propno= CON(n,4);
    E=MAT(matno,1);
    v=MAT(matno,3);
    I=PROP(propno);
    Av=PROP(propno,2);
    len=L(n);
    EI=E*I;
    G=E/(2*(1+v));
    d=zeros(2,2);
    if Av==0
      d(1,1)=len^3/(3*EI);
    end
    if Av~=0
      d(1,1)=(len^3/(3*EI))+(len/(G*Av));
    end
   d(1,2)=len^2/(2*EI);
```

```
   d(2,1)=d(1,2);
   d(2,2)=len/(EI);
   a=[-1,-len,1,0;
       0,-1,0,1];
   k=a'*(inv(d))*a;
   khat(:,:,n)=k;

end
% The given routine calculates the element stiffness matrix and stores it
% as a nested array in the matrix khat. Thus the matrix khat contains nels
% number of subarray where nels is the number of elements of the system.

% Since the local axis of beams are parallel to the global X axis , no need
% to form transformation matrix from level 2 to level 3. The element
stiffness
% in the local and global cordinates are the same.

% Assemble the local stiffness matrix to form the global stiffness matrix

neq=max(max(ID));
% The maximum number in the ID matrix is stored in the variable neq. This
% is equal to the total degree of freedom of the structure.

KG=zeros(neq,neq);

for n=1:nels
    K=khat(:,:,n);
    iend=CON(n,1);
    jend=CON(n,2);
    gn(1)=ID(iend,1);
    gn(2)=ID(iend,2);
    gn(3)=ID(jend,1);
    gn(4)=ID(jend,2);
    for i=1:4
        for j=1:4
            r=gn(i);
            s=gn(j);
            test=r*s;
            if test~=0
                Kadd=K(i,j);
                KG(r,s)=KG(r,s)+Kadd;

            end
        end
    end
end
% The global stiffness matrix is formed by directly assembling the
% stiffness matrix from level 2 using the ID matrix.



% Add the support spring stiffness

   [nr,nc]=size(R);
   for i=1:nr
       for j=1:nc
           if R(i,j)<0
```

```
                S=-R(i,j);
                eqn=ID(i,j);
                KG(eqn,eqn)=KG(eqn,eqn)+S;

            end
        end
    end

    % The structure can be modelled with springs attached to supports. For
    % example when the structure rests on an elastic foundation the support
    % can be idealised as springs with some constant stiffness value. Thus
    % these stiffness has to be added to the structure global stiffness
    % matrix. A negative number in the restraint matrix is used to represent
    % the spring stiffness. In later routines for frames, these is modified
    % and complex numbers are used to represent spring stiffness.


% Calculate the fixed end forces for each element for the following loading

% [ uniformly distributed load, Point loads upto 3 in an element]


for n=1:nels
    loadno=CON(n,5);
    matno=CON(n,3);
    propno=CON(n,4);
    E=MAT(matno,1);
    v=MAT(matno,3);
    G=E/(2*(1+v));
    Av=PROP(propno,2);
    GA=G*Av;
    FDT(1,1)=0;
    FDT(2,1)=0;
    FDT(3,1)=0;
    FDT(4,1)=0;
    if loadno~=0
        W=MLOAD(loadno,1);
        len=L(n);
        FDT(1,1)=-(W*len)/2;
        FDT(2,1)=(-W*(len^2))/12;
        FDT(3,1)=FDT(1,1);
        FDT(4,1)=-FDT(2,1);

    for j=1:3
        PL=MLOAD(loadno,2*j);
        alpha= MLOAD(loadno,2*j+1);
        a=alpha*len;
        b=len-a;
        if G*Av==0
            GA=(10^10)*E*I;
        end
        delta=(((PL*(alpha^2)*(len^3)/(2*E*I))*(1-
(alpha/3)))+((PL*alpha*len)/(GA)));
        r=PL*(alpha^2)*(len^2)/(2*E*I);
        d(1,1)=(len^3/(3*E*I))+(len/(G*Av));
```

```
        d(1,2)=len^2/(2*EI);
        d(2,1)=d(1,2);
        d(2,2)=len/(E*I);
        displace(1,1)=delta;
        displace(2,1)=r;
        fef=(inv(d))*(displace);
        fef=-fef;
        f(1,1)=-(PL+fef(1,1));
        f(2,1)=(-PL*alpha*len)-(fef(1,1)*len)-fef(2,1);
        f(3,1)=fef(1,1);
        f(4,1)=fef(2,1);


        FDT(1,1)=FDT(1,1)+f(1,1);
        FDT(2,1)=FDT(2,1)+f(2,1);
        FDT(3,1)=FDT(3,1)+f(3,1);
        FDT(4,1)=FDT(4,1)+f(4,1);
    end

     end
            FEF(:,:,n)=[FDT];
end

% The fixed end force for each element is a 4 x 1 matrix . The fixed end
% forces are stored as a submatrix in the matrix FEF.


% Assemble the fixed end force to form the global fixed end force vector


neq=max(max(ID));
[nels,cols]=size(CON);
for i=1:neq
    Q(i,1)=0;
end

for i=1:nels
    q=FEF(:,:,i);
    iend=CON(i,1);
    jend=CON(i,2);
    geq1=ID(iend,1);
    geq2=ID(iend,2);
    geq3=ID(jend,1);
    geq4=ID(jend,2);
    if geq1~=0
        Q(geq1,1)=Q(geq1,1)+q(1);
    end
    if geq2~=0
        Q(geq2,1)=Q(geq2,1)+q(2);
    end
    if geq3~=0
        Q(geq3,1)=Q(geq3,1)+q(3);
    end
   if geq4~=0
        Q(geq4,1)=Q(geq4,1)+q(4);
   end
end
```

```
Q=-Q;

% The fixed end force vector in global cordinates is also calculated by a
% direct assembly of fixed end forces from the level 2 using the ID matrix.
% The sign of the fixed end forces is changed at the end to convert it into
% an equivalent nodal force.


% Calculate the nodal displacments

D=inv(KG)*(FVEC+Q);

% The above is an equilibrium representation of the forces. The output
% obtained from this routine is in the form of a vector which represents
% the displacements at each degree of freedom.


% Format the displacements into tabular form


[nr,nc]=size(ID);
for i=1:nr
    for j=1:nc
        k=ID(i,j);
        UOUT(i,j)=0;
        if k~=0
            UOUT(i,j)=D(k,1);
       end
    end
end

% Calculate the element forces


for n=1:nels
    iend=CON(n,1);
    jend=CON(n,2);
    u(1,1)=UOUT(iend,1);
    u(2,1)=UOUT(iend,2);
    u(3,1)=UOUT(jend,1);
    u(4,1)=UOUT(jend,2);
    f=((khat(:,:,n))*u)+FEF(:,:,n);
     F(:,:,n)=f;

end

 % Remember to add back the element fir=xed end forces in the local
 % cordinates.


% Calculate the spring forces

   [nr,nc]=size(R);
   S=zeros(nr,nc);
   for i=1:nr
       for j=1:nc
```

```
            k=R(i,j);
            if k<0
                S(i,j)=-k*UOUT(i,j);

            end
        end
    end


% Calculate the reactions
[nels,cols]=size(CON);
[nodes,cols]=size(R);
REACT=zeros(nodes,2);
for n=1:nels
    s1=F(:,:,n);
    s(1,1)=s1(1,1);
    s(2,1)=s1(2,1);
    s(3,1)=s1(3,1);
    s(4,1)=s1(4,1);
    iend=CON(n,1);
    jend=CON(n,2);
    REACT(iend,1)=REACT(iend,1)+s(1,1);
    REACT(iend,2)=REACT(iend,2)+s(2,1);
    REACT(jend,1)=REACT(jend,1)+s(3,1);
    REACT(jend,2)=REACT(jend,2)+s(4,1);

end

React=REACT-P;

[nodes,cols]=size(R);
EQ=zeros(1,2);
for i=1:nodes
    EQ(1,1)=EQ(1,1)+REACT(i,1);

end

% The routine checks for the global equilibrium of forces in the vertical
direction.
% The result of this routine should give zero. The react used in the routine
% is the reactions at the nodes before deducting the nodal forces.

% Plot the deflected and undeflected shape of the given continuous beam

for c=1:2
    mag=mg(c);
for n=1:nels
    iend=CON(n,1);
    jend=CON(n,2);
    xi=X(iend);

    Len=L(n);
    dx=Len/nsegD;
    U1=UOUT(iend,1);
    U2=UOUT(iend,2);
    U3=UOUT(jend,1);
    U4=UOUT(jend,2);
```

```
    nload=CON(n,5);
    %for i=1:nsegD+1
        %x=(i-1)*dx;
        %y(i,1)=(((2*(x^3))/(Len^3))-((3*(x^2))/(Len^2))+1)*(U1*mag);
        %y(i,1)=y(i,1)+((((x^3))/(Len^2))-((2*(x^2))/Len)+x)*(U2*mag);
        %y(i,1)=y(i,1)+(((3*(x^2))/(Len^2))-((2*(x^3))/(Len^3)))*(U3*mag);
        %y(i,1)=y(i,1)+(((x^3)/(Len^2))-((x^2)/Len))*(U4*mag);

        %if nload~=0
            %nmat=CON(n,3);
            %nprop=CON(n,4);
            %EI=(MAT(nmat,1))*(PROP(nprop));
            %w=MLOAD(nload,1);
            %y(i,1)=y(i,1)+((w*x^2)/(24*EI))*((Len-x)^2);
            %for np=1:3
                %P=MLOAD(nload,2*np);
                %a=Len*(MLOAD(nload,((2*np)+1)));
                %b=Len-a;
                %if x<=a
                    %y(i,1)=y(i,1)+(P*(b^2)*(x^2))/(6*EI*(Len^3))*((3*a*Len)-
(3*a*x)-(b*x));

                %end
                %if x>a
                    %x2=Len-x;
                    %b2=a;
                    %a2=b;

%y(i,1)=y(i,1)+(P*(b2^2)*(x2^2))/(6*EI*(Len^3))*((3*a2*Len)-(3*a2*x)-
(b2*x2));
                %end
            %end

            %s(i,1)=x+xi;
        %end
    end

        %if n==1
            %Rx=s;
            %Ry=y;
        %end

        %if n>1
            %Rx=[Rx;s];
            %Ry=[Ry;y];
        %end
    end


%ESHAPEX(:,:,c)=Rx;
%ESHAPEY(:,:,c)=Ry;
%end

% For the given structure two deflected shapes are plotted . The
% undeflected shape is plotted using the X cordinate of the structure.
```

```
%deflex1=ESHAPEX(:,:,1); % The first vector in the matrix 'und' is stored as
a vector 'undx'
%defley1=ESHAPEY(:,:,1); % The second vector in the matrix 'und' is stored as
a vector 'undy'


%deflex2=ESHAPEX(:,:,2); % The first vector in the matrix 'defle' is stored
as a vector 'deflex'
%defley2=ESHAPEY(:,:,2); % The first vector in the matrix 'defle' is stored
as a vector 'defley'


%ESHAPE=plot(X,0*X,deflex1,defley1,deflex2,defley2);
%savefig(strcat(rootdir,'\',Folder1,'\',Folder2,'\deflectedshape',string(jj),
'.fig'))
% Plot the shear force diagram


%for n=1:nels
    %iend=CON(n,1);
    %jend=CON(n,2);
    %nload=CON(n,5);
    %xi=X(iend);
    %Len=L(n);
    %EF=F(:,:,n);
    %Vi=EF(1);
    %Vj=EF(3);
    %if nload==0
        %x(1,1)=xi;
        %x(2,1)=xi;
        %x(3,1)=x(2,1);
        %x(4,1)=x(3,1);
        %x(5,1)=x(4,1);
        %x(6,1)=x(5,1);
        %x(7,1)=x(6,1);
        %x(8,1)=x(7,1);
        %x(9,1)=x(1,1)+Len;
        %x(10,1)=x(9,1);
        %v(1,1)=Vi;
        %v(2,1)=v(1,1);
        %v(3,1)=v(2,1);
        %v(4,1)=v(3,1);
        %v(5,1)=v(4,1);
        %v(6,1)=v(5,1);
        %v(7,1)=v(6,1);
        %v(8,1)=v(7,1);
        %v(9,1)=v(8,1);
        %v(10,1)=v(9,1);
    %end


    %if loadno~=0
        %w=MLOAD(nload,1);
        %x(1,1)=xi;
        %x(2,1)=xi;
        %x(3,1)=x(1,1)+Len*MLOAD(nload,3);
        %x(4,1)=x(3,1);
```

```
        %x(5,1)=x(4,1);
        %if MLOAD(nload,5)~=0
            %x(5,1)=x(1,1)+Len*MLOAD(nload,5);
        %end
             %x(6,1)=x(5,1);
             %x(7,1)=x(6,1);
        %if MLOAD(nload,7)~=0
            %x(7,1)=x(1,1)+Len*MLOAD(nload,7);
        %end
        %x(8,1)=x(7,1);
        %x(9,1)=x(1,1)+Len;
        %x(10,1)=x(9,1);
        %v(1,1)=Vi;
        %v(2,1)=v(1,1);
        %v(3,1)=v(2,1)+w*(x(3,1)-x(2,1));
        %v(4,1)=v(3,1)+MLOAD(nload,2);
        %v(5,1)=v(4,1)+w*(x(5,1)-x(4,1));
        %v(6,1)=v(5,1)+MLOAD(nload,4);
        %v(7,1)=v(6,1)+w*(x(7,1)-x(6,1));
        %v(8,1)=v(7,1)+MLOAD(nload,6);
        %v(9,1)=v(8,1)+w*(x(9,1)-x(8,1));
        %v(10,1)=v(9,1);

    %end

    %if n==1
        %vv=v;
        %xx=x;
    %end

    %if n>1
        %vv=[vv;v];
        %xx=[xx;x];
    %end

    %R=[xx,vv];

%end

%PlotV=[R(:,1),R(:,2)];
%SHEAR=plot(X,0*X,R(:,1),R(:,2));
%savefig(strcat(rootdir,'\',Folder1,'\',Folder2,'\shear',string(jj),'.fig'))
% Plot the bending moment diagram

for n=1:nels
    iend=CON(n,1);
    jend=CON(n,2);
    xi=X(iend);
    Len=L(n);
    dx=Len/nsegBM;
    BM=F(:,:,n);
    Mi=BM(2);
    Mj=BM(4);
    Vi=BM(1);
    Vj=BM(3);
    nload=CON(n,5);
    if SIDE=='T'
```

```
    Mj=-Mj;
    Vj=-Vj;
end
if SIDE=='C'
    Mi=-Mi;
    Vi=-Vi;
end
dM=(Mj-Mi)/nsegBM;
dV=(Vj-Vi)/nsegBM;
for i=1:(nsegBM+1)
    yM(i,1)=Mi+((i-1)*dM);
    yV(i,1)=Vi+((i-1)*dV);
    s=(i-1)*dx;
    x(i,1)=xi+s;
    if nload~=0
        w=MLOAD(nload,1);
        if SIDE=='C'
            Mw=-((w*s)*(Len-s))/2;
        end
        if SIDE=='T'
            Mw=((w*s)*(Len-s))/2;
        end
        yM(i,1)=yM(i,1)+Mw;
        for load=1:3
            P=MLOAD(nload,2*load);
            a=(MLOAD(nload,((2*load)+1)))*Len;
            b=Len-a;
            if s<=a
                if SIDE=='C'
                    Mp=-(P*b*s)/Len;
                end
                if SIDE=='T'
                    Mp=(P*b*s)/Len;
                end
                yM(i,1)=yM(i,1)+Mp;
            end
            if s>a
                if SIDE=='C'
                    Mp=-((P*a)*(Len-s))/Len;
                end
                if SIDE=='T'
                    Mp=((P*a)*(Len-s))/Len;
                end
                yM(i,1)=yM(i,1)+Mp;
            end
        end
    end
end
r=[yM];
q=[yV];
if n==1
    R=r;
    FullX=x;
end
if n>1
    R=[R;r];
    FullX=[FullX;x];
```

```
    end
    if n==1
        Q=q;
    end
    if n>1
        Q=[Q;q];
    end

end
    FullMoment=[R];
    FullShear=[Q];
    FullPlotX=[FullX];

%BMD=plot(X,0*X,R(:,1),R(:,2));
%savefig(strcat(rootdir,'\',Folder1,'\',Folder2,'\moment',string(jj),'.fig'))
```

APPENDIX F: Code for creating continuous beam function inputs for ASCE-7 Loads

```
clear all
clc

interiorsupports=[25;50;75;100]; %in feet
Vdesign=100; %design wind speed, mph
exp='o';
Roof_Height=16; %in feet
%the purlins on this building are symmetric. Because of this, the loads
%will be calculated from the eave to the ridge and the loads for purlin 1
%will be equivalent to edge purlin on leeward side, 2 to 19, 3 to 18, etc.
tribwidth=[0;1.9321;5.7963;9.3951;13.5617;18.5617;22.9784;27.3951;31.8117;
            36.2284;40;]; %tributary width of a purlin, ft
numangles=19;
rooflength=125; %in feet
numtimes=15;
EWA=25*(25/3);  %in feet

%finds zg and alpha based on exposure category (from ASCE 7)
if isequal(exp,'s')
    zg=1200;
    alpha=7.0;
else
    zg=900;
    alpha=9.5;
end
%calculates Kz based on roof height and zg and alpha (from ASCE 7)
if Roof_Height<15
    Kz=2.01*(15/zg)^(2/alpha);
else
    Kz=2.01*(Roof_Height/zg)^(2/alpha);
end
Kd=0.85; %per criteria in ASCE 7
qz=0.00256*Kz*Kd*Vdesign^2; %equation for velocity pressure based on
    %ASCE 7

X=[0;3.2;9.6;19.2;25;50;75;100;105.8;115.4;121.8;125]; %in feet
X=X*12; %convert to inches

CpTW=[-3.48314, -3.48314,-3.09417,-3.09417, -3.09417, -3.48314, -3.48314;
      -6.96628, -6.44359, -6.18834, -6.18834, -6.28834, -6.44359, -6.96628;
      -6.48783, -5.76331, -5.76331, -5.76331, -5.76331, -5.76331, -6.48783;
      -6.71387, -6.67262, -4.91052, -4.91052, -4.91052, -6.67262, -6.71387;
      -8.00727, -8.00727, -5.78336, -5.78336, -5.78336, -8.00727, -8.00727;
      -7.07314, -7.07314, -5.10867, -3.53666, -5.10867, -7.07314, -7.07314;
      -7.07314, -7.07314, -5.10867, -3.2711, -5.10867, -7.07314, -7.07314;
      -7.07298, -7.07298, -5.10855, -3.27103, -5.10855, -7.07298, -7.07298;
      -7.07314, -7.07314, -5.10867, -3.2711, -5.10867, -7.07315, -7.07314;
      -6.04004, -6.04004, -4.3625, -2.79332, -4.3625, -6.04004, -6.04004];

pressure=CpTW*qz; %in plf
```

```
% PROP=[Moment of inertia (in inches^4), Shear area (in inches^2)]
PROP=[9.177, 0.976];
% MAT= [Modulus of Elasticity (ksi),coefficent of thermal expansion,
Poisson's ratio]
MAT=[29000,0.00000108,.27];

%finds the number of nodes and number of elements
nnodes=size(X,1);
nels=nnodes-1;

for PURLIN_COUNTER=1:(size(tribwidth,1)-1)
    % Restraint Matrix is given by
    % R=[X displacement , Y displacement restraint]
    % this input to R puts supports at each end of the strucure and
    % creates a matrix of zeros in the middle
    R=[1,0;
       zeros(nnodes-2,2);
       1,0];
    % matrix containing the point load values that would be located at
    %the supports (all zero for this case)
    P=zeros(nnodes,2);

    % Connectivity Matrix is given by
    % CON=[iend,jend,material property no:,section property no:,member load
type]
    %first set it equal to zero for all elements
    CON=zeros(nels,5);

    ii=1;
    for i=1:nels
        %writes in the i and j end values and property and material
        %type identifiers
        CON(i,:)=[i, i+1,  1,  1,  0];
        if ismember(X(i),interiorsupports*12)
            %this if statement finds the interior supports and carries
            %over the previous MLOAD number since the load isn't
            %changing at a new pressure tap. It also adds a support in
            %the R matrix.
            CON(i,5)=ii-1;
            R(i,:)=[1,0];
        else
            %these statements continue to add MLOAD values and increase
            %this counter
            CON(i,5)=ii;
            ii=ii+1;
        end
    end

    for j=1:size(CpTW,2)
        % For member load type zero indicate there is no member load where as
any
        % number greater than zero indicate the corresponding row in the
member
        % load matrix.
        MLOAD(j,:)=[pressure(PURLIN_COUNTER,j)/12/1000,   0,  0,  0,  0,  0,
0];
    end
```

```
    % The number of segments to which the structure needs to be divided
    % plot the deflected and undeflected shape
    nsegD=[100];
    % The magnification of displacement for plotting the shape of the
structure.
    % The magnification factor of 0 is used to plot the undeflected shape and
    % the magnification factor greater than 1 is used to plot the undflected
shape.

    mg=[1,2];

    % For the given example the undeflected shape is plotted with the
    % magnification factor  of 10

    % The number segments to which the elements has to be divided to plot the
    % bending moment diagram is given by
    nsegBM=[200];

    % The side on which the bending moment digarm needs to be plotted is
given
    % by
    SIDE='T';
    % The character T represents tension side and the character C represenst
    % the compression side


[L,ID,FVEC,khat,KG,FEF,Q,D,UOUT,F,S,React,EQ,FullMoment,FullShear,FullPlotX]=
Beam_Functions(CON,X,R,P,MAT,PROP,MLOAD,nsegD,mg,nsegBM,SIDE);

%[L,ID,FVEC,khat,KG,FEF,Q,D,UOUT,F,S,React,EQ,ESHAPE,SHEAR,BMD]=Beam_Function
s(CON,X,R,P,MAT,PROP,MLOAD,nsegD,mg,nsegBM,SIDE,rootdir,Folder1,Folder2,jj);

    kk=1;
    jj=1;
    for k=1:nnodes
        if abs(React(k,1))>0.00001
            R_Force(:,kk)=React(k,1);
            kk=kk+1;
        end
        if abs(React(k,2))>0.00001
            R_Moment(:,jj)=React(k,2);
            jj=jj+1;
        end
        D_VERT(:,k)=UOUT(k,1);
        D_ROT(:,k)=UOUT(k,2);
    end
    for l=1:nels
        V_ELEM_i(:,l)=F(1,1,l);
        V_ELEM_j(:,l)=F(3,1,l);
        M_ELEM_i(:,l)=F(2,1,l);
        M_ELEM_j(:,l)=F(4,1,l);
    end

    %MaxMin file will be 4 columns, 1 row per time step. [MaxV,
    %MaxM, MinV, MinM]
    MaxMin(:,2)=max(FullMoment);
    MaxMin(:,1)=max(FullShear);
```

```
MaxMin(:,4)=min(FullMoment);
MaxMin(:,3)=min(FullShear);

FullX=FullPlotX/12;

for mm=1:125
    [val,idx]=min(abs(FullX-mm));
    FullX2(mm)=FullX(idx);
    FullV2(mm)=FullShear(idx);
    FullM2(mm)=FullMoment(idx);
end
FullX3=FullX2;
FullV3=FullV2;
FullM3=FullM2;

rootdir='D:\Mary\Beam analysis\All Angles.v2\EE1_Results';
Folder1='ASCE7';
Folder2=strcat('Purlin',string(PURLIN_COUNTER));

filen='NegReactions.txt';
fileID=fopen(fullfile(rootdir,Folder1,Folder2,filen),'w+');
formatting='%g\t';
for m=1:size(R_Force,2)-1
    formatting=strcat(formatting,' %g\t');
end
for mm=1:size(R_Force,1)
    fprintf(fileID,strcat(formatting,'\n'),R_Force(mm,:));
end

filen='NegDisp.txt';
fileID=fopen(fullfile(rootdir,Folder1,Folder2,filen),'w+');
formatting='%g\t';
for n=1:size(D_VERT,2)-1
    formatting=strcat(formatting,' %g\t');
end
for nn=1:size(D_VERT,1)
    fprintf(fileID,strcat(formatting,'\n'),D_VERT(nn,:));
end

filen='NegRotationalDisp.txt';
fileID=fopen(fullfile(rootdir,Folder1,Folder2,filen),'w+');
formatting='%g\t';
for o=1:size(D_ROT,2)-1
    formatting=strcat(formatting,' %g\t');
end
for oo=1:size(D_ROT,1)
    fprintf(fileID,strcat(formatting,'\n'),D_ROT(oo,:));
end

filen='NegShearIEnd.txt';
fileID=fopen(fullfile(rootdir,Folder1,Folder2,filen),'w+');
formatting='%g\t';
for p=1:size(V_ELEM_i,2)-1
    formatting=strcat(formatting,' %g\t');
end
for pp=1:size(V_ELEM_i,1)
    fprintf(fileID,strcat(formatting,'\n'),V_ELEM_i(pp,:));
```

```
end

filen='NegShearJEnd.txt';
fileID=fopen(fullfile(rootdir,Folder1,Folder2,filen),'w+');
formatting='%g\t';
for q=1:size(V_ELEM_j,2)-1
    formatting=strcat(formatting,' %g\t');
end
for qq=1:size(V_ELEM_j,1)
    fprintf(fileID,strcat(formatting,'\n'),V_ELEM_j(qq,:));
end

filen='NegMomentIEnd.txt';
fileID=fopen(fullfile(rootdir,Folder1,Folder2,filen),'w+');
formatting='%g\t';
for r=1:size(M_ELEM_i,2)-1
    formatting=strcat(formatting,' %g\t');
end
for rr=1:size(M_ELEM_i,1)
    fprintf(fileID,strcat(formatting,'\n'),M_ELEM_i(rr,:));
end

filen='NegMomentJEnd.txt';
fileID=fopen(fullfile(rootdir,Folder1,Folder2,filen),'w+');
formatting='%g\t';
for q=1:size(M_ELEM_j,2)-1
    formatting=strcat(formatting,' %g\t');
end
for qq=1:size(M_ELEM_j,1)
    fprintf(fileID,strcat(formatting,'\n'),M_ELEM_j(qq,:));
end
filen='NegFullMoment.txt';
fileID=fopen(fullfile(rootdir,Folder1,Folder2,filen),'w+');
formatting='%g\t';
for r=1:size(FullM3,2)-1
    formatting=strcat(formatting,' %g\t');
end
for rr=1:size(FullM3,1)
    fprintf(fileID,strcat(formatting,'\n'),FullM3(rr,:));
end
filen='NegFullX.txt';
fileID=fopen(fullfile(rootdir,Folder1,Folder2,filen),'w+');
formatting='%g\t';
for s=1:size(FullX3,2)-1
    formatting=strcat(formatting,' %g\t');
end
for ss=1:size(FullX3,1)
    fprintf(fileID,strcat(formatting,'\n'),FullX3(ss,:));
end
filen='NegFullShear.txt';
fileID=fopen(fullfile(rootdir,Folder1,Folder2,filen),'w+');
formatting='%g\t';
for t=1:size(FullV3,2)-1
    formatting=strcat(formatting,' %g\t');
end
for tt=1:size(FullV3,1)
    fprintf(fileID,strcat(formatting,'\n'),FullV3(tt,:));
```

```
    end
    filen='NegMaxMin.txt';
    fileID=fopen(fullfile(rootdir,Folder1,Folder2,filen),'w+');
    formatting='%g\t';
    for t=1:size(MaxMin,2)-1
        formatting=strcat(formatting,' %g\t');
    end
    for tt=1:size(MaxMin,1)
        fprintf(fileID,strcat(formatting,'\n'),MaxMin(tt,:));
    end
    fclose('all');
end
```

APPENDIX G: Code for creating shear and moment envelope

```
clear all
clc

tribwidth=[0;1.9321;5.7963;9.3951;13.5617;18.5617;22.9784;27.3951;31.8117;
            36.2284;40;43.6515;48.0682;52.4848;56.9015;61.3182;
            66.3182;70.4649;74.0836;77.9478;80]; %tributary width of a
purlin, ft
numangles=19;
rooflength=125;

rootdir2='D:\Mary\Beam analysis\All Angles.v2\EE1_Results\ASCE7';

%PURLIN_COUNTER=2;
for PURLIN_COUNTER=1:(size(tribwidth,1)-1)
    for ANGLE_COUNTER=1:numangles
        ang=2700+(ANGLE_COUNTER-1)*50;

        rootdir='D:\Mary\Beam analysis\All Angles.v2\EE1_Results';

        Folder1=string(ang);
        Folder2=strcat('Purlin',string(PURLIN_COUNTER));
        filen1='FullMoment.txt';
        filen2='FullShear.txt';
        filen3='MaxMin.txt';
        filen4='FullX.txt';

        filen5='NegFullMoment.txt';
        filen6='NegFullShear.txt';
        filen7='NegMaxMin.txt';
        filen8='NegFullX.txt';
        filen9='PosFullMoment.txt';
        filen10='PosFullShear.txt';
        filen11='PosMaxMin.txt';

        filename1 = strcat(rootdir,'\',Folder1,'\',Folder2,'\',filen1);
        filename2 = strcat(rootdir,'\',Folder1,'\',Folder2,'\',filen2);
        filename3 = strcat(rootdir,'\',Folder1,'\',Folder2,'\',filen3);
        filename4 = strcat(rootdir,'\',Folder1,'\',Folder2,'\',filen4);
        filename5 = strcat(rootdir2,'\',Folder2,'\',filen5);
        filename6 = strcat(rootdir2,'\',Folder2,'\',filen6);
        filename7 = strcat(rootdir2,'\',Folder2,'\',filen7);
        filename8 = strcat(rootdir2,'\',Folder2,'\',filen8);
        filename9 = strcat(rootdir2,'\',Folder2,'\',filen9);
        filename10 = strcat(rootdir2,'\',Folder2,'\',filen10);
        filename11 = strcat(rootdir2,'\',Folder2,'\',filen11);

        delimiterIn = '\t';
        headerlinesIn = 0;
        MFull = importdata(filename1,delimiterIn,headerlinesIn);
        VFull = importdata(filename2,delimiterIn,headerlinesIn);
        MaxMin = importdata(filename3,delimiterIn,headerlinesIn);
        XFull = importdata(filename4,delimiterIn,headerlinesIn);
        NMFull = importdata(filename5,delimiterIn,headerlinesIn);
```

```
    NVFull = importdata(filename6,delimiterIn,headerlinesIn);
    NMaxMin = importdata(filename7,delimiterIn,headerlinesIn);
    NXFull = importdata(filename8,delimiterIn,headerlinesIn);
    PMFull = importdata(filename9,delimiterIn,headerlinesIn);
    PVFull = importdata(filename10,delimiterIn,headerlinesIn);
    PMaxMin = importdata(filename11,delimiterIn,headerlinesIn);

    VFull_Max_1ANG(ANGLE_COUNTER,:)=max(VFull);
    VFull_Min_1ANG(ANGLE_COUNTER,:)=min(VFull);
    MFull_Max_1ANG(ANGLE_COUNTER,:)=max(MFull);
    MFull_Min_1ANG(ANGLE_COUNTER,:)=min(MFull);

    VFull_Max_All=max(VFull_Max_1ANG);
    VFull_Min_All=min(VFull_Min_1ANG);
    MFull_Max_All=max(MFull_Max_1ANG);
    MFull_Min_All=min(MFull_Min_1ANG);
end
[val,idx]=max(VFull_Max_All);
VMaxMin(5,PURLIN_COUNTER)=val;
VPos(5,PURLIN_COUNTER)=idx;
[val,idx]=max(MFull_Max_All);
MMaxMin(5,PURLIN_COUNTER)=val;
MPos(5,PURLIN_COUNTER)=idx;
[val,idx]=min(VFull_Min_All);
VMaxMin(6,PURLIN_COUNTER)=val;
VPos(6,PURLIN_COUNTER)=idx;
[val,idx]=min(MFull_Min_All);
MMaxMin(6,PURLIN_COUNTER)=val;
MPos(6,PURLIN_COUNTER)=idx;

[val,idx]=max(NVFull);
VMaxMin(1,PURLIN_COUNTER)=val;
VPos(1,PURLIN_COUNTER)=idx;
[val,idx]=max(NMFull);
MMaxMin(1,PURLIN_COUNTER)=val;
MPos(1,PURLIN_COUNTER)=idx;
[val,idx]=min(NVFull);
VMaxMin(2,PURLIN_COUNTER)=val;
VPos(2,PURLIN_COUNTER)=idx;
[val,idx]=min(NMFull);
MMaxMin(2,PURLIN_COUNTER)=val;
MPos(2,PURLIN_COUNTER)=idx;

[val,idx]=max(PVFull);
VMaxMin(3,PURLIN_COUNTER)=val;
VPos(3,PURLIN_COUNTER)=idx;
[val,idx]=max(PMFull);
MMaxMin(3,PURLIN_COUNTER)=val;
MPos(3,PURLIN_COUNTER)=idx;
[val,idx]=min(PVFull);
VMaxMin(4,PURLIN_COUNTER)=val;
VPos(4,PURLIN_COUNTER)=idx;
[val,idx]=min(PMFull);
MMaxMin(4,PURLIN_COUNTER)=val;
MPos(4,PURLIN_COUNTER)=idx;

%VPlot=[VFull_Max_All;VFull_Min_All];
```

```
    %MPlot=[MFull_Max_All;MFull_Min_All];
    %plot(XFull(1,:),VFull(1,:));
end
```